

NEW CONCEPTS IN SURFACE MODIFICATION FOR BIOSENSOR
APPLICATION-POLYANILINE AND BACTERIOPHAGE SURFACE
MODIFICATION

Except where reference is made to the work of others, the work described in this dissertation is my own or was done in collaboration with my advisory committee. This dissertation does not include proprietary or classified information.

Hongxia Zhang

Certificate of Approval:

Vince Cammarata
Associate Professor
Chemistry and Biochemistry

Curtis G. Shannon, Chair
Professor
Chemistry and Biochemistry

Wei Zhan
Assistant Professor
Chemistry and Biochemistry

Anne E. V. Gorden
Assistant Professor
Chemistry and Biochemistry

George T. Flowers
Dean
Graduate School

NEW CONCEPTS IN SURFACE MODIFICATION FOR BIOSENSOR
APPLICATION-POLYANILINE AND BACTERIOPHAGE SURFACE
MODIFICATION

Hongxia Zhang

A Dissertation

Submitted to

the Graduate Faculty of

Auburn University

in Partial Fulfillment of the

Requirements for the

Degree of

Doctor of Philosophy

Auburn, Alabama
December 19, 2008

NEW CONCEPTS IN SURFACE MODIFICATION FOR BIOSENSOR
APPLICATION-POLYANILINE AND BACTERIOPHAGE SURFACE
MODIFICATION

Hongxia Zhang

Permission is granted to Auburn University to make copies of this dissertation at its discretion, upon request of individuals or institutions and at their expense. The author reserves all publication rights.

Signature of Author

Date of Graduation

VITA

Hongxia Zhang, daughter of Qinshan Zhang and Fengying Yan, was born on December 17, 1975, in Ningxia, China. After graduated from Pingluo High School in 1994, she went to Peking University where she obtained a Bachelor degree of Chemistry in 1998. She got a Master degree of Philosophy in Chemistry from Hong Kong Baptist University in 2002. In the fall of 2003, she entered Graduate School at Auburn University to pursue a Doctoral degree in Chemistry under the guidance of Dr. Curtis G. Shannon.

DISSERTATION ABSTRACT

NEW CONCEPTS IN SURFACE MODIFICATION FOR BIOSENSOR
APPLICATION-POLYANILINE AND BACTERIOPHAGE SURFACE
MODIFICATION

Hongxia Zhang

Doctor of Philosophy, December 19, 2008
(M. Phil., Hong Kong Baptist University, 2002)
(2002 B. S., Peking University, 1998)

181 Typed Pages

Directed by Curtis G. Shannon

Polyaniline is one of the most promising conductive polymers for technological applications because of its unique electrooptical properties, ease of synthesis and low cost. An additional attribute is that polyanilines can be chemically modified straightforwardly in an electrochemical cell. Specifically, nucleophiles can reduce the polyaniline backbone from the oxidized emeraldine form to the leucoemeraldine form, leading to the formation of chemically modified polyaniline. In chapter 2 of this dissertation, we investigate electrochemically directed chemical modification of polyanilines for applications in heterogeneous immunosorbent assays. Electrochemical methods and surface enhanced Raman Spectroscopy (SERs) were used to characterize

polyaniline films covalently modified with IgG antibody fragments containing nucleophilic thiol groups. The cyclic voltammetry signals from the protein sandwich assay were much higher on the oxidized state of polyaniline than those on the reduced state of polyaniline, indicating that the antibody fragment is covalently attached only to oxidized polyaniline. SERs results also provide evidence that the emeraldine form of polyaniline converted into the leucoemeraldine form after reacting with antibody solution.

Assembly of biological molecules and nanoparticles to generate novel hybrid materials is an active area of investigation with applications ranging from sensor development to the diagnosis and treatment of certain diseases. Typically, the bonding between biomolecules and nanoparticles is based on hydrophobic interactions, van der Waals contact, and/or electrostatic forces. In chapter 3 of this work, we report on the covalent attachment of filamentous bacteriophage thiolated with 2-iminothiolane to gold nanoparticles. Results from UV-VIS spectroscopy indicate that the reaction between primary amines on phage and 2-iminothiolane takes place very rapidly. TEM and AFM imaging clearly shows that the formation of networks of bacteriophage and nanoparticles has occurred. Surface enhanced Raman spectroscopy was used to investigate nature of the interaction between thiol-functionalized fd bacteriophage and gold nanoparticles. The conjugate network generated in our work has promising applications in biosensor field. Preliminary investigations on the use of these materials to modify electrode surfaces will be discussed.

ACKNOWLEDGMENT

There is a long list of people I wish to express my sincerest gratitude. At first, I would like to thank my research advisor, Professor Curtis Shannon, a erudite and kindly person. During the four years working with him, I was deeply impressed by his meticulous and aggressive attitude to research.

I would also like to thank my committee members, Dr. Vince. Cammarata, Dr. Wei Zhan, and Dr. Anne Gorden for their precious advice and help within this dissertation.

I would like to thank the group members, Anand, Yuming, Fengping, Lunsheng, Joseph, Chaokang, Amy, Uhur, for their friendship and useful discussions. Dr. I-Hsuan Chen, thank you for giving me so much help to prepare bacteriophage solution for me. Dr. Kai Jiang, thank you for your help in the experiment of chapter 4.

In addition, I would like to express my appreciation to Dr. Michael Miller for his kindness of answering my questions in TEM during the course of my research and to be my outside reader.

Style manual or journal used:

American Chemical Society Style

Computer software used:

Microsoft Word 2003, Microsoft Excel, ChemDRAW 8.0, Microcal Origin 6.0

TABLE OF CONTENTS

LIST OF FIGURES	xiii
LIST OF TABLES	xv
CHAPTER 1. Literature Review	1
1.1. Introduction to Biosensors	1
1.2. Electrochemical Immunosensors	5
1.3. Introduction to Polyaniline (PANI)	14
1.4. Nanoparticles in Biotechnology.....	21
1.5. Bacteriophage	26
1.6. Surface Enhanced Raman Spectrometry-Principle and Application in Biospecies Detection	30
1.7. Polyoxometalate for Electrochemical Catalysis	33
References	39
CHAPTER 2. ELECTROCHEMICAL ENZYME IMMUNOASSAY ON POLYANILINE MODIFIED GOLD ELECTRODES	51
2.1. Introduction.....	51
2.2. Experimental	54
2.2.1. Chemicals and reagents.....	54
2.2.2. Covalent immobilization of immunoreagents.....	55

2.2.3. Cyclic voltammetry.....	56
2.2.4. Raman spectroscopy	57
2.2.5. Matrix assisted laser desorption ionization-time of flight mass spectroscopy	57
2.3. Results.....	58
2.3.1. Matrix assisted laser desorption ionization-time of flight mass spectroscopy	58
2.3.2. Cyclic Voltametry.....	62
2.3.2.1. Determination of rabbit IgG sandwich assay on oxidized polyaniline electrode	62
2.3.2.2. Crossed reaction of anti-rabbit IgG and anti-sheep IgG.....	67
2.3.2.3. Reactivity of Fab fragment of anti-rabbit IgG	71
2.3.2.4 The influence of 11-mercapto-1-undecanol on the interaction between antibodies and oxidized polyaniline.....	73
2.3.2. Surface Enhanced Raman Spectroscopy (SERs)	77
2.3. Discussion	80
2.5. Conclusions and future application.....	86
References.....	89

CHAPTER 3. PREPARATION AND CHARACTERIZATION OF COVALENTLY

LINKED BACTERIOPHAGE-NANOPARTICLE

3.1. Introduction.....	92
------------------------	----

3.2. Experimental	95
3.2.1. Materials and reagents	95
3.2.2. Sample preparation	95
3.2.3. Cyclic Voltammetry	96
3.2.4. AFM	96
3.2.5. TEM	97
3.2.6. UV-Vis	97
3.2.7. Raman	97
3.2.8. SEM	98
3.3. Results and Discussion	98
3.3.1. Results for reaction between 2-iminothiolane and lysine or bacteriophage	98
3.3.2. Formation of gold nanoparticles	104
3.3.3. TEM results for gold-bacteriophage conjugate formation...	108
3.3.4. SERS results for gold-bacteriophage conjugate formation..	115
3.3.5. Bioactivity of bacteriophage in networks	119
3.4. Conclusion and potential applications	126
References.....	129

CHAPTER 4. PREPARATION AND CHARACTERIZATION OF

POLYOXOMETALATE/PROTEIN ULTRATHIN FILMS GROWN ON ELECTROD

SURFACE USING LAYER-BY-LAYER ASSEMBLY

4.1. Introduction.....	134
4.2. Experimental	136

4.2.1. Chemicals and reagent	136
4.2.2. Film assembly	136
4.2.3. UV-Vis Spectroscopy	137
4.2.4. AFM measurements	137
4.2.5. Electrochemistry	138
4.3. Results and Discussion	138
4.3.1. Film assembly	138
4.3.2. Characterization of LBL films	139
4.3.3. AFM characterization of $\{P_2W_{18}O_{62}^{6-}/cyt\ c\}_n$ films	147
4.3.4. Effect of film thickness on overall electron transfer rate.....	149
4.3.5. Electrocatalysis of hydrogen peroxide reduction using $\{P_2W_{18}O_{62}^{6-}/cyt\ c\}_n$ films.....	149
4.4. Conclusions.....	154
References.....	156
CHAPTER 5. SUMMARY.....	159
References.....	162

LIST OF FIGURES

Figure 1.1. The working principle of biosensor.....	2
Figure 1.2. The structure of antibody.....	7
Figure 1.3. The different formats of immunoassays generally used in immunosensors from Ref 37	10
Figure 1.4. The structures of polyanilines (Ref. 72, 73).....	15
Figure 1.5. Polyaniline synthesis mechanism (Ref. 74, 75).....	17
Figure 1.6. Reaction pathways of nucleophilic addition to polyaniline. (Ref. 78,79).....	19
Figure 1.7. Mechanism of nucleophilic addition (Ref. 78, 79).....	20
Figure 1.8. Structure of bacteriophage PIII, pVI, pVII, pVIII and pXIX represent phage proteins (A) (from Ref. 110).....	28
Figure 1.9. Structure of Polyoxometalate commonly used in Catalysis (a: Keggin structure; and b: Wells–Dawson structure (Ref. 147, 148).....	36
Figure 2.1. MALDI-MS spectrum of (a) oxidized polyaniline (OPANI) and reduced polyaniline (RPANI) and (b) oxidized polyaniline (OPANI) and polyaniline reacted with butanethiol (OPANI-Bu)	60
Figure 2.2. Cyclic voltammograms of Rabbit sandwich assay on oxidized (blue solid line), reduced polyaniline modified gold electrodes(green solid line) and baseline caused by pAPP non-enzymatic hydrolysis (brown dash line).....	66

Figure 2.3. Cyclic voltammograms of Rabbit, Sheep IgG sandwich assay and cross reaction between Rabbit and Sheep IgG on oxidized polyaniline modified gold electrodes	68
Figure 2.4. Cyclic voltammogram of the electrodes with Rabbit IgG sandwich assay on oxidized polyaniline (blue line); Sheep IgG sandwich assay on reduced polyaniline (brown dash line); and Rabbit IgG sandwich assay prepared by reducing Polyaniline firstly at -200 mV for 5 min, and then immersed in anti-Sheep IgG after that oxidizing polyaniline on the electrode and modified with anti-rabbit IgG.....	70
Figure 2.5. Cyclic voltamgram for the electrode with monoclonal anti-rabbit IgG sandwich assay and F(ab) fragment of anti-rabbit IgG sandwich assay on oxidized polyaniline film	72
Figure 2.6. Cyclic voltammograms on the electrod with the following modifications monoclonal anti-rabbit IgG sandwich assay (black solid line); rabbit anti IgG on oxidizd polyaniline surface firstly and then immersing this electrode into 1mM 11mercapto-1-undecanol solution in buffer A for 1 hr. After that, reacting electrode with rabbit IgG and then labeled rabbit an IgG consequently (black dash line); c: Immersing the electrode with polyaniline film into 1mM 11mercapto-1-undecanol solution in buffer A for 1 hr firstly and then put this electrode into rabbit anti IgG solution for 1 hr. After that, electrode was reacted with rabbit IgG and then labeled rabbit anti-IgG consequently (solid brown line).....	75

Figure 2.7. Cyclic voltammogram for the electrode with: F(ab) fragment of anti-rabbit IgG sandwich assay on oxidized polyaniline film(black dash line) and electrode by modifying rabbit anti IgG (Fab fragment) on oxidized polyaniline surface firstly and then immersing this electrode into 1mM 11-mercapto-1-undecanol solution in buffer A for 1 hr. After that, reacting electrode with rabbit IgG and then labeled anti-rabbit IgG	76
Figure 2.8. Raman spectrum of a) reduced polyaniline film ; b) oxidized polyaniline film and (c) polyaniline film after oxidized form reacting with F(ab) fragment of Rabbit IgG. The excitation wavelength is 632.5 nm	78
Figure 2.9. Raman spectra of oxidized polyaniline film (a); polyaniline film after oxidized form reacting with F(ab) fragment of Rabbit IgG (b); and polyaniline film after oxidized form reacting with F(ab) fragment of Rabbit IgG and then exposing in the water for 2 hours (c) . The excitation wavelength is 632.5 nm	85
Figure 2.10. Proposed application of immunosensor prepared on polyaniline film.....	88
Figure 3.1. Change of UV-Vis absorbance at 268 nm by reaction time adding lysine (a) into 2-IT solution or adding fd bacteriophage (b) into 2-IT solution	100
Figure 3.2. Blocked electrochemical reaction on IT reacted bacteriophage modified gold electrode.....	102
Figure 3.3. AFM image of IT reacted bacteriophage modified gold surface.....	103
Figure 3.4. UV-Vis spectrum of 100 times diluted originally prepared gold colloidal solution.....	105

Figure 3.5. TEM of gold colloid with concentration originally prepared (a) and 100 times diluted concentration	106
Figure 3.6. AFM image of IT reacted bacteriophage modified gold surface	109
Figure 3.7. Raman spectra of gold nanoparticles conjugate with bacteriophage through 2-IT (phage-IT-AuNP), gold nanoparticles and phosphate buffer (AuNP-buffer) and bacteriophage, buffer and gold nanoparticles mixture (AuNP-phage-buffer).....	116
Figure 3.8. SEM image of <i>Salmonella typhimurium</i> -bacteriophage E2 infection	120
Figure 3.9. Raman spectra of bacteriophage- <i>E. coli</i> infection (Phage-IT-AuNP: gold bacteriophage-nanoparticles conjugate through IT; Phage-IT-ecoli: <i>E. coli</i> infection of IT reacted bacteriophage ; Ecoli-AuNP: mixture of <i>E. coli</i> solution and gold colloid solution; Phage-IT-AuNP-ecoli: <i>E. coli</i> infection of gold bacteriophage-nanoparticles conjugate through IT)	122
Figure 3.10. Proposed sensor application of the gold nanoparticles-bacteriophage network described in this chapter.....	128
Figure 4.1. Layer-by-layer formation of $P_2W_{18}O_{62}^{6-}$ and <i>cyt c</i> (or $Ru(bpy)_3^{2+}$) thin films characterized by cyclic voltammetry (CV). The multilayered films were formed by alternately dipping a glassy carbon electrode (GCE) in respective POM and protein (or $Ru(bpy)_3^{2+}$) solutions. The first layer (dash line) of $P_2W_{18}O_{62}^{6-}$ was electrostatically attracted onto the electrode surface by a pre-adsorbed $Ru(bpy)_3^{2+}$ layer. See Experimental section. Supporting electrolyte: 0.1 M H_2SO_4 aqueous solution; scan rate: 0.1 V/s. (a) $\{P_2W_{18}O_{62}^{6-}/cyt c\}_n, n$	

= 1-4; (b) $\{\text{P}_2\text{W}_{18}\text{O}_{62}^{6-}/\text{Ru}(\text{bpy})_3^{2+}\}_n$, $n = 1-4$; (c) Comparison of $\{\text{P}_2\text{W}_{18}\text{O}_{62}^{6-}/\text{cyt } c\}_2$ and $\{\text{P}_2\text{W}_{18}\text{O}_{62}^{6-}/\text{Ru}(\text{bpy})_3^{2+}\}_4$ (dot line).....142

Figure 4.2. Electrochemical responses of a $\{\text{P}_2\text{W}_{18}\text{O}_{62}^{6-}/\text{cyt } c\}_n$ film under different CV scan rate. (a) Normalized peak (B_2' as in Figure 1a) current of $\{\text{P}_2\text{W}_{18}\text{O}_{62}^{6-}/\text{cyt } c\}_n$ ($n = 1-12$) at different scan rate; (b) Cyclic voltammograms of $\{\text{P}_2\text{W}_{18}\text{O}_{62}^{6-}/\text{cyt } c\}_n$ at 0.005 V/s (solid line: $n = 1, 3, 5, 7, 9$ and 11; dot line: $n = 12$).....145

Figure 4.3. UV-vis absorption spectra of $\{\text{P}_2\text{W}_{18}\text{O}_{62}^{6-}/\text{cyt } c\}_n$ ultrathin film layer-by-layer assembled on a glass slide. dotted line: blank; solid lines show stepwise growth of $\{\text{P}_2\text{W}_{18}\text{O}_{62}^{6-}/\text{cyt } c\}_n$ on both sides of glass slide, $n = 1-12$; the arrow indicates the film growth direction. Inset: layer-by-layer growth of *cyt c* absorption at 409146

Figure 4.4. Determination of LBL film thickness using AFM. (a) Tapping mode AFM imaging was used to profile lithographically defined patterns in LbL films. An area of the patterned film containing regions of bare mica as well as a $\{\text{P}_2\text{W}_{18}\text{O}_{62}^{6-}/\text{cyt } c\}_{10}$ film is shown (b). The height profile as measured along the dashed line in the image (a)148

Figure 4.5. Determination of the apparent electron transfer rate constants (k_{app}) for $\{\text{P}_2\text{W}_{18}\text{O}_{62}^{6-}/\text{cyt } c\}_1$ and $\{\text{P}_2\text{W}_{18}\text{O}_{62}^{6-}/\text{Rubpy}\}_1$ films following Laviron method. Peak potentials were collected from the CVs t different scan rates in degassed 0.1 M H_2SO_4 aqueous solution150

Figure 4.6. Electrocatalysis of hydrogen peroxide reduction using $\{\text{P}_2\text{W}_{18}\text{O}_{62}^{6-}/\text{cyt } c\}_n$ films. (a) Dependence of catalysis efficiency on film thickness. $\{\text{P}_2\text{W}_{18}\text{O}_{62}^{6-}$

$/cyt\ c\}_n$ ($n = 1 - 3$) films were examined using 50 mM H_2O_2 ; supporting electrolyte: 0.1 M KCl in 0.1 M phosphate buffer (PBS), pH = 7.3; (b) Catalysis of hydrogen peroxide reduction using $\{P_2W_{18}O_{62}^{6-}/cyt\ c\}_n$ ($n = 1$) modified GCEs at different H_2O_2 concentrations; other conditions are the same as in (a)153

LIST OF TABLES

Table 1.1. Representative examples for enzymes used in electrochemical immunoassays.....	12
Table 2.1. The MALDI-MS peak assignment of oxidized polyaniline and butanthiol reacted polyaniline	61
Table 2.2. Assignment of Raman peaks of Polyaniline	79
Table 2.3. Oxidized peak current for PAPP enzymatic hydrolysis on electrodes with different modification	82
Table 3.1. The assignment of spectral regions of fd bacteriophage.....	11
Table 3.2. The assignment of spectral regions of bacterial cells.	124
Table 4.1. Change of k_{app}° as a function of number of LbL layers.....	151

CHAPTER 1

LITERATURE REVIEW

1.1 Introduction to biosensors

Biosensors show tremendous commercial potential in fields such as medical and health care, veterinary science, environmental monitoring and control, food processing, military technology and agriculture¹⁻³. As a consequence, in the last twenty years biosensors have been the subject of intense research worldwide.

In 1999, the International Union of Pure and Applied Chemistry (IUPAC) defined a biosensor as "a self-contained integrated device ... capable of providing specific quantitative or semi-quantitative analytical information using a biological recognition element (biochemical receptor) which is retained in direct spatial contact with a transduction element", going on to caution "Because of their ability to be repeatedly calibrated ... a biosensor should be clearly distinguished from a bioanalytical system, which requires additional processing steps, such as reagent addition"⁴.

Considerable progress has been made in monitoring and diagnosing metabolites such as glucose, hormones, neurotransmitters, antibodies, and antigens for clinical purposes since the first biosensing device was developed by Leland C. Clark⁵, who integrated an enzyme into an electrode. In principle, a biosensing device is composed of two parts: a

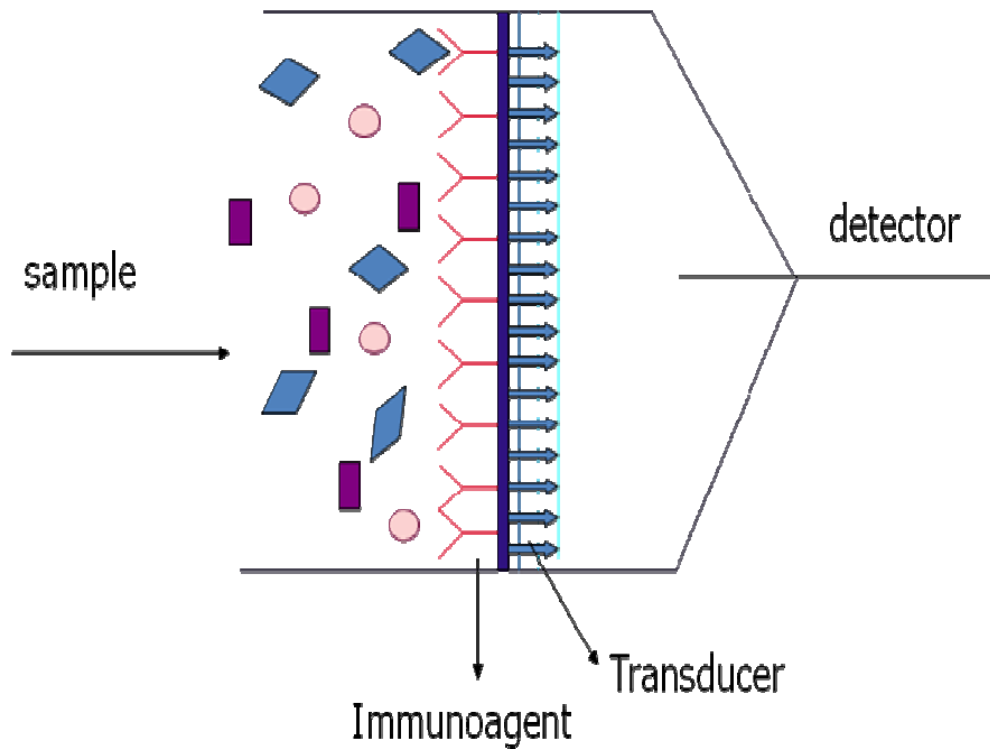


Figure 1.1. The working principle of a biosensor

biomolecular recognition element (receptor) and a transducer. The basic concept of biosensor's operation is illustrated in Figure 1.1. The biomolecular recognition element, which is generally an enzyme or an antibody (immunoagent), recognizes the target analyte and the transducer then converts the recognition event into a measurable signal.

The ideal biosensor should be able to detect target molecules both selectively and quantitatively within the required concentration range and in a reasonable time and should be capable of generating a signal without the need for externally added reagents. Therefore, the bio-recognition element should be very specific and sensitive to the target analyte only. The most common forms of biorecognition mechanisms can be classified in four major categories, namely: (i) antibody/antigen interactions, (ii) nucleic acid/DNA interactions, (iii) enzymatic interactions, and (iv) cellular structure/cell interactions⁶.

The integration of the bioreceptor and the transducer into a single sensor is the key property of a biosensor. The bio-recognition element and transducer surface can be coupled together using one of several methods: a membrane or matrix entrapment⁷⁻⁹, physical adsorption¹⁰⁻¹², or covalent bonding¹³⁻¹⁸. Problems may arise as entrapment and physical adsorption result in a weak bond and the molecules in the biorecognition element have random orientation, leading to non-uniform adsorption patterns. Although covalent attachment procedures are more complicated than entrapment ones, they are especially useful when the sensor is so small that the membrane or film must be fabricated directly onto the transducer. Under such conditions, more stable and reproducible activities can be obtained using a covalent attachment approach.

Based on the transduction mechanism used for target detection and measurement, biosensors can be divided into several types, namely electrochemical, optical, mechanical and thermal. Electrochemical measurements include amperometry, potentiometry, Ion Sensitive Field-Effect Transistors (ISFETs), conductometry and capacitance biosensors. Amperometry measurement is based on measuring the current resulting from electrochemical oxidation or reduction of an electroactive species¹⁹. Potentiometry measurement determines the potential difference between an indicator and a reference electrode when there is no significant current flowing between them²⁰. An ISFET is used to determine ion concentrations and consists of an electrochemical sensor that utilizes thin films or selective membranes as recognition elements²¹. Conductometry detects changes in conductivity between two electrodes. Capacitance biosensors directly detect a change in the dielectric constant of the medium caused by biorecognition reaction.

Optical biosensors have successfully been used for the detection of target analytes of interest in a variety of applications. The primary function of this type of sensor is to correlate changes in concentration, mass, or number of molecules with direct changes in the characteristics of light as a result of the interaction between bioreceptors and analytes. There are a number of optical techniques used for monitoring biorecognition on the surface of a sensor, including Surface Plasmon Resonance²², internal reflection spectroscopy²³, Surface Enhanced Raman Spectroscopy(SERS), fluorescence²⁴ and Fourier Transform Infrared Spectroscopy (FTIR)²⁵.

Mechanical measurements detect changes in mass, strain, surface stress, or viscosity using piezoelectric or acoustic techniques. For any piezoelectric crystal, the change in its resonant frequency is proportional to the mass of material absorbed on its surface up to about a 2% change. When bioreceptors capture a molecule of the analyte, the resulting change in the mass of the piezoelectric crystal leads to a frequency shift which can be measured. The major drawbacks of these devices are problems due to interference from atmospheric humidity and the difficulty in using them for the determination of material in solution. In resonant biosensors, an acoustic wave transducer is coupled with a bioreceptor. When analyte molecules become attached to the membrane, the change in mass affects the membrane characteristics, quantitatively changing the resonant frequency of the transducer. This frequency change can then be measured.

Thermal detection biosensors exploit the absorption or production of heat generated in biological reactions that, in turn, changes the temperature of the medium. These biosensors are generally constructed by combining immobilized enzyme molecules with temperature sensors. When the analyte comes in contact with the enzyme, the exothermic or endothermic reaction that results can be measured and calibrated against the analyte concentration. The measurement of the temperature is typically accomplished via a thermistor.

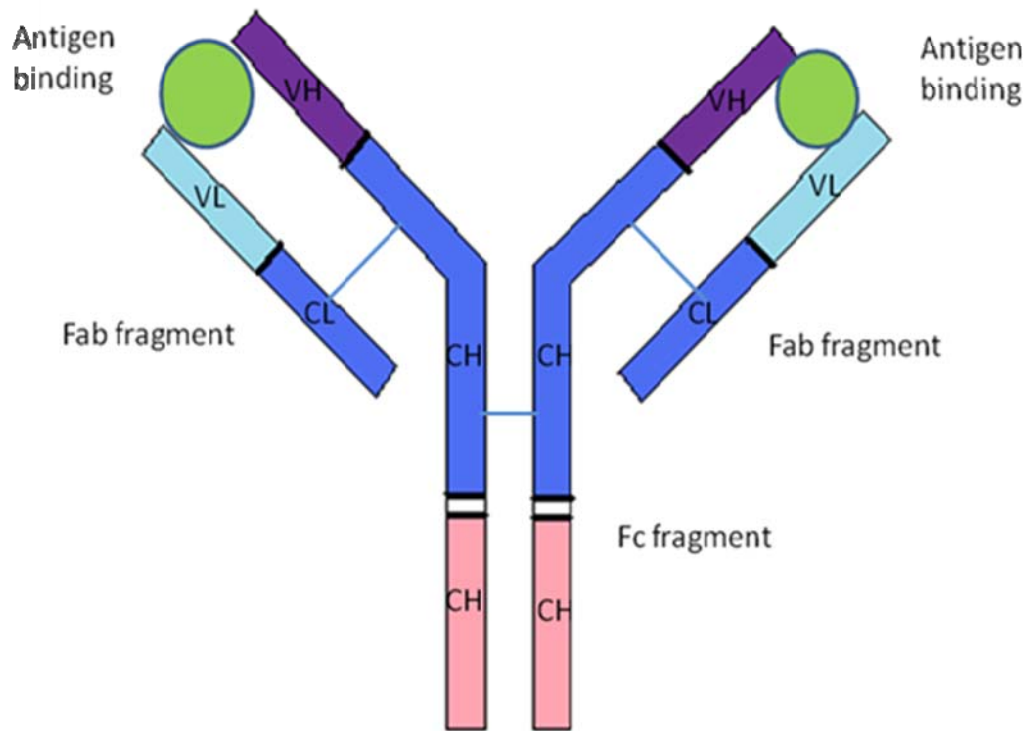
1.2 Electrochemical Immunosensors

Immunosensors are biosensors that detect the binding of an antigen to its specific antibody by coupling the immunochemical reaction to the surface of a transducer²⁶. The

first application of immunosensors was reported in 1970, when Centeno and Johnson developed antibodies that selectively bound malathion²⁷. A few years later, radioimmunoassays were developed for aldrin and dieldrin²⁸ and for parathion²⁹. In 1972, Engvall and Perlman introduced the use of enzymes as labels for immunoassays, naming the new technique Enzyme-Linked ImmunoSorbent Assay, or ELISA³⁰.

Antibodies, which are also referred to as immunoglobulins, are proteins that are produced by the immune system to defend the organism against foreign species. All antibodies have a basic structure that includes an identical pairs of heavy chain polypeptides and light chain polypeptides. These two sets of polypeptides chains are held together by disulfide bridges and form a “Y” shape (Figure 1.2). The amino acid sequence in the tips of the "Y" varies greatly among different antibodies and is thus referred to as the variable region. The constant region, which makes up the bulk of the antibody, determines the mechanism used to destroy the antigen. Each of the heavy chains is encoded for by a variable region (VH) and a constant region (CH); similarly each of the light chains is encoded for by VL and CL segments.

Alternatively, the antibody can be divided into three fragments, with two identical *Fab* fragments hinged to an *Fc* fragment (Figure 1.2). The variable region of the *Fab* fragments provides a binding site for the specific antigen, and there are two binding sites per antibody. The *Fc* fragment of the antibody does not combine with the antigen but contains carboxy terminal amino acids, which allows it to link to solid substrates such as the transducer surface.



Heavy chain and light chain are interconnected by disulfide bridge

Figure 1.2 The structure of an antibody

Immunosensors are based on the principles of solid-phase immunoassays, with either an antibody or antigen immobilized on the sensor surface. To obtain an efficient sensing device, the antibody must first be immobilized on the solid phase. The immobilization technique requires that: a) the biological activity must not be affected by attachment to the sensor surface; b) the immunoagent film must retain its structure and function; c) the bioreceptor must remain tightly associated with the sensor surface; and d) the sensor film should have long-term stability and durability.

There are several commonly used immobilization methods. First, the antibody or antigen can be immobilized on the substrate by physical adsorption. Physical adsorption can involve van der Waals forces, ionic binding or hydrophobic forces. Catts et al. successfully immobilized protein to various solid substrates, including derivatized glass, plastics and silicone rubber by adsorption³¹. The main advantage of physical adsorption onto solid surfaces is that it is a simple method that can be performed under mild conditions. Immunoagents adsorbed on solid surfaces through adsorption exhibit a certain degree of reversibility and generally the forces involved in the binding are not very strong; however, irregular distributions of randomly oriented proteins are commonly observed on the surface^{32, 33}. Physical adsorption produces non-specific interactions between the surface and protein, which may lead to deactivation due to the deformation of protein molecules on the surface³⁴.

Secondly, the protein can be entrapped within a membrane, surfactant matrix, polymer or microcapsule. The procedure of entrapping biological components in polymer

gels, membranes or surfactant matrices has been used with success in the past. For example, protein entrapment can occur by photo- or irradiation-polymerization of a solution containing the acrylate monomers³⁵. The entrapment of proteins in thin surfactant films fabricated by Langmuir-Blodgett deposition is also common³⁶. The entrapment of protein has the significant drawback of leakage of the biological species during use, however, resulting in a loss of activity.

Another approach often used to attach proteins to sensor surfaces is covalent binding, where biomolecules have been immobilized on solid surfaces through the formation of defined linkages^{13,14}. Covalent binding is a widely favored method as it generally results in minimal loss of biomolecular activity. It has been employed to improve the uniformity, density and distribution of the bound proteins, as well as the reproducibility of the surfaces. By forming covalent bonds, proteins can be strongly immobilized on the surface and therefore are not easily detached from the surface during use. Also, as part of the structure of the immunoagent, a wide variety of functional groups is available for covalent immobilization so that the active site of the binding can be avoided.

Many different formats for immunoassays³⁷ have been described and four of the most commonly used are shown in Figure 1.3. In a direct assay, the antigen is incubated with excess amounts of an immobilized antibody and the interaction detected. The measured signal is directly proportional to the amount of antigen present. In competitive assay formats, the detection of the target is based on the competition between an analyte derivative and the analyte in the sample for a limited number of antibody binding sites. In

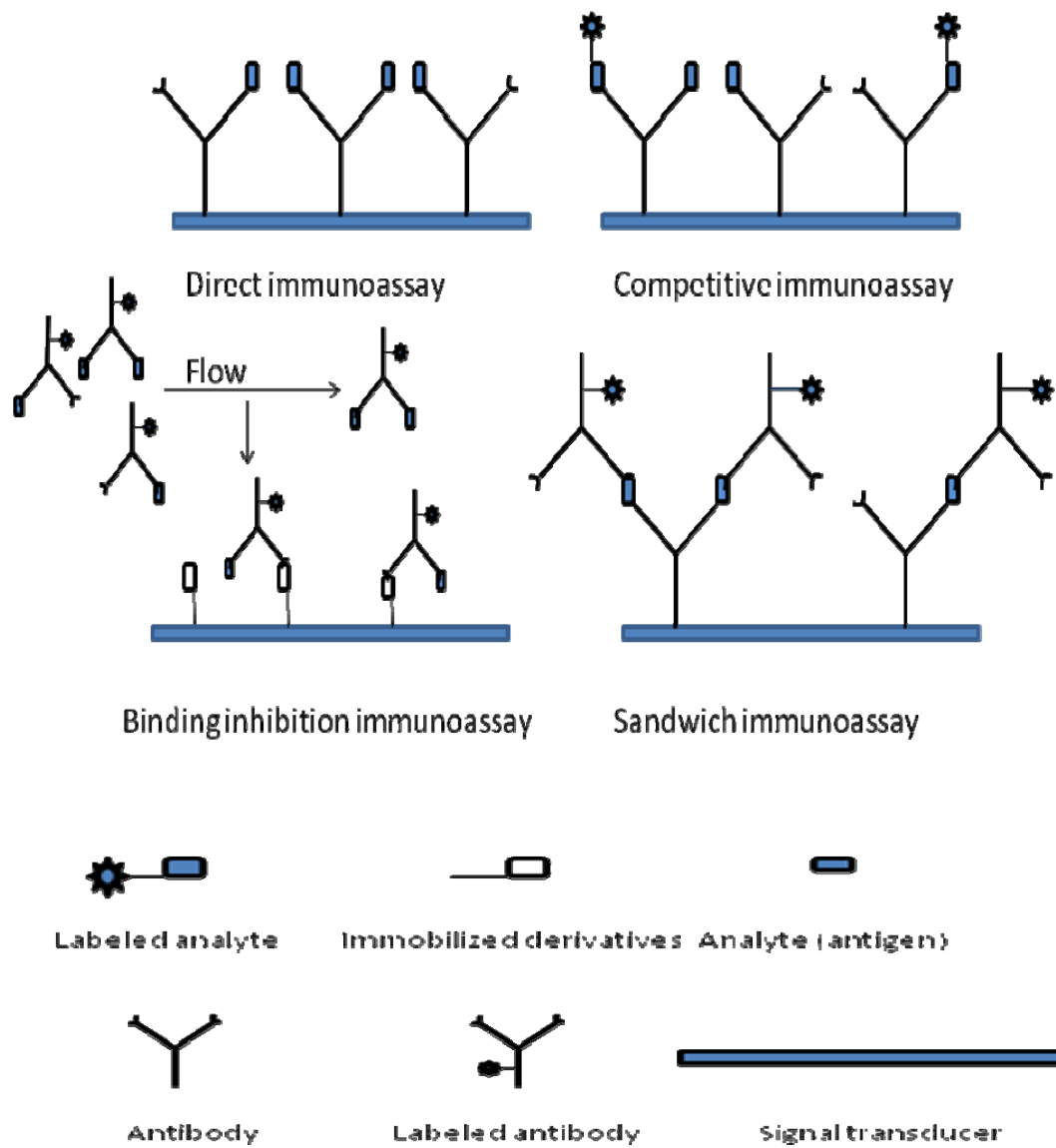


Figure 1.3. The different formats of immunoassays generally used in immunosensors

(Ref 37)

binding inhibition assays, the antibody and the analyte are first pre-incubated and, after equilibration, the solution is placed in contact with the immobilized antigen. Only the non-inhibited antibodies (unbound) will bind to the transducer and generate a detectable signal. As for the sandwich assay format, the antigens are incubated with an excess of a primary antibody and the resulting antigen-antibody complex is incubated with a second labeled antibody, which binds to a second antigenic site. The amount of labeled antibody bound is related to the analyte concentration.

Electrochemical immunosensors determine the level of analyte by detecting changes in the potential³⁸⁻⁴¹, current⁴²⁻⁴⁵, capacitance⁴⁶, conductance⁴⁷, or impedance^{48, 49} caused by the immunoreaction. Electrochemical detection of the interaction between antibody and antigen can be performed both with and without labeling.

For electrochemical detection, several processes have been investigated that detect antibody and antigen interaction directly, for example potentiometric and impedimetric methods^{50, 51}. However, due to the highly ionic and electrically noisy environment in which such interactions take place, many of these methods are unreliable. One frequently used format is an amperometric immunosensor, where proteins are labeled with enzymes that produce an electroactive product from an added substrate. Electrochemical detection of the labels offers several advantages, including high sensitivity and the low cost of the resulting sensors and instrumentation. The first amperometric immunosensor for tumor markers was reported in 1979⁵², where a competitive immunoassay was used for the determination of hCG. Monoclonal anti-hCG was immobilized on an amperometric

Table 1.1. Examples of enzymes used in electrochemical immunoassays

Enzyme	Substrate	Detected compound	Reference
<i>Alkaline phosphatase</i>	<i>p</i> -Aminophenyl phosphate	<i>p</i> -Aminophenol	53, 54
	3-Indoxyl phosphate	Indigo Blue	55, 56
	<i>p</i> -Cyanophenyl phosphate	<i>p</i> -Cyanophenol	57
	1-Naphthyl phosphate	1-Naphthol	58, 59
	Ascorbic acid 2-phosphate	Ascorbic acid	60
Peroxidase	H ₂ O ₂ + iodide	Iodine	61
	H ₂ O ₂ + hydroquinone	Benzoquinone	62
Glucose-6-phosphate dehydrogenase	Glucose-6-phosphate + NAD ⁺	Gluconate-6-phosphate + NADH	63
Catalase	H ₂ O ₂	O ₂	64
Lactase	O ₂ + hydroquinone	O ₂	65
Cholinesterase	Butyrylthiocholine iodide	Thiocholine	66
		Mercury mercaptide	67
Galactosidase	<i>p</i> -aminophenyl-β-D-galactopyranoside	<i>p</i> -Aminophenol	68
Glucose oxidase	Glucose + ferrocene	O ₂	69
Urease	Urea	NH ₄ ⁺ +CO ₂	38
β-Lactamase	Benzyl penicillin	H ⁺	70

oxygen electrode and catalase-labeled-hCG and hCG in the sample competed for binding sites in anti-hCG immobilized on the electrode surface. After removing nonspecifically bound hCG, the sensor was then reacted with the substrates. The membrane-bound catalase generated oxygen that was sensed by the oxygen electrode.

For an electrochemical immunoassay, a labeled enzyme has the following requirements: 1) electrochemically active products must be produced by the enzyme; 2) the enzyme must have a high catalysis coefficient; 3) the enzyme and enzyme substrates must be stable in buffer solution; and 4) there must be as few by-products as possible in the enzyme reaction. Several commonly used enzymes are listed in Table 1.1.

Alkaline phosphatase is one of the most commonly used enzyme labels in electrochemical immunoassay⁵⁴⁻⁵⁹. Various organic phosphates can be dephosphorylated to remove phosphate under catalysis with alkaline phosphatase, and the reaction product can be easily monitored by electrochemical detectors. Alkaline phosphatase and its conjugates are highly stable; the only disadvantage of this enzyme is that it is rather expensive. 4-aminophenyl phosphate is the most frequently used substrate and the concentration of *p*-aminophenol produced in catalytic reaction can be determined at a nanomolar level⁵³ or even below⁵⁴ by the oxidation current.

Xu et al.⁷¹ reported the detection of antigen mouse IgG using a sandwich electrochemical enzyme immunoassay with flow injection analysis. After incubating in *p*-aminophenyl phosphate solution for 30 minutes, mouse IgG attached on a glassy carbon working electrode was analyzed. The results revealed that alkaline phosphatase exhibited

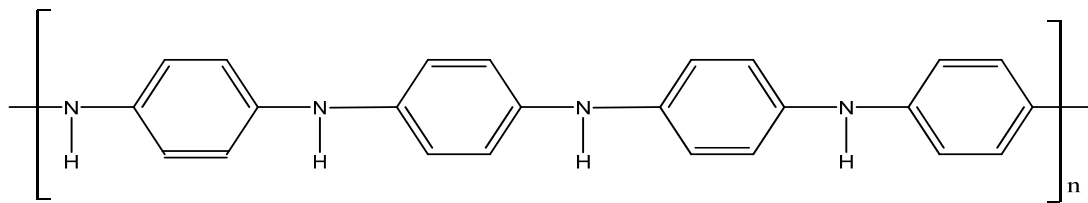
the best activity and smallest base line signal due to *p*-aminophenyl phosphate non-enzymatic hydrolysis in tris buffer solution.

1.3 Introduction to Polyaniline (PANI)

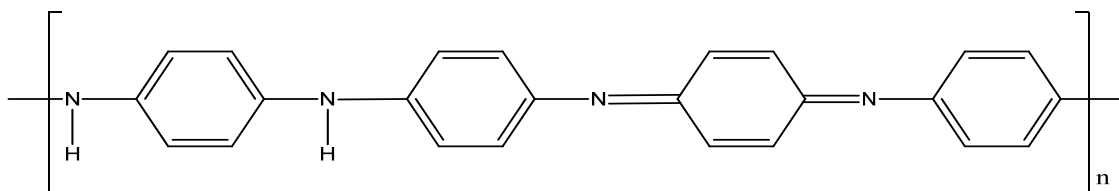
In the last thirty years, organic conducting polymers (CP) obtained by electropolymerization or chemical oxidation have been extensively studied for various technological applications. Due to their unique optical properties, their electrochemical reversibility, their stability in both air and aqueous medium and their market potential, polyanilines have been the focus of a great deal of research in the field of conducting polymers in recent years.

The first reports on polyaniline date back to 1862⁷², and its four oxidation states were discovered at the beginning of the 20th century⁷³. PANI consists of phenyl rings in the benzenoid and quinoid form, and nitrogen heteroatoms in either amine (–NH–) or imine (–N=) form (Figure 1. 4). The four oxidation states of polyaniline are both pH and potential dependent. Polyaniline can take a fully reduced form (leucoemeraldine), which is composed of benzenoid rings throughout, a half oxidized form (emeraldine base), where it is 25% quinoid rings, and a fully oxidized form (pernigraniline), where it is 50% quinoid rings. All are insulators except for the emeraldine salt form, protonated from the half oxidized emeraldine form, which conducts electricity.

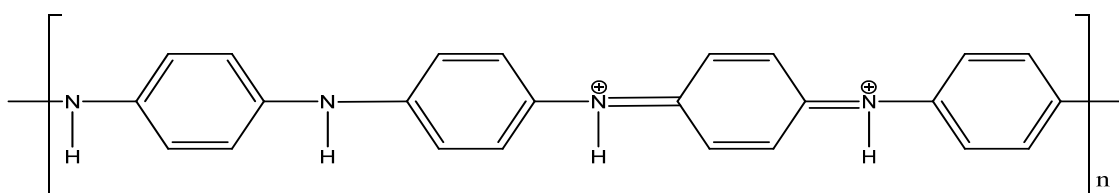
Polyaniline (PANI) was selected for use as the substrate for this study and coupled with antibody rabbit and sheep IgG to construct the biosensor used for the electroimmunoassay reported here.



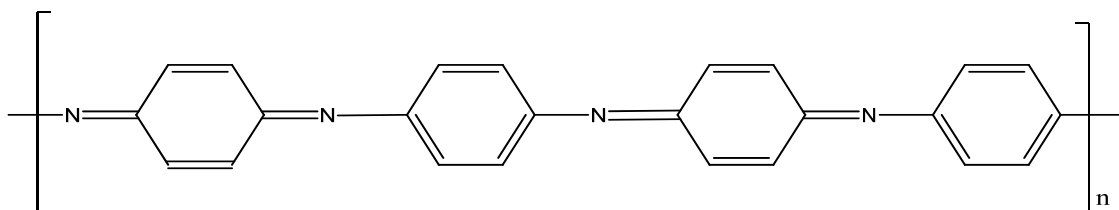
Leucoemeraldine



Emeraldine base



Emeraldine salt



Pernigraniline

Figure 1.4 Structure of polyaniline (Ref. 72, 73)

PANI can be prepared chemically or electrochemically by oxidative polymerization. Chemical synthesis produces powdered polyaniline, while electrochemical synthesis can be used to generate thin films on a conductive substrate. The electrochemical polymerization of aniline consists of several stages. The first step is the oxidation of the monomer to form cation radicals^{74, 75} (Figure 1.5), which is followed by dimerization due to the association of radical ions^{74, 75}. At the potential required to oxidize the monomer, the dimer or higher oligomer is also oxidized and thus reacts further with the radical cation of the monomer to build up the aniline chain.

The electro-oxidative polymerization method is preferentially used for the preparation of PANI films because the deposition of the films can easily be controlled by electrochemical techniques. There are two electrochemical methods used to synthesize polyaniline, namely cyclic voltammetry and direct current potential amperometry, where a constant potential is applied on a working electrode. The morphology of electrochemically prepared PANI depends strongly on the experimental conditions. The growth rate of a PANI film depends on the type of supporting electrolyte, in the order: $\text{H}_2\text{SO}_4 > \text{HCl} > \text{HNO}_3 > \text{HClO}_4$ ⁷⁶. As shown in Figure 1.5, in the electrochemical oxidation of PANI, associated anions, or counter ions, are also involved in the oxidation since oxidation generates both a positively charged PANI cation and a corresponding anion. Redox reactions in polyaniline introduce charges into the polymer material, and in order to maintain electroneutrality, counter ions must be incorporated. Both the ionic

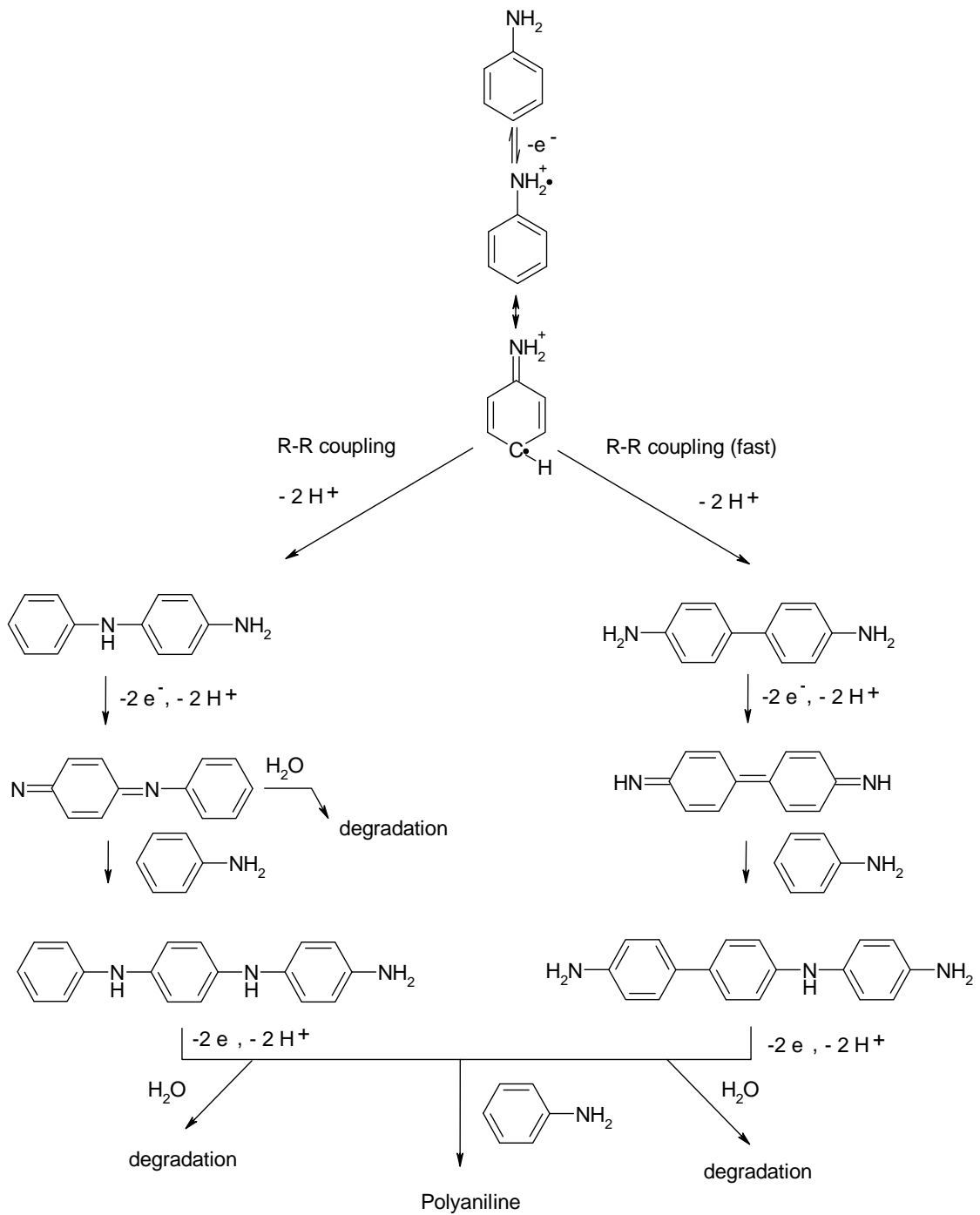


Figure 1.5 Polyaniline synthesis mechanism (Refs 74, 75)

species and the solvent molecules are transported into and out of the film during redox reactions.

The aniline oxidation reaction is pH dependent. In $\text{pH} < 2$ solution, protonated aniline species participate in the reaction, and the oxidation is accompanied by the loss of protons.

During synthesis of polyaniline, PANI may be overoxidized, which results in the degradation of the product when the potential is too positive. Kobayashi⁷⁷ and Hand⁷⁸ pointed out that the final degradation products consist of p-benzoquinone, hydroquinone, p-aminophenol, quinoneimine, and still-oxidized PANI.

The quinonimine units present in PANI may be attacked by nucleophiles such as amine or thiol groups in the compound, on the ring and polyaniline backbone, and thus reduced from the emeraldine state to the leucoemeraldine state. The nucleophiles generally used are shown in Figure 1.6^{79, 80}. Nucleophilic addition of amines and thiols to quinonimine rings has been proposed as a powerful method for polyaniline post-modification⁸¹⁻⁸⁴.

A possible reaction mechanism is shown in Figure 1.7^{79, 80}. Protonation of the imine nitrogen could potentially improve the nucleophilic attack of thiols or other nucleophiles to the protonated quinoid ring. It has been reported that the pernigraniline state is more reactive than emeraldine, while leucoemeraldine is not reactive^{85, 86}. The higher amount of quinonimine units in pernigraniline (100 %) results in greater activity than in emeraldine (50%). This is of particular interest for this study because there are a number of nucleophilic groups, for example amine groups and sulfhydryl groups, in antibody

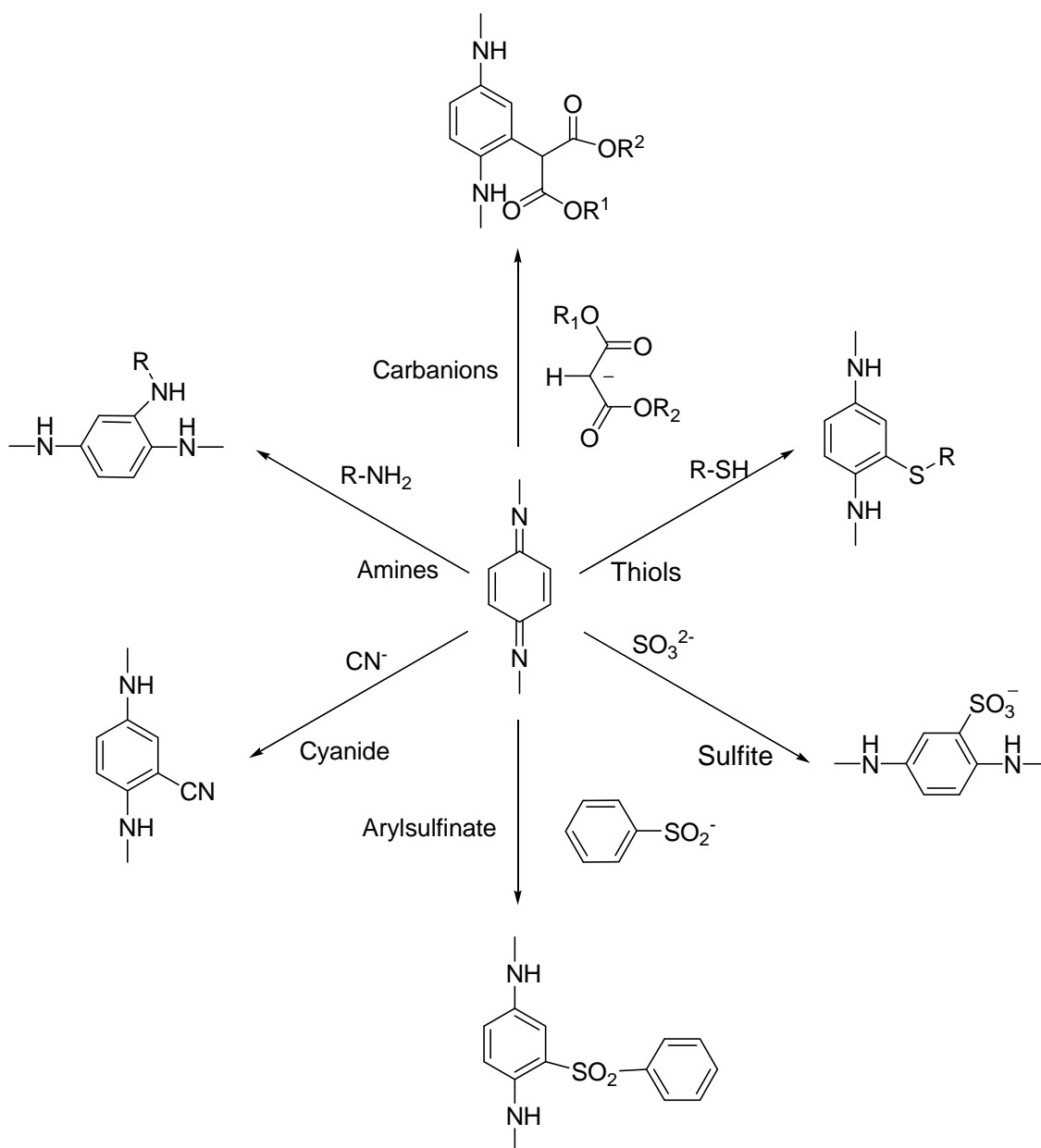


Figure 1.6 Reaction pathways of nucleophilic addition to polyaniline. (Ref. 78,79)

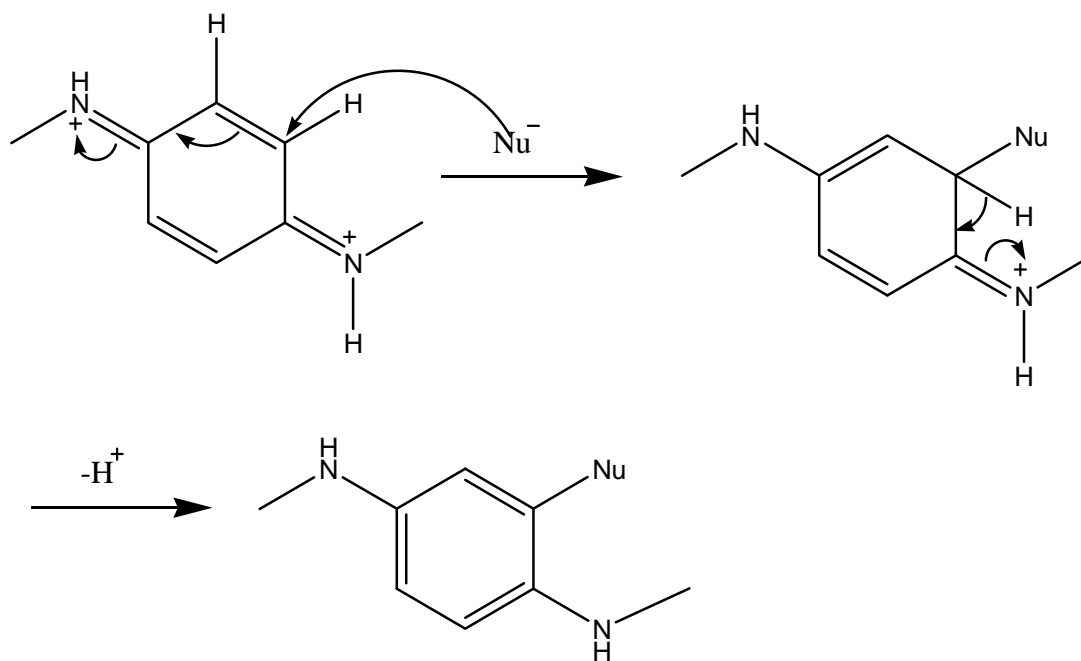


Fig 1.7 Mechanism of nucleophilic addition (Ref. 78, 79)

structures. Based on the information presented in this section, therefore, in this research the polyaniline film used as the substrate was formed by electrochemical deposition synthesis and anti-rabbit or goat IgG was immobilized on the PANI film by nucleophilic reaction to produce the electrochemical immunosensor. The properties of the new sensor will be discussed in more detail in the next chapter.

1.4. Nanoparticles in biotechnology

Nanoparticles are small clusters of atoms about 1 to 100 nanometers in size. Although in the natural world there are many examples of structures that exist with nanometer dimensions, including essential molecules within the human body, for example, Virus, and components of foods, it has only been possible to develop molecules and structures within this size range in the laboratory in the last quarter of a century.

The electronic and optical properties and chemical reactivity of nanopartilces are completely different from those of bulk materials. There are two factors that lead to the major property changes that result from this transition from bulk solids to nanoparticles, namely the huge increase in the ratio of surface area to volume and fact that the small size of the particles places them in the realm where quantum mechanics determines their behavior. The ratio of surface area to volume gradually increases as the particle size decreases; a high ratio is a critical factor governing the performance of catalysis and structures such as electrodes in fuel cell and batteries. Also, once particles become sufficiently small, they begin to exhibit quantum mechanical behavior, and therefore acquire unique electronic and optical properties.

There are two methods generally used to produce nanoparticles. The top-down approach starts with a bulk material, and then breaks it into smaller pieces using mechanical, chemical or other forms of energy, while the bottom-up approach synthesises the material from atomic or molecular species via chemical reactions, allowing the precursor particles to grow in size. Top-down processes do not easily allow the large-scale production of parts that are significantly smaller than 100 nanometers. Current nanotechnology research therefore places greater emphasis on the development of bottom-up strategies, especially in coupling and functionalizing nanoparticles with biomaterials. Usually, “wet chemistry” procedures are used to prepare nanoparticles in bio-applications. In these procedures, capping agents (often citrates, phosphanes, or thiols) are applied as stabilizers to the atoms exposed at the surface of the nanoparticles to prevent uncontrolled growth and aggregation of the nanoparticles.

The application of small particles in diagnostics, particularly in medications and for cell targeting, has been the focus of research for decades. One of the earliest examples of applying nanotechnology to solving problems in biology was the use of liposomes as drug delivery vehicles⁹⁰. The unique electronic, optical, and catalytic properties of nanoparticles, along with the wide variety of synthetic methods that can be used to control particle shape or/and size, offer great promise for the development of revolutionary new nanoscale assemblies, structures, and devices.

Nanoparticles are similar in size to large biological macromolecules, which are typically in the range of about 5 to 200 nm. Modification of nanoparticles to be capable

of targeting specific cells, delivering drugs with pinpoint accuracy, imaging biomolecular processes, sensing molecular responses to therapeutic agents, and guiding surgical procedures have all been accomplished in the last twenty years. For example, nanoparticles smaller than 20 nm have been used to travel through blood vessel walls and penetrate the blood-brain barrier or the stomach epithelium⁸⁷⁻⁹¹, barriers that normally make it difficult for therapeutic and imaging agents to reach their intended targets. In drug delivery applications, nanoparticles must be small enough to avoid rapid filtration by the spleen, which is composed of filaments spaced at roughly 200 nm⁹² that serve as a meshwork for phagocytotic cells⁹³. In order to successfully traverse the liver, particles must be small enough to pass through the organ's 150–200 nm fenestra⁹⁴.

The size of nanoscale devices also allows them to interact readily with biomolecules on the cell surface and within the cell, often in ways that do not change the behavior and biochemical properties of those molecules. Nanoparticles usually form the core of nano-biomaterials that can then be functionalized with biomolecules. The biomolecules can be coupled with nanoparticles stabilized by anionic ligands such as citrate or lipoic acid. Cells, proteins and enzymes with positive charges may preserve their native structures and activities when they are directly adsorbed on anionic stabilized nanoparticles through electrostatic interactions. However, as in the case of immobilization on a biosensor surface, biomolecules that are physically adsorbed onto nanoparticles can be readily lost from the surface, and adsorbed proteins are often prone to denaturation, thereby losing their biocatalytic or biorecognition activities. Some

proteins and enzymes that were directly adsorbed on nanoparticles showed conformational changes and loss of biological activity⁹⁵. However, by covalently attaching biomolecules to nanoparticle surfaces, problems of instability and inactivation can be overcome. The covalent bond is usually applied in the form of a coating of colloidal gold with thiol-containing biomolecules, which have cysteine residues. If no thiol residues are available in the native proteins, thiol groups can be produced chemically (e.g. with Traut's reagent, 2- iminothiolane)⁹¹ or by genetic engineering. Traut's reagent is a water soluble reagent that reacts with primary amines at pH 7-10 to introduce sulfhydryl groups spontaneously and efficiently⁹⁶. Thiolation of protein primary amines with Traut's reagent is generally complete in less than 1 hour.

Another approach to covalent bonding is based on biomolecules that contain terminal carboxy, amino, or maleimide groups. These can be used for the coupling of biological components by means of carbodiimide-mediated esterification and amidation^{97, 98}.

The biotin and streptavidin couple is an ideal model for bioconjugate nanoparticles with biomaterials because of its high binding affinity and high specificity^{99, 100}. Each streptavidin has four binding sites for biotin, positioned in pairs on opposite domains of the protein molecule. Nanoparticle-protein binding occurs between the amine residues on the nanoparticle surface and the carbodiimide-activated carboxylic group of streptavidin.

Biological macromolecules and their derived supramolecular complexes can be used in the synthesis and assembly of nanoparticles and biomaterials conjugate for cell targeting, drug delivery and cancer treatment. Researchers have demonstrated large scale

covalent network assembly of quantum dots (QDs) and carbon nanotubes (CNTs) with CPMV and mutant FHV hybrid systems^{101, 102}.

Regular two-dimensional lattices of bacterial cell surface proteins, nano- and micrometer-sized nucleic acid components, as well as hollow biomolecular compartments such as virus particles, have already been exploited for the generation of nanoparticle bioconjugates. Virus particles typically consist of several hundred to several thousands of protein molecules that assemble in the form of a hollow compartment that holds the viral nucleic acid. Viruses have long been suggested as nanoparticle vectors for drug delivery, vaccines, and gene therapy¹⁰³. Figure 1.8 shows some examples of viruses developed to work in conjunction with gold nanoparticles, carbon nanotubes and quantum dots for nanotechnology applications including cell targeting, vaccines, imaging and thermal treatments¹⁰². Linking nanoparticles with known molecular signatures of human cancer could provide innovative solutions to early cancer detection, *in vivo* tumor imaging, personalized diagnostics, and targeted therapeutics. A variety of nanoscale particles have already been applied for imaging tumors and the tumor microenvironment in animal models and human clinical trials. It has been reported¹⁰⁴ that NIR imaging of targeted gold-coated nanoparticles containing a dielectric silicon core shows promise for detecting an individual cancer's molecular environment. By changing the thickness of the coating and the dielectric core's diameter, it is possible to tune the particle's optical absorption and scattering spectra from the localized area to focus specifically on the tumor tissue. Increasing the power of the NIR beam for 4 min increased the particle's temperature by

an average of 37.4°C, leading to irreversible heat induced damage in the carcinoma cells. A bacteriophage is a type of virus that infects bacteria. Souza reports the creation of an assembly composed of fd bacteriophage and gold particles that has the potential to seek out and treat disease in situ in the human body^{105, 106}. Building on these reports, the research conducted for this dissertation examined a filament bacteriophage with gold nanoparticles covalently bonded using Traut's Reagent.

1.5. Bacteriophages

Although the therapeutic nature of bacteriophages in treating infectious disease was discovered by Felix d'Herelle in 1917¹⁰⁷, their use was greatly facilitated by the development of the phage display technique, first reported for the *Escherichia coli* specific bacteriophage M13 in 1985 by Smith¹⁰⁸. Phage display allows researchers to select peptides and proteins with binding affinity similar or higher than monoclonal antibodies, making it possible to generate antibody-like molecules that bind specifically to target molecules, i.e. antigens, without involving the immune system of an animal. Compared to the production of monoclonal antibodies, large quantities of high affinity peptides can now be produced inexpensively in much less time using the filamentous bacteriophage display technique. The bacteriophage library, one of the best-known protein library methods, is a powerful technology for selecting and engineering polypeptides with novel functions.

Although different bacteriophages may contain different materials, all bacteriophages use DNA or RNA as their genetic material and all are covered with a coating of protein.

By far, the most popular phage that has been used for antibody display is the filamentous bacteriophage. Filamentous phages are highly stable in harsh conditions such as high salt concentration and acidic pH. They have a fixed diameter of about 6.5 nm, and their length is determined by the size of their genome. For example, fd phage particles have a long cylindrical protein capsid that is 930 nm in length. These proteins enclose a single-stranded DNA genome of about 6400 nucleotides, consisting of 11 genes. In contrast, a 221-nucleotide microphage variant is only 50 nm long¹⁰⁹.

Filamentous phage particles are coated with five proteins, pIII, pVI, pVII, pVIII and pIX^{110, 111} (Figure 1.8). The hollow tube that surrounds ssDNA is composed of several thousand copies of the 50-amino acid protein, pVIII, which overlaps like fish scales to form a right-handed helix. The filament is held together by the interactions between the hydrophobic midsections of adjacent subunits. Because the amino end of pVIII protrudes towards the outside of the capsid, it can be modified to express a different peptide. The length of the peptides displayed by pVIII is limited to five to six amino acids unless intact molecules of pVIII are also present on the surface of the phage. Longer peptides interfere with phage propagation.

There are 3-5 copies of each of pVII and pIX in the blunt end of the phage. These two small hydrophobic peptides, with masses of 33 and 32 kDa, respectively, play an important role in the early stages of phage assembly, where they serve as a nucleus for the subsequent deposition of pVIII. Endeman et al. have shown some evidence to indicate

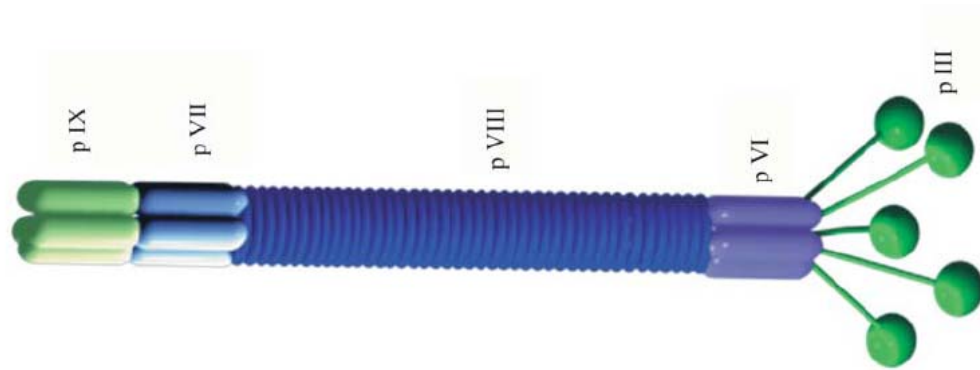


Figure 1.8 Structure of a typical bacteriophage. pIII, pVI, pVII, pVIII and pXIX represent phage proteins (A) (Ref. 110)

that at least some of the pIX is exposed¹¹² and Gao et al. also proved that antibody variable regions can be displayed on the amino termini of pVII and pIX¹¹³.

The pointed end of the particle contains about five copies each of pIII and pVI. pVI is degraded in cells which lack pIII, suggesting that these proteins may assemble in the cell membrane before being incorporated into phage particles¹¹⁴. A pIII protein is expressed at the end of a virus, with usually 3-5 proteins of 406 amino acids being produced. Relatively large proteins can be expressed, enabling it to be used for the production of whole protein or antibody molecule libraries. Smith was the first to demonstrate that the amino terminus of pIII, which protrudes away from the phage surface, can tolerate insertions of foreign polypeptides¹⁰⁸. Most of the currently used phage display vectors use the N-terminus of pIII protein to display the foreign peptide or protein.

Because the pIII , pVIII and pIX proteins on the phage can be easily genetically engineered to display ligand peptides that will specifically bind to target cells in selected tissues, filamentous phages show promise for application in biosensors, cell targeting and drug delivery. For example, the filamentous phage M13 has been used as a virus-NPs network for tissue-specific targeting. Vascular-targeted phages displaying binding peptides and a biotin tag were introduced *in vivo*, followed by detection with streptavidin-conjugated quantum dots¹¹⁵. The targeted phage was able to specifically guide the QDs to the tumor, indicating that M13-based nanoparticles may be useful for future *in vivo* use.

Based on reports by Souza et al. that Au-phage networks can target specific cells, in this research gold nanoparticles were used as signal reporters for fluorescence and dark-field microscopy and near-infrared (NIR), surface-enhanced Raman scattering (SERS) spectroscopy¹¹⁶.

1.6. Surface Enhanced Raman Spectrometry-principle and application in biospecies detection

Raman spectroscopy is a well-established technique that provides information on the vibrational frequencies of molecules. In conventional Raman spectroscopy, incident light is considered as an electromagnetic wave that induces polarization in a target molecule. The induced dipole then emits or scatters light at the optical frequency of the incident light wave, with the wavelength shifted slightly due to transitions between molecular vibration levels.

Raman spectroscopy is increasingly used in materials characterization, biochemistry and even art conservation. However, conventional Raman spectroscopy suffers from low signal strength and is ineffective for surface studies because the photons of the incident laser light simply propagate through the bulk, generating a signal that overwhelms any signal from the analytes on the surface.

Surface enhanced Raman scattering (SERS) was accidentally discovered while attempting to examine an electrode using Raman spectroscopy in 1974. SERS provides greatly enhanced Raman signals from Raman-active analyte molecules that have been adsorbed onto certain specially prepared metal surfaces. The importance of SERS is that

its surface selectivity and sensitivity extends the utility of Raman spectroscopy to a wide variety of interfacial systems that had previously been inaccessible to conventional Raman spectroscopy due to their lack of surface sensitivity. SERs allows Raman spectroscopy to be applied to molecules located on very small (nanoscale) metallic objects. It has been reported that increases in the intensity of the Raman signal on the order of 10^4 - 10^6 have been regularly observed, rising as high as 10^8 or 10^{14} in certain special systems^{117, 118}.

The mechanism underlying this large enhancement in Raman signal for SERs is not yet fully understood and controlled, but it is generally agreed that there are two primary mechanisms involved: an electromagnetic and a chemical enhancement. Of these, the electromagnetic effect is the primary contributor to the SERS effect. Electromagnetic enhancement (EME) depends on the roughness of the metal surface and arises due to the significantly amplified electromagnetic fields (E) generated by the localized surface plasmon resonance (LSPR) of nanoscale metal surface roughness features.

Electromagnetic enhancement should be a nonselective enhancement for Raman scattering by all the molecules adsorbed on a particular surface. However, there is evidence to suggest that there is a second enhancement mechanism that operates independently of the electromagnetic mechanism and is related to the type of analyte present^{119, 120}.

Chemical enhancement (CE) involves changes to the adsorbate electronic states due to chemisorption of the analyte¹²¹. This enhancement provides an order or two of

magnitude enhancement to the Raman signal intensity. Because electromagnetic enhancement is the dominant contributor to SERS and there are a large variety of substrate materials and geometries available, optimizing the electromagnetic enhancement provides the most convenient and effective way to improve SERS in a typical empirical setting.

SERS is usually performed on Ag¹²², Au¹²³ or Cu¹²⁴ surfaces because these metals have appropriate values of the dielectric constant¹²⁵ and can be easily handled in ambient, electrochemical and ultra-high vacuum environments. Commonly used substrates in surface enhanced Raman spectroscopy include colloids in sol-gel¹²⁶, electrochemically roughened electrodes^{122, 127}, vapor-deposited metal island films¹²⁸ and lithography-produced nanostructures¹²⁹.

Any electromagnetic field decreases in strength with distance from the point source. According to theoretical calculations, the SERS enhancement, G, has been found to scale with distance according to

$$G=[r/(r+d)]^{12}$$

where r is the radius of the spherical metal roughness feature and d is the distance of the analyte to that feature. Experimentally, the enhancement decreases ten-fold with a distance of 2-3 nm^{121, 130, 131}.

In 1980, Cotton and Van Duyne demonstrated that it was possible to study very small quantities of biological materials using SERS¹³². SERS has since been successfully used for the characterization and detection of individual nucleosides, oligonucleotides and

nucleic acids at physiologically relevant concentrations¹³³⁻¹³⁷. Graham et al. have been able to use modified DNA and novel aggregating agents for silver colloids to detect DNA down to concentrations of $8 \times 10^{-13} \text{ M}$ ¹³⁸.

SERS has also been used in immunosensor development. For example, Raman dyes have been used to label antibodies that are attached to gold nanoparticle probes. Desiree et al.¹³⁹ have reported using SERS in a sandwich-immunoassay format to detect prostate-specific antigen (PSA), the best serum marker currently available for the detection of prostate cancer and the forensic marker of choice for determining the presence of azoospermic semen in some sexual assault cases, down to levels of 1 pg/ml of antigen. SERS has also been used for *in vivo* tumor targeting and spectroscopic detection by Nie et al.¹⁴⁰, where gold nano-particles were used to conjugate to tumor-targeting ligands such as single-chain variable fragment (ScFv) antibodies to target tumor biomarkers. SERS, combined with nanotechnology, clearly has a promising future in biomedicine, diagnosis, cell targeting and cancer treatment applications.

1.7. Polyoxometalates for Electrochemical catalysis

Polyoxometalates (POMs) are a class of inorganic compounds that have fascinated chemists for almost two centuries. These inorganic complexes are negatively charged aggregates of transition metals (mainly molybdenum, tungsten and vanadium) with oxygen and their chemical properties can be controlled by transition metal substitution and the counteranion used. They are typically composed of metal ions in their highest oxidation state bridged by oxo-ligands (O^{2-}). Almost any other element can be

incorporated into the POM framework, leading to a huge array of possible structures and properties¹⁴¹⁻¹⁴⁴.

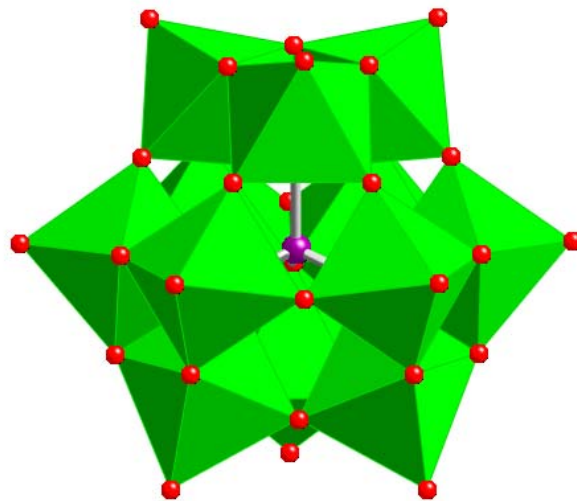
POMs have been widely applied in many fields, including catalysis, medicine, magnetic properties, materials, surface chemistry. Polyoxometalates offer several advantages as catalysts. First, POMs are easily synthesized and a variety of compounds can be made available. Second, they are very stable. Since negatively charged oxygen atoms are polarized towards the positive metal atoms on the interior of the structure, the oxygen atoms are relatively inert, making POMs resistant to both acidic and basic decomposition. Third, POMs can be made soluble in water or organic solvents by changing their counterions¹⁴⁵. For example, tetrabutylammonium (TBA) can be used as the counterion for organic phase reactions, and Na⁺ or K⁺ for aqueous phase reactions. As POMs have a negative charge, they can be attached to a positively charged support medium, thus changing a homogeneous catalyst to a heterogeneous catalyst¹⁴⁶. In addition, the incorporation of transition metals provides a source of weakly attached electrons that can be transferred to other compounds. POMs are also known to be very good oxidation-reduction catalysts, since they are capable of absorbing and stabilizing electrons from substrates in oxidation reactions, thus lowering the energy state of reaction intermediates.

Much of the research on the catalytic properties of POMs has focused on the Keggin (XM₁₂O₄₀) and Wells–Dawson (X₂M₁₈O₆₂) structures (where M =W or Mo and X = a tetrahedral template), shown in Figure 1.9. In these structures a metal atom is located in

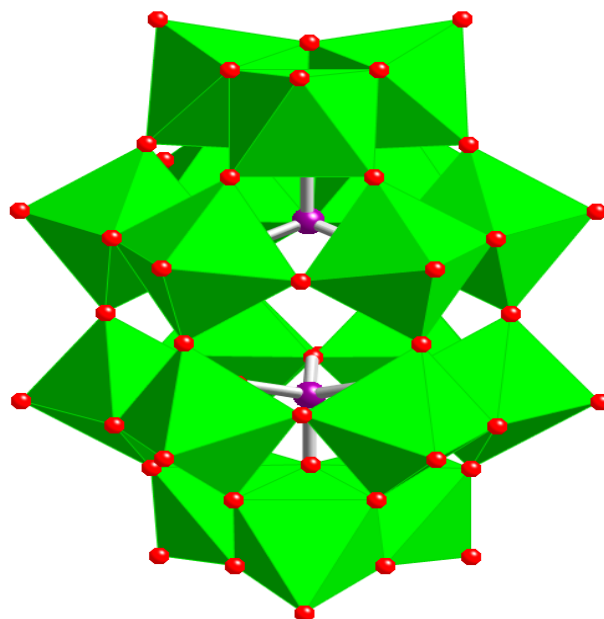
the center of the octahedron with an oxygen atom in each corner^{141, 147, 148}. The Keggin structure is roughly spherical and gives a general formula of XM_{12} , where X is the heteroatom and M is the d^0 metal. Each corner of the heteroatom tetrahedron is associated with an M_3O_{13} unit. The Wells–Dawson type structure is ellipsoidal, with a formula X_2M_{18} . This structure consists of two heteroatoms stacked one atop the other, and each end is composed of an M_3O_{13} cap, with two six-metal belts circling the molecule. The electrochemical properties of POMs have been intensively studied, as the ability of POMs anions to accept various numbers of electrons has made these compounds very attractive for electrode modification and electrocatalytic research. Immobilization of POMs on electrodes not only simplifies their electrochemical study but also facilitates their use in applications such as biosensors and electrocatalysis. Some promising results have been reported¹⁴⁹⁻¹⁵², and both Keggin- and Dawson-type heteropolyanions have been extensively applied as electrocatalysts.

In electrocatalytic reactions, POM can be used either homogeneously dissolved in the electrolyte solution or attached to the electrode surface. Generally three different methods can be applied to immobilize POM on the electrode surface. The first of these is to entrap POM in various conducting polymer films such as polyaniline¹⁵³⁻¹⁵⁵.

POM can also be attached onto the surface of electrodes through an electrodeposition method¹⁵⁶, but the easiest way to coat electrodes with a heteropolyanion monolayer is by simply soaking the electrode in an acidic aqueous heteropolyanion solution. It has been reported that $\text{PMo}_{12}\text{O}_{40}^{3-}$, $\text{P}_2\text{Mo}_{18}\text{O}_{62}^{6-}$, $\text{P}_2\text{W}_{18}\text{O}_{62}^{6-}$, $\text{SiW}_{11}\text{O}_{39}\text{Fe}^{\text{III}}(\text{H}_2\text{O})^{5-}$, and



a



b

Figure 1.9 Structure of polyoxometalate commonly used in catalysis (a: Keggin poly(3-methylthiophene)¹⁵⁷, and poly(pyrrole)/poly(*N*-methylpyrrole)¹⁵⁸⁻¹⁶⁰ structure; and b: Wells–Dawson structure) (Ref. 147, 148)

$\text{PW}_{11}\text{O}_{39}\text{Fe}^{\text{III}}(\text{H}_2\text{O})^{4-}$ were absorbed spontaneously on glassy carbon and edge pyrolytic graphite electrodes¹⁶¹. Faulkner's group¹⁶² immersed a negatively charged film in a solution containing large mono-, multi-, and polyvalent cations, which were coated onto the electrode due to electrostatic interaction. Subsequently, a layer of the heteropolyanions (POM) was coated onto the cation phase. Repeating this procedure allows three-dimensional multilayer molecular assemblies to be formed in a controlled way. This method is often referred to as the layer-by-layer (LBL) method. Electrostatic layer-by-layer (LBL) assembly was first proposed by Decher and coworkers in the early 1990s^{163, 164}. This film assembly approach offers a simple way to prepare nanoscale ultrathin films with defined composition and uniform thickness. With the LBL technique, a wide variety of materials may be employed and film fabrication is performed under mild conditions, which is particularly important for preserving the activity of biomolecules^{165, 166}.

POM have also been used for the catalysis of electroreduction reactions, such as the reduction of bromate¹⁶⁷, nitrite¹⁶⁸ and hydrogen peroxide^{162, 169, 170}. Molecular oxygen or H_2O_2 are often used as oxidizing agents because they are considered green reagents when used in conjunction with POMs. The detection of hydrogen peroxide generated by a range of enzymes (e.g., oxidase) is the essential component of many biosensors and a variety of electrocatalysts such as peroxidases and transition metals have been used for this purpose. For example, Matel et al. reported polyoxometalate to be an efficient electrocatalyst for hydrogen peroxide reduction by cyclic voltammetry¹⁵². Chapter 4 of

this dissertation reports the fabrication of multilayer ultrathin films by alternating deposition of protein and polyoxometalate based on electrostatic interaction as the driving force, along with a study of the catalysis of hydrogen peroxide reduction. This work was performed in collaboration with Dr. Kai Jiang, a member of Dr. Wei Zhan's group. I was responsible for conducting the image scanning required by the project.

References

1. Dong, S.; Chen, X., *Rev. Mol. Biotechnol.* **2002**, 82, 303.
2. Sharma, S. K.; Sehgal, N.; Kumar, A., *Curr. Appl. Phys.* **2003**, 3, 307.
3. Malhotra, B. D.; Chaubey, A., *Sens. Actuators B: Chem.* **2003**, 91, 117.
4. Thévenot, D. R.; Toth, K.; Durst, R. A.; Wilson, R. A., *Biosens. Bioelectron.* **2001**, 16, 121.
5. Clark, L. C.; Lyons, C., *Acad. Sci.* **1962**, 102, 29.
6. Vo-Dinh, T.; Cullum, B., *J. Anal. Chem.* **2000**, 366, 540.
7. Updike, S. J.; Hicks, G. P., *Nature* **1967**, 214, 986.
8. Gunasingham, H.; Teo, P. Y. T.; Lai, Y. H.; Tang, S. G., *Biosensors and Bioelectronics* **1989**, 4, 349.
9. Huang, J.; Hooijmans, C. M.; Briasco, C. A.; Geraats, S. G. M.; Luyben, K. C. A. M.; Thomas, D.; Barbotin, J. N.; 619, *Appl. Microbiol. Biotechnol.* **1990**, 33, 619.
10. Ngeh-Ngwainbi, J.; Foley, P. H.; Kuan, S. S.; Guilbault, G. G., *J. Am. Chem. Soc.* **1986**, 108, 5444.
11. Prusak-Sochaczewski, E.; Loung, J. H. T., *Anal. Lett.* **1990**, 23, 401.
12. Suleiman, A. A.; Guilbault, G. G., *Analyst (Cambridge UK)* **1994**, 119, 2279.
13. Lin, J. N.; Herron, J.; Brizgys, M., *IEEE Trans Biomed. Eng.* **1988**, 35, 466.
14. Peterman, J. H.; Tarcha, P. J.; Butler, J. E., *J. Immunol. Methods* **1988**, 111, 27.
15. Muramatsu, H.; Dicks, J. M.; Tamiya, E.; Karube, I., *Anal. Chem.* **1987**, 59, 2760.
16. Muramatsu, H.; Kajiwarra, K.; Karube, I., *Anal. Chim. Acta.* **1986**, 188, 257.

17. Thompson, M.; Arthur, C. L.; Dhaliwal, G. K., *Anal. Chem.* **1986**, 58, 1206.
18. Leggett, G. J.; Roberts, C. J.; Williams, P. M.; Davies, M. C.; Jackson, D. E.; Tendler, S. J. B., *Langmuir* **1993**, 9, 2356.
19. Siegmann-Thoss, C.; Renneberg, R.; Glatz, J. F. C.; Spener, F., *Sens. Actuators B: Chem.* **1996**, 30, 71.
20. Buck, R. P.; Kinder, E., *Pure Appl. Chem.*, **1994**, 2527.
21. Covington, A. K., *Pure Appl. Chem.*, **1994**, 66, 565.
22. Liedberg, B.; Nylander, C.; Lundstrom, I., *Sens. Actuators.*, **1983**, 4, 299.
23. Sutherland, R. M.; Dahne, C.; Place, J. F., *Anal. Lett.* **1984**, 17, 43.
24. Li, X.; Rosenzweig, Z., *Anal. Chim. Acta.* **1997**, 353, 263.
25. Geddes, N. J.; Paschinger, E. M.; Furlong, D. N.; Caruso, F.; Hoffmann, C. L.; Rabolt, J. F., *Thin Solid Films* **1995**, 260, 192.
26. North, i., *Trends Biotechnol.* **1985**, 3, 180.
27. Centeno, E. R.; Johnson, W. G., *Int. Arch. Allergy Appl. Immunol.* **1970**, 37, 1.
28. Langone, J. J.; Van Vunakis, H., *Res. Commun. Chem. Pathol. Pharmacol.* **1975**, 10, 163.
29. Ercegovich, C. D.; Vallejo, R. P.; Gettig, R. R.; Woods, L.; Bogus, E. R.; Mumma, R. O., *J. Agric. Food Chem.* **1981**, 29, 559.
30. Engvall, E.; Perlmann, P., *J. Immunol.* **1972**, 109, 129.
31. Catt, K.; Tregear, G. W.; Burger, H. G.; Skermer, G., *Clin. Chim. Acta.* **1970**, 27, 267.

32. Caruso, F.; Rodda, E.; Furlong, D. N., *J. Colloid Interface Sci.* **1995a**, 178, 104.
33. Lin, J. N.; Drake, B.; Lea, A. S.; Hansma, P. K.; Andrade, J. D., *Langmuir* **1990**, 6, 509.
34. Geddes, N. J.; Martin, A. S.; Caruso, F.; Urquhart, R. S.; Furlong, D. N.; Sambles, J. R.; Than, K. A.; Edgar, J. A., *J. Immunol. Methods* **1994b**, 175, 149.
35. Hall, E. A.; Hall, C. E.; Marttens, N.; Mustan, M. N.; Datta, D., *Uses of Immobilized Biological Compounds*. Dordrecht: Kluwer: p 11.
36. Li, J. R.; Cai, M.; Chen, T. F.; Jiang, L., *Thin Solid Films* **1989**, 18, 205.
37. Marazuela, M. D.; Moreno-Bondi, M. C., *Anal. Bioanal. Chem.* **2002**, 372, 664.
38. Campanella, L.; Attioli, R.; Colapicchioni, C.; Tomassetti, M., *Sens. Actuators B Chem.* **1999**, 55, 23.
39. Gerdes, M.; Spener, F.; Meusel, M., *Quim. Anal.* **2000**, 19, 8.
40. Milligan, C.; Ghindilis, A., *Electroanalysis* **2002**, 14, 415.
41. Solé, S.; Alegret, S.; Céspedes, F.; Fàbregas, E.; Díez-Caballero, T., *Anal. Chem.* **1998**, 70, 1462.
42. Darain, F.; Park, S. U.; Shim, Y. B., *Biosens. Bioelectron.* **2003**, 18, 773.
43. Liu, B. H.; Yan, F.; Kong, J. L.; Deng, J. Q., *Anal. Chim. Acta.* **1999**, 386, 31.
44. Liu, G. D.; Wu, Z. Y.; Wang, S. P.; Shen, G. L.; Yu, R. Q., *Anal. Chem.* **2001**, 73, 3219.
45. Wang, J.; Pamidi, P. V. A.; Rogers, K. R., *Anal. Chem.* **1998**, 70, 1171.
46. Hu, S. Q.; Wu, Z. Y.; Zhou, Y. M.; Cao, Z. X.; Shen, G. L.; Yu, R. Q., *Anal. Chim.*

- Acta.* **2002**, 458, 297.
47. Hianik, T.; Snejdarkova, M.; Sokolikova, L.; Meszar, E.; Krivanek, R.; Tvarozek, V.; Novotny, I.; Wang, J., *Sens. Actuators B Chem.* **1999**, 57, 201.
 48. Alfonta, L.; Willner, I.; Throckmorton, D. J.; Singh, A. K., *Anal. Chem.* **2001**, 73, 5287.
 49. Ma, J.; Chu, Y. M.; Di, J.; Liu, S. C.; Li, H. N.; Feng, J.; Ci, Y. X., *Electrochem. Commun.* **1999**, 1, 425.
 50. Hu, S. Q., *Talanta* **2003**, 61, 769.
 51. Katz, E.; Willner, I., *Electroanalysis* **2003**, 15, 913.
 52. Aizawa, M.; Morioka, A.; Suzuki, S.; Nagamura, Y., *Anal. Biochem.* **1979**, 94, 22.
 53. Niwa, O.; Xu, Y.; Halsall, H. B.; Heineman, W. R., *Anal. Chem.* **1993**, 65, 1559.
 54. Ghindilis, A. L.; Makower, A.; Bauer, C. G.; Bier, F. F.; Scheller, F. W., *Anal. Chim. Acta.* **1995**, 304, 25.
 55. Costa-Garcia, A., *Anal. Chim. Acta.* **2001**, 442, 55.
 56. Diaz-Gonzalez, M.; Fernandez-Sanchez, C.; Costa-Garcia, A., *Anal. Sci.* **2002**, 18, 1209.
 57. Kreuzer, M. P.; Osullivan, C. K.; Guilbault, G. G., *Anal. Chim. Acta.* **1999**, 393, 95.
 58. Garcia Sanchez, F.; Navas Diaz, A.; Ramos Peinado, M. C.; Belledone, C., *Anal. Chim. Acta.* **2003**, 484, 45.
 59. Palecek, E.; Kizek, R.; Havran, L.; Billova, S.; Fojta, M., *Anal. Chim. Acta.* **2002**,

469, 73.

60. Moore, E. J.; Pravda, M.; Kreuzer, M. P.; Guilbault, G. G., *Anal. Lett.* **2003**, 36, 303.
61. Mazziotti, G.; Premawardhana, L. D. K. E.; Parkes, A. B.; Adams, H.; Smyth, P. P. A.; Smith, D. F.; Kaluarachi, W. N.; Wijeyaratne, C. N.; Jayasinghe, A.; de Silva, D. G. H.; Lazarus, J. H., *Eur. J. Endocrinol.* **2003**, 149, 103.
62. Loubaud, M.; van Doorn, W. G., *Postharvest Biol. and Tech.* **2004**, 32, 281.
63. Athley, D.; McNeil, C. J.; Bailey, W. R.; Hager, H. J.; Mullen, W. H.; Russell, L. J., *Biosens. Bioelectron.* **1993**, 8, 415.
64. Campanella, L.; Sammartino, M. P.; Tomassetti, M.; Zannella, S., *Sens. and Actuators B* **2001**, 76, 158.
65. Skorobogatko, O. V.; Ghindilis, A. L.; Shuster, A. M.; Troitskaya, E. N., *Prikl. Biokhim. Mikrobiol.* **1994**, 27, 2997.
66. Shaidarova, L. G.; Fomin, A. Y.; Ziganshina, S. A.; Medyantseva, E. P.; Budnikov, G. K., *J. Anal. Chem.* **2002**, 57, 150.
67. Medyantseva, E. P.; Shen, L. F.; Fedoseeva, O. V.; Budnikov, G. K.; Skorodelis, O. E.; Zeidaka, A. A., *Prikl. Biokhim. Mikrobiol.* **1993**, 29, 619.
68. Thomas, J. H.; Kim, S. K.; Hesketh, P. J.; Halsall, H. B.; Heineman, W. R., *Anal. Biochem.* **2004**, 328, 113.
69. Armada, M. P. G.; Losada, J.; Cuadrado, I.; Alonso, B.; Gonzalez, B.; Casado, C. M., *Electroanal.* **2003**, 15, 1109.

70. Sergeyeva, T. A.; Soldatkin, A. P.; Rachkov, A. E.; Tereschenko, M. I.; Piletsky, S. A.; El'skaya, A. V., *Anal Chim Acta* **1999**, 390, 73.
71. Xu, Y.; Halsall, H. B.; Heineman, W. R., *J. Pharm. Biomed. Anal.* **1989**, 7, 1301.
72. Letheby H., *J. Chem. Soc.* **1862**, 15, 161.
73. Green, A. G.; Woodhead, A. E., *J. Chem. Soc. Trans.* **1912**, 101, 1117.
74. Hong, S.; Yound, M. J.; Park, S. M., *J. Phys. Chem. B.* **2005**, 109, 3844.
75. DurC, L.; MANDI, Z.; KOVAES, S., *Eelectrochimica Acta* **1995**, 40, 1681.
76. Nunziante, P.; Pistoia, G., *Electrochim Acta.* **1989**, 2, 22.
77. Kobayashi, T.; Yoneyama, H.; Tamura, H., *J. Electroanal. Chem.* **1984**, 177, 293.
78. Hand, R.; Nelson, R., *J. Am. Chem. Soc.* **1974**, 6, 850.
79. Diego, F. A.; Horacio, J. S.; César, A. B., *J. Braz. Chem. Soc.* **2005**, 16, 259.
80. César, B.; Horacio, J. S.; Diego, F. A.; Doris, E. G.; Fernando, G.; Gabriel, A. P.; Gustavo, M. M.; Maria, C. M., *Electrochimica Acta.* **2004**, 49, 3671.
81. Han, C. C.; Hong, S. P.; Yang, K. F.; Bai, M. Y.; Lu, C. H.; Huang, C. S., *Macromolecules* **2001**, 34, 587.
82. Han, C. C.; Hseih, W. D.; Yeh, J. Y.; Hong, S. P., *Chem. Mater.* **1999**, 11, 480.
83. Han, C. C.; Jeng, R. C., *Chem. Commun.* **1997**, 553.
84. Han, C. C.; Lu, C. H.; Hong, S. P.; Yang, K. F., *Macromolecules* **2003**, 36, 7908.
85. Barbero, C.; Morales, G. M.; Grumelli, D.; Planes, G.; Salavagione, H. J.; Marengo, C. R.; Miras, M. C., *Synth. Metals.* **1999**, 101, 694.
86. Salavagione, H. J.; Morales, G. M.; Miras, M. C., *Acta. Polymerica.* **1999**, 50, 40.

87. Kreuter, J., *J. Nanosci. Nanotechnol.* **2004**, 4, 484.
88. Lockman, P. R.; Oyewumi, M. O.; Koziara, J. M.; Roder, K. E.; Mumper, R. J.; Allen, D. D., *J. Control. Release* **2003**, 93, 271.
89. Russell-Jones, G. J.; Arthur, L.; Walker, H., *Int. J. Pharm.* **1999**, 179, 247.
90. Steiniger, S. C.; Kreuter, J.; Khalansky, A. S.; Skidan, I. N.; Bobruskin, A. I.; Smirnova, Z. S.; Severin, S. E.; Uhl, R.; Kock, M.; Geiger, K. D.; Gelperina, S. E., *Int. J. Cancer* **2004**, 109, 759.
91. Vinogradov, S. V.; Batrakova, E. V.; Kabanov, A. V., *Bioconjug. Chem.* **2004**, 15, 50.
92. Chen, L. T.; Weiss, L., *Blood Cells* **1973**, 41, 529.
93. Bailey, F. R.; Copenhaver, W. M.; Bunge, R. P.; Bunge, M. B., *Bailey's Textbook of Histology*. Williams & Wilkins: 1971.
94. Braet, F.; De Zanger, R.; Baekeland, M.; Crabbe, E.; Van Der Smissen, P.; Wisse, E., *Hepatology* **1995**, 21, 180.
95. Yongli, C.; Xiufang, Z.; Yandao, G.; Nanming, Z.; Tingying, Z.; Xinqi, S., *J. Colloid Interface Sci.* **1999**, 214, 38.
96. Soumitra S. G.; Philip M. K.; Ann W. M.; C., H. L., *Bioconjugate Chem.* **1990**, 1, 71.
97. Dubertret, B.; Calame, M.; Libchaber, A. J., *Nat. Biotechnol.* **2001**, 19, 365.
98. Safer, D. E.; Bolinger, L.; Leigh, J. S., *J. Inorg. Biochem.* **1986**, 26, 77.
99. Gisela, B.; Anette, H.; Erik, W.; Ulf, L., *Biomolecular Engineering* **1999**, 16, 105.

100. Pei, R.; Cheng, Z.; Wang, E.; Yang, X., *Biosens. Bioelectron.* **2001**, 16, 355.
101. Nicole, F. S.; George, P. L.; David, J. E., *Langmuir* **2006**, 22, 3488.
102. Portney, N. G.; Singh, K.; Chaudhary, S.; Destito, G.; Schneemann, A.; Manchester, M.; Ozkan, M., *Langmuir* **2005**, 21, 2098.
103. Lin, E.; Nemunaitis, J., *Cancer Gene Therapy* 11, 643.
104. Stern, J. M.; Stanfield, J.; Park, S.; Hsieh, J.-T.; Cadeddu, J. A., *Journal of Endourology* **2007**, 21, 939.
105. Souza, G. R., *Proc. Natl. Acad. Sci.* **2006**, 103, 1215.
106. Souza, G. R., *Anal. Chem.* **2006**, 78, 6232.
107. D'Herelle, F., *Sur un microbe invisible antagoniste des bacilles dysenteriques* **1917**, 165, 373.
108. Smith, G. P., *Science* **1985**, 228, 1315.
109. Specthrie, L.; Bullitt, E.; Horiuchi, K.; Model, P.; Russel, M.; Makowski, L., *J. Mol. Biol.* **1992**, 228, 720.
110. Marco, A. A., *Genetics and Molecular Biology* **2005**, 28, 1.
111. Marvin, D. A., *J. Mol. Biol.* **2006**, 355, 294.
112. Endemann, H.; Model, P., *J. Mol. Biol.* **1995**, 250, 496.
113. Gao, C.; Mao, S.; Lo, C. H.; Wirsching, P.; Lerner, R. A.; Janda, K. D., *Proc. Natl. Acad. Sci.* **1999**, 96, 6025.
114. Rakonjac, J.; Feng, J. N.; Model, P., *J. Mol. Biol.* **1999**, 289, 1253.
115. Chen, L.; Giordano, R. J.; Arap, W.; Pasqualini, R., *Chem. Biol.* **2004**, 11, 1081.

116. Souza, G. R.; Christianson, D. R.; Staquicini, F. I.; Ozawa*, M. G.; Snyder, E. Y.; Sidman, R. L.; Miller, J. H.; Arap, W.; Pasqualini, R., *Proceedings of National Academy of Sciences of the United States of America* **2006**, 103, 1215.
117. Kneipp, K.; Kneipp, H.; Itzkan, I.; Dasar, R. R.; Feld, M. S., *Chem. Rev.* **1999**, 99, 2957.
118. Lecomte, S.; Wackerbart, H.; Soulimane, T.; Buse, G.; Hildebrandt, P., *J. Am. Chem. Soc.* **1998**, 120, 7381.
119. Otto, A.; Mrozek, I.; Grabhorn, H.; Akemann, W., *J. Phys.: Condens. Matter.* **1992**, 4, 1143.
120. Doering, W. E.; Nie, S. M., *J. Phys. Chem. B* **2002**, 106, 311.
121. Weaver, M. J.; Zou, S.; Chan, H. Y., *Anal. Chem.* **2000**, 73, 38A.
122. Jeanmaire, D. L.; Van Duyne, R. P., *J. Electroanal. Chem. Interfacial Electrochem.* **1977**, 84, 1.
123. Grabar, K. C.; Freeman, R. G.; Hommer, M. B.; Natan, M. J., *Anal. Chem.* **1995**, 67, 735.
124. Allen, C. S.; Van Duyne, R. P., *J. Am. Chem. Soc.* **1981**, 103, 7497.
125. Kreibig, U.; Gartz, M.; Hilger, A.; Hovel, H., *Advances in metal and semiconductor clusters*. JAI Press Inc.: Stamford, 1998; Vol. 4, p 345.
126. Volkan, M.; Stokes, D. L.; Vo-Dinh, T., *J. Raman Spectrosc.* **1999**, 30, 1057.
127. Fleischmann, M.; Hendra, P. J.; McQuillan, A. J., *Chem. Phys. Lett.* **1974**, 26, 163.

128. Zeisel, D.; Deckert, V.; Zenobi, R.; Vo-Dinh, T., *Chem. Phys. Lett.* **1998**, 283, 381.
129. Dick, L. A.; McFarland, A. D.; Haynes, C. L.; Van Duyne, R. P., *J. Phys. Chem. B.* **2002**, 106, 853.
130. Champion, A.; Kambhampati, P., *Chem. Soc. Rev.* **1998**, 27, 241.
131. Kneipp, K.; Kneipp, H.; Itzkan, I.; Dasar, R. R.; Feld, M. S., *Chem. Rev.* **1999**, 99, 2957.
132. Cotton, T. M.; Schultz, S. G.; Vanduyne, R. P., *J. Am. Chem. Soc.* **1980**, 102, 7960.
133. Jang, N. H., *Bull. Korean Chem. Soc.* **2002**, 23, 1790.
134. Kneipp, K. a.; Flemming, J., *J. Mol. Struct.* **1986**, 145, 173.
135. Kneipp, K.; Pohle, W.; Fabian, H., *J. Mol. Struct.* **1991**, 244, 183.
136. Thorton, J.; Force, R. K., *Appl. Spectrosc.* **1991**, 45, 1522.
137. Kim, S. K.; Joo, T. H.; Suh, S. W.; Kim, M. S., *J. Raman Spectrosc.* **1986**, 17, 381.
138. Graham, D.; Smith, W. E.; Linacre, A. M. T.; Munro, C. H.; Watson, N. D.; White, P. C., *Anal. Chem.* **1997**, 69, 4703.
139. Grubisha, D. S., *Anal. Chem.* **2003**, 75, 5936.
140. Qian, X.; Peng, X.; Ansari, D. O.; Yin-Goen, Q.; Chen, G. Z.; Shin, D. M.; Yang, L.; Young, A. N.; Wang May D.; Nie, S., *Nat. Biotechnol.* **2008**, 26, 83.
141. Pope, M. T., *Heteropoly and Isopoly Oxometalates*. Springer Verlag: Berlin, 1983.

142. Pope, M. T.; Müller, A., *Polyoxometalates: From Platonic Solids to Anti-Retroviral Activity*. Kluwer Academic Publishers: Dordrecht, 1994.
143. Pope, M. T.; Müller, A., *Polyoxometalate Chemistry: From Topology via Self-Assembly to Applications*. Kluwer Academic Publishers: Dordrecht, 2001.
144. Borrás-Almenar, J. J.; Coronado, E.; Müller, A.; Pope, M. T., *Polyoxometalate Molecular Science*. Academic Publishers: Dordrecht, 2003.
145. Hill, C. L., *Coord. Chem. Rev.* **1998**, 143, 1.
146. Okun, N. M.; Anderson, T. M.; Hill, C. L., *J. Mol. Cat.* **2003**, 197, 283.
147. Pope, M. T.; Müller, A., *Angew. Chem., Int. Ed. Engl.* **1991**, 30, 34.
148. Contant, R.; Herve, G., *Inorg. Chem.* **2002**, 22, 63.
149. Kasem, K. K.; Schultz, F. A., *Can. J. Chem.* **1995**, 73, 858.
150. Hill, C. L.; Prosser-McCartha, C. M., *Coord. Chem. Rev.* **1995**, 143, 407.
151. Okuhara, T.; Misuno, N.; Misono, M., *Adv. Catal.* **1996**, 41, 113.
152. Martel, D.; Kuhn, A., *Electrochimica Acta* **2000**, 45, 1829.
153. Keita, B.; Belhouari, A.; Nadjo, L.; Contant, R., *J. Electroanal. Chem.* **1995**, 381, 243.
154. Bidan, G.; Genies, E. M.; Lapkowski, M., *J. Chem. Soc., Chem. Commun.* **1998**, 533.
155. Keita, B.; Bouaziz, D.; Nadjo, L. J., *Electroanal. Chem.* **1988**, 255, 303.
156. Keita, B.; Nadjo, L., *J. Electroanal. Chem.* **1985**, 191, 441.
157. Fabre, B.; Bidan, G.; Fichou, D., *J. Chim. Phys.* **1992**, 89, 1053.

158. Keita, B.; Bouaziz, D.; Nadjjo, L.; Deronzier, A., *J. Electroanal. Chem.* **1990**, 279, 187.
159. Wang, P.; Li, Y., *J. Electroanal. Chem.* **1996**, 408, 77.
160. Dong, S.; Jin, W., *J. Electroanal. Chem.* **1985**, 191, 441.
161. Rong, C.; Anson, F. C., *Inorg. Chim. Acta* **1996**, 242, 11.
162. Ingersoll, D.; Kulesza, P. J.; Faulkner, L. R., **1994**, 141, 140.
163. Decher, G.; Hong, J. D., *Macromol. Chem. Macromol. Symp.* **1991**, 46, 321.
164. Lvov, Y.; Essler, F.; Decher, G., *J. Phys. Chem.* **1993**, 97, 13773.
165. Liu, H.; Hu, N., *J. Phys. Chem. B* **2005**, 109, 10464.
166. Yang, S.; Li, Y.; Jiang, X.; Chen, Z.; Lin, X., *Sens. Actuators* **2006**, B114, 774.
167. Papadakis, A.; Souliotis, A.; Papaconstantinou, E., *J. Electroanal. Chem.* **1997**, 435, 17.
168. Toth, J. E.; Anson, F. C., *J. Am. Chem. Soc.* **1989**, 111, 2444.
169. Toth, J. E.; Melton, J. D.; Cabeli, D.; Bielski, B. H. J.; Anson, F. C., *Inorg. Chem.* **1952**, 29, 1990.
170. Sun, C.; Zhao, J.; Xu, H.; Sun, Y.; Zhang, X.; Shen, J., *J. Electroanal. Chem.* **1997**, 435, 63.

CHAPTER 2

ELECTROCHEMICAL ENZYME IMMUNOASSAY ON POLYANILINE MODIFIED GOLD ELECTRODES

2.1 Introduction

Conducting electroactive polymers are relatively new materials, having being discovered just over 20 years ago. They have aroused considerable interest due to their ability to conduct electricity and their unique chemical and biochemical properties and already have numerous bioanalytical and technological applications¹⁻⁴. Conductive polymers are easily synthesized and can be deposited onto the conductive surface of a given substrate from monomer solutions by electrochemical polymerization with precise electrochemical control of their formation rate and thickness¹. Polyaniline is one of the most promising conductive polymers for technological applications because of its unique electro-optical properties, environmental stability and inexpensive monomer².

As described in the previous chapter, there are four main forms of polyaniline^{3, 4}, namely leucoemeraldine, emeraldine base, emeraldine salt and pernigraniline. The completely reduced form, leucoemeraldine consists of phenylene rings with amine type nitrogens. This reduced leucoemeraldine base is very easily oxidized, requiring only minimal amounts of oxygen. In the half oxidized polymer, emeraldine, the ratio of benzenoid type rings to quinoid type rings is 3:1. Both the isolated form (emeraldine base) and conducting form (emeraldine salt) have good stability. For the fully oxidized

polyaniline, pernigraniline, the numbers of phenylene rings with a benzenoid type sequence and rings with a quinoid type sequence are equal and are separated by imine nitrogens.

Several studies have suggested that small nucleophilic molecules, such as amines and thiols, can form covalent bonds to the polyaniline backbone⁵⁻⁷. These reports suggest that a variety of nucleophiles are capable of reducing the polyaniline backbone from the oxidized emeraldine to the reduced leucoemeraldine structure to form the corresponding derivatives of polyanilines through nucleophilic reactions.

A major application of protein analysis is the early diagnosis of certain diseases by detecting the presence of specific peptides and proteins in plasma or serum. The direct detection of the protein relies on the specific interactions of proteins, for example the interaction between antibody and antigen. Immuno-interaction of proteins in solution with their complementary proteins immobilized on a surface produces changes in, for example, the refractive index⁸, thickness and dielectric constant of the immobilized layer⁹. Electrochemical enzyme immunoassays have already been developed to analyze antibodies and antigens (Ab-Ag complexes) under enzyme catalysis¹⁰⁻¹².

Immunosensors are devices with a fast response, coupled with a high specificity and sensitivity. Preferably, immunosensors should also be able to regenerate, allowing them to be reused immediately or after dissociation of the Ab-Ag complex. Immunosensors with electrochemical detection methods have been widely used due to their high sensitivity and selectivity, low expense and small size.

The first step in developing a new immunosensor is the immobilization of a suitable antibody to the surface of a transducer using electrochemical, optical, or piezoelectric

methodologies. This step can be carried out by either a covalent attachment, physical adsorption, or electrostatic entrapment in a polymer matrix. It has been pointed out⁵⁻⁷ that nucleophilic molecules, such as amines and thiols can covalently attach to the polyaniline backbone. Furthermore, nucleophilic groups, such as the amine group in lysine or the thiol groups that connect the three fragments of antibodies are already present in antibodies' structure. Thus, it should be straightforward to develop a synthetic method to couple protein molecules to the surface of polyaniline by nucleophilic reaction.

Surface-enhanced Raman scattering (SERS) was discovered twenty years ago. SERS spectra often differ considerably from regular Raman spectra. As the Raman effect is inherently weak, it is usually difficult to use normal Raman scattering either for trace analysis or for the study of highly fluorescent samples¹³. In SERS, however, molecules at or near a noble metal surface with nanoscale structural features exhibit a dramatic increase in the incident electromagnetic field, yielding high intensity Raman spectra. SERS can dramatically increase the Raman intensity of a molecule in proximity to a nanoscale roughened surface^{14, 15}. Several studies of polyaniline structures deposited on rough metallic surfaces that utilize SERs had been performed in recent years¹⁶⁻¹⁹.

In the research reported here, polyaniline film was electrochemically deposited onto a gold foil surface. Cyclic voltammetry and Raman spectroscopy were used to characterize polyaniline films covalently modified with Rabbit IgG immunoassay containing nucleophilic amine and thiol groups. The results suggested that only the oxidized emeraldine form of polyaniline can covalently bond with anti-rabbit IgG to produce a good immunosensor. Applications of this novel surface modification methodology will be discussed in this chapter. Matrix Assisted Laser

Desorption/Ionization Time-of-Flight (MALDI-TOF) Mass Spectrometry was utilized to prove that the emeraldine form of polyaniline reacts easily with nucleophilic groups such as thiol. MALDI-TOF Mass Spectrometry is a technique that offers great promise for the fast and accurate determination of a number of polymer characteristics. This analytical technique, first reported in 1987²⁰, generates a mass spectrum that can give information about repeat units, end groups, and the molecular weight distribution of the polymer. In this MS method, a solid matrix is used, which absorbs light at the laser wavelength²¹. The sample is mixed with a matrix solution and allowed to co-crystallize on a target plate. The target matrix absorbs the pulsed laser light energy and is vaporized, carrying some of the sample with it.

2.2. Experimental

2.2.1 Chemical and reagent

Aniline monomer (Fisher) was distilled at 80 °C under reduced pressure prior to use and stored in the dark over zinc metal at 4 °C in a nitrogen gas atmosphere. All other chemicals were reagent grade and used as received. Sodium chloride, magnesium chloride, sulfuric acid, hydrochloric acid and sodium hydroxide were bought from Fisher.

Tris(hydroxymethyl)aminomethane and Tween-20 were bought from ACROS. 4-nitrophenylphosphate disodium salt (99 %) and sodium sulfide were bought from Alfa Aesar. Affinipure anti-rabbit IgG (rAb), rabbit IgG (rAg), alkaline phosphatase conjugated monoclonal anti-rabbit IgG (γ -chain-specific) (rAb^{*}), anti-sheep IgG (sAb), sheep IgG (sAg), alkaline phosphatase conjugated monoclonal anti-sheep IgG (γ -chain-specific) (sAb^{*}) were all obtained from Sigma Chemical Co. and used as received.

4-Aminophenylphosphate (pAPP) was synthesized by reduction of 4-nitrophenyl phosphate with sodium sulfide²². Briefly, 2.3 g of 4-nitrophenyl phosphate disodium salt ($\text{Na}_2 - \text{pNPP}$) was dissolved in 5.6 mL of distilled water and pH adjusted to 9 with NaOH solution. Then 3.0g $\text{Na}_2\text{S}\cdot 9\text{H}_2\text{O}$ was added and the mixture was heated to 90 – 95 °C for 1 hour. The solution was cooled and acidified with concentrated HCl (pH < 2). The acidified solution was filtered and the pH was adjusted to 4-5 by NaOH solution. The white crystals were collected (i.e. the monosodium salt of pAPP) and recrystallized from methanol to remove inorganic impurities. The product pAPP was refrigerated for later use.

The buffer solutions used in the experiment were as follows: Buffer A: 0.135 M NaCl + 1% (v/v) Tween-20; Buffer B: 0.1 M Tris (hydroxymethyl) aminomethane, 1 mM magnesium chloride, and 0.02% (w/v) sodium azide. The pH was adjusted to 9.0 with concentrated hydrochloric acid solution;

5 $\mu\text{g}/\text{mL}$ anti-rabbit IgG solution, rabbit IgG solution and anti-rabbit IgG alkaline phosphatase conjugate (Ab^*) solution were prepared by diluting from stock solutions separately with 0.135 M NaCl + 1% (v/v) Tween-20.

The support electrolyte for cyclic voltammetry was 4 mM 4-aminophenyl phosphate in Tris (hydroxymethyl) aminomethane (pH 9) buffer.

2.2.2 Covalent immobilization of immunoreagents

Au foil (99.999% purity, Alfa) was cleaned with piranha solution (1: 3 $\text{H}_2\text{O}_2:\text{H}_2\text{SO}_4$), and distilled water. Polyaniline films were then grown on the gold foil electrode using 0.1 M aniline monomer in 0.5 M H_2SO_4 aqueous solution. The electropolymerization of aniline was carried out by controlled potential electrolysis at 800 mV (*vs.* Ag/AgCl) for 3

minutes. Polyaniline films were forced to the reduced form at -200 mV (vs. Ag/AgCl) in 0.5 M sulfuric acid solution for about 3 minutes. The oxidized form was prepared by applying 600 mV on the polyaniline electrode for 3 minutes in 0.5 M sulfuric acid solution. The oxidized and reduced polyaniline-coated electrodes were cleaned by soaking in deionized water to remove aniline and acid residue.

For the immuno-sandwich assay, the electrode with the polyaniline film was soaked in 5 $\mu\text{g/mL}$ anti-body solution for 1 hr, and then the modified electrode was soaked in antigen solution, followed by soaking in alkaline phosphatase labeled antibody, for half an hour each. The electrode was rinsed by buffer with 0.135 M NaCl + 1% (v/v) Tween-20 three times and dried by N_2 before being transferred to another solution. The substrate was then transferred into a Teflon electrochemical cell containing 4 mM 4-aminophenyl phosphate in 0.1 M Tris buffer (pH 9.0) solution. The alkaline phosphatase label catalyzes the conversion of 4-aminophenyl phosphate to 4-aminophenol, which can be easily detected by cyclic voltammetry. Oxidative peak currents were recorded.

2.2.3 Cyclic Voltammetry

All cyclic voltammetry experiments were performed in a homemade Teflon cell with a total volume of 10 mL using a BAS Epsilon Potentiostat workstation.

A standard three-electrode system was used in which a gold foil was the working electrode, a Pt wire was the counter electrode and Ag/AgCl was the reference electrode. Since reduced polyaniline is not conductive, after reacting the polyaniline film with the antibody this modified gold foil could no longer be used as a working electrode, so instead was placed close to the working electrode in the electrolyte. All potentials were referenced to the reference electrode. The scanning rate was 100 mV/s. The

electrochemical cell was isolated from light with aluminum foil and maintained in a nitrogen atmosphere during the immunoassay experiments.

2.2.4 Raman Spectroscopy

Thin polyaniline film was deposited on a rough gold surface via cyclic voltammetry between 0 and +800 mV versus an Ag/AgCl reference electrode at 100 mV s⁻¹ in a three electrode cell containing an aqueous solution of 0.5M H₂SO₄ and 0.05 M aniline. The polyaniline film was then either reduced at -200 mV or oxidized at +600 mV. The oxidized polyaniline film was reacted with anti-rabbit IgG F(ab)₂ fragment solution for 1 hour. The surfaces were characterized using a custom made Raman spectrometer equipped with a HeNe Laser (632.5 nm) and an Ocean Optics HR2000 spectrometer. Au supports with rough surfaces were prepared using electrochemical methods according to the previously reported procedure^{23,24}. For roughening the surface, the gold foil served as the working electrode, and platinum wire and silver–silver chloride (Ag/AgCl) were employed as the counter and reference electrodes. The gold substrate was cycled in a deoxygenated 0.1M KCl aqueous solution from -0.28V (holding 10 s) to +1.22V (holding 5 s) versus Ag/AgCl at 500 mV/s for 25 cycles.

2.2.5 Matrix assisted laser desorption ionization-time of flight mass spectroscopy

Matrix assisted laser desorption ionization-time of flight mass spectroscopy (MALDI-TOF MS) experiments were performed on a Microflex™ MALDI-TOF mass spectrometer (Bruker Daltonic, Billerica, MA) equipped with a nitrogen laser operating at 337 nm.

Polyaniline was prepared by control potential at 800 mV for 15 minutes and oxidized at 600 mV for 5 minutes, after which the solid was washed by distilled water and peeled

from the electrode surface. The polyaniline solid was reacted with 1 mM butanethiol in aqueous solution for 1 hours and then washed with distilled water and dried in N₂ flowing container. For solventless MALDI, samples were all prepared in as that previously reported²⁵⁻²⁷. Polyaniline and matrix dithranol were mixed and ground in a mortar with a pestle for 15 min in order to reduce the size of the polyaniline particles. A molar ratio of analyte to matrix of 1:50 was used (assuming a molecular weight of 1000 Da for polyaniline, as calculated from previous studies on these samples²⁸) with approximately 1 mg of polyaniline being used for each sample. In order to adhere the ground sample to the plate, a small amount of mixed sample was spread out over several spots on the plate, giving a minimal amount of surface coverage. Gentle pressure was applied to the top of the polyaniline with a spatula in order to compress the solid on the plate. Excess solid was then blown off of the sample plate with a gentle stream of nitrogen to avoid contamination prior to insertion of the sample stage in the mass spectrometer. These resulting sample “films” were kept very thin in order to prevent any calibration errors and losses in sensitivity.

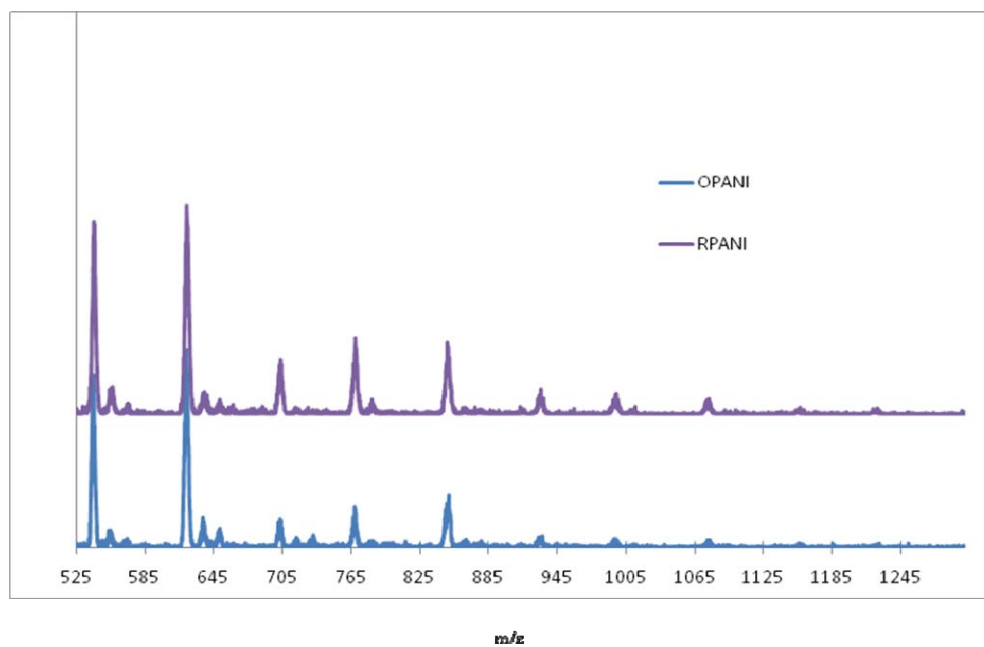
2.3. Results

2.3.1. Matrix assisted laser desorption ionization-time of flight mass spectroscopy

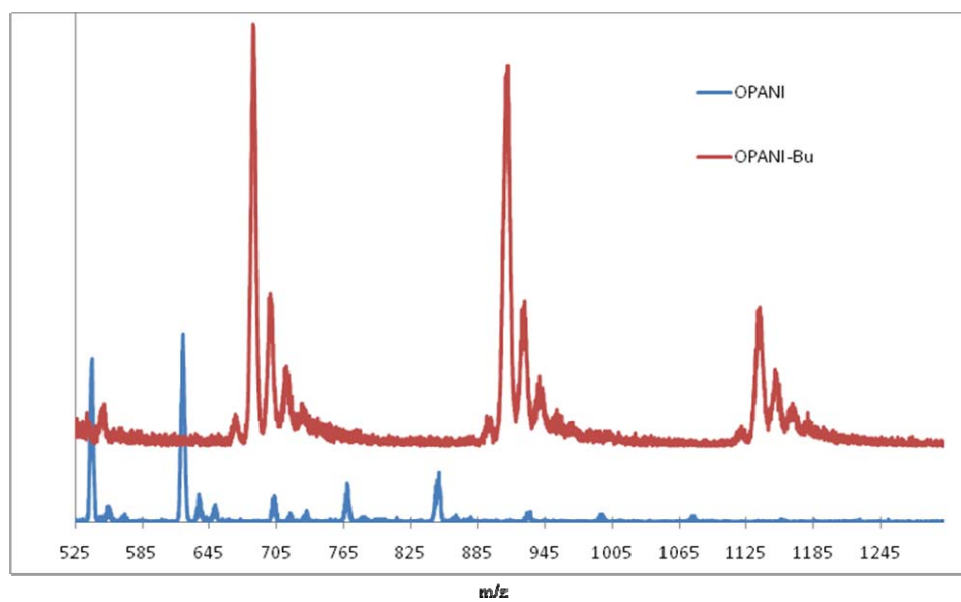
Most reported nucleophilic reactions of polyaniline were conducted in ethanol solution, but in the work reported here the biomolecules were dissolved in aqueous solution. In order to test the nucleophilic reaction of polyaniline in aqueous solution, water soluble butanethiol (BT) was used to react with oxidized polyaniline. Solventless MALDI spectra of oxidized polyaniline, reduced polyaniline and BT reacted polyaniline are shown in Figure 2.1. It should be noted that two groups of peaks appear adjacent to the main peak at

differences of 14-16 mass units in oxidized polyaniline and reduced polyaniline. According to the structure of the sample, these differences can only correspond to NH₂ groups. It is logical to assume that the subsidiary groups at 14-16 units may be due to the loss of a final amine group during fragmentation of the sample in the desorption/ionization process. Depending on the end groups present, the structure of the polyaniline given in Table 2.1 is represented by different symbols. Some structures result from the loss of the terminal amine groups, leaving the polyaniline oligomers to be terminated by two phenyl groups. This series of oligomers is designated by the symbol # followed by two numbers in brackets. The first number within a bracket represents the number of benzenoid groups, while the second represents the number of quinoid units. A quinoid unit consists of one nitrogen atom involved in a double-bond with a six-membered ring. A polyaniline chain terminated by amine group at one end and by phenyl groups at another end is denoted by the symbol *, while the symbol @ represents a polyaniline chain with amine groups at both ends.

Because the reduced and oxidized polyaniline forms differ by only 2 to 4 mass units, it is hard to differentiate their spectra. Therefore, in Figure 2.1a the data gives almost identical mass spectra for oxidized PANI and reduced PANI. However, after reacting with butanethiol, the mass spectrum for polyaniline changed compared to the original spectrum for polyaniline. For example, groups with three adjacent peaks at m/z 624, 850, and 999, disappeared and new groups with six adjacent peaks at m/z 726, 942, 1148 appeared after the reaction between oxidized polyaniline and butanethiol. The molecular weight of butanethiol (CH₃CH₂CH₂CH₂SH) is 90. It has several fragments whose molecular weight could be 75 (-CH₂-CH₂-CH₂-SH), 61 (-CH₂-CH₂-SH) and



a



b

Figure 2.1 MALDI-MS spectrum of (a) oxidized polyaniline (OPANI) and reduced polyaniline (RPANI) and (b) oxidized polyaniline (OPANI) and polyaniline reacted with butanethiol (OPANI-Bu)

Table 2.1 The MALDI-MS peak assignment of oxidized polyaniline and butanethiol reacted polyaniline

OxidizedPANI Peaks	PANI-Bu calculation (m/z)	PANI-Bu spectra (m/z)
542 (5,1)#	652+90	741
558 (5, 1)*	635+90=725, 652+75=726	726
574 (5, 1)@	624+90=714, 638+75=713 652+61=713	715
624 (5,2)#	624+75=699, 638+61=699 652+47=699	700
638 (5,2)*	624+61=685, 638+47=685	684
652 (5,2)@	624+47=671,	670
771 (5,1)#+226		
	880+90=970	971
850 (5.2)#+226	865+90=955 880+75=955	958
865 (5.2)*+226	850+90=941 865+75=940 880+61=941	942
880 (5.2)@+226	850+75=927 865 +61=926 880+47=927	928
	850+61=911 865+47=912	911
	850+47=897	898
918 (8,2)*	993+47+90=1130, 1008+47+75=1130	1132
932 (8,2)@	993+90+32=1115, 1008+47+61=1116	1118
993 (9,3)#	993+90+61=1144, 1008+47+90=1145	1148
1008 (9,3) *	993+90+75=1158 1008+75+75=1158	1162
1023 (9,3)@	993+90+90=1173 1008+90+75=1173	1175

47(-CH₂-SH). Based on the calculations in Table 2.1, the new peaks may be due to a new kind of polymer produced from a reaction between butanethiol and oxidized polyaniline.

Maldi-MS results indicate that butanethiol may have reacted with oxidized polyaniline and attached on the polyaniline backbone.

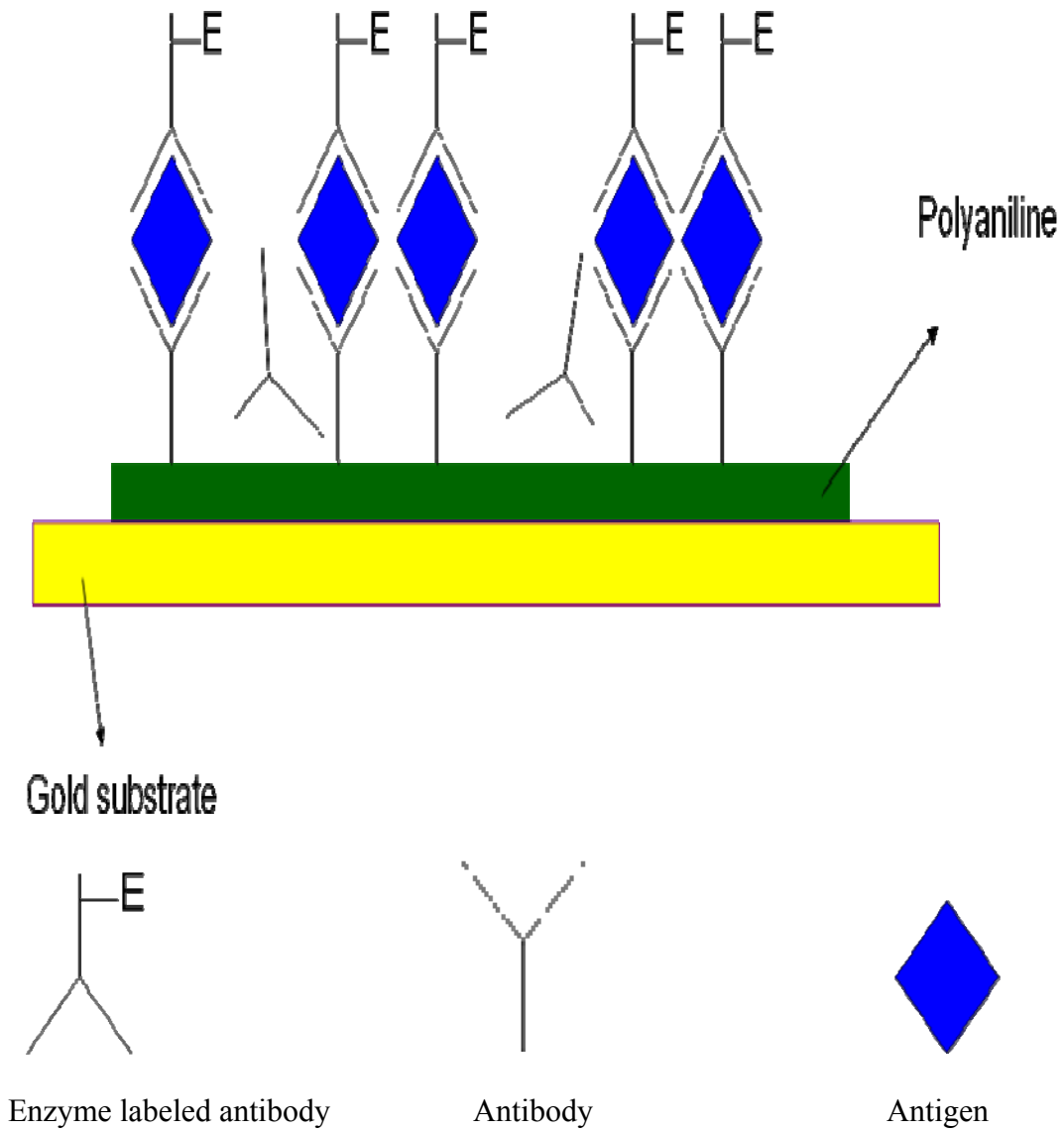
2.3.2 Cyclic voltammetry

2.3.2.1 Determination of rabbit IgG sandwich assay on oxidized polyaniline electrode

In an electrochemical sandwich assay, the antigen specifically interacts with the antibody, and then the alkaline phosphatase labeled antibody combines with the antigen (Scheme 2.1). The activity of the alkaline phosphatase can be detected electrochemically using a nonelectroactive substrate that produces an electroactive product as a result of enzymatic dephosphorylation.

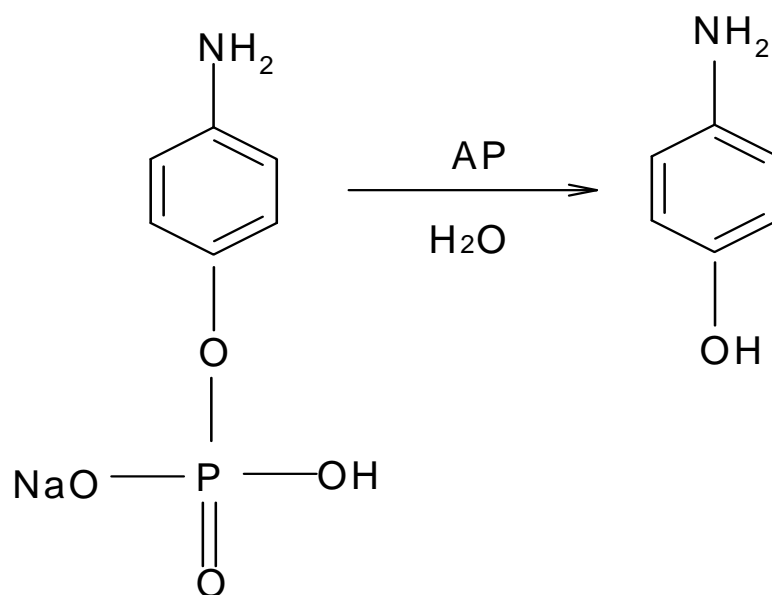
For this research anti-rabbit IgG and sheep IgG sandwich assays were prepared. The label, alkaline phosphatase, catalyzes the conversion of 4-aminophenyl phosphate to 4-aminophenol, which is electrochemically active. The electrochemical reactions are shown in Scheme 2.2. 4-Aminophenyl phosphate (PAPP) has been widely used as a substrate, because alkaline phosphatase catalyzes dephosphorylation of PAPP to generate 4-aminophenol (PAP), which can be measured amperometrically at a low potential²⁹.

However, PAPP decomposes only slowly in alkaline solution, which means that the electrochemical measurement of alkaline phosphatase by PAP is usually limited by the background signal produced from the electrochemical reduction of the PAPP decomposition product. This decreases both the sensitivity and the reproducibility of the alkaline phosphatase detection. Moreover, the product of the enzymatic reaction, PAP, is

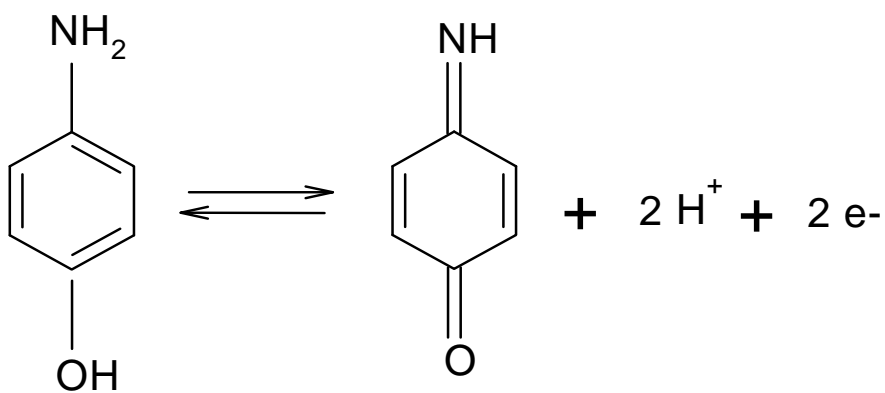


Scheme 2.1 Electrochemical Sandwich Immunoassay in our research

a.



b.



Scheme 2.2 a. The conversion of 4-aminophenyl phosphate (PAPP) to 4-aminophenol

(AP- alkaline phosphatase)

b. The electrochemical behavior of 4-aminophenol (PAP)

easily oxidized by air and is light sensitive. Thus, the time available for accumulation of product is limited.

Figure 2.2 shows cyclic voltammograms of 4-aminophenol produced on rabbit IgG sandwich assay surfaces on oxidized and reduced polyaniline modified gold electrodes. As previously reported by our group³⁰, after reacting with antibody the film become nonconductive. It has also been reported that the leucoemeraldine form (reduced polyaniline form) is not conductive. We therefore thought it likely that after reacting with antibody the polyaniline is reduced to the leucoemeraldine form through a nucleophilic reaction with the antibody. Therefore, in order to obtain a better signal, a bare gold electrode was used as the working electrode and was positioned as close as possible to the functionalized electrode.

As reported previously^{31, 32}, peak heights of the observed voltammetric anodic oxidation signals at 0.1 v are proportional to the concentration of PAP in the sample solution and can therefore be used for analytical evaluations. As Figure 2.2 shows, in tris-buffer solution the 4-aminophenol oxidation peak current for an electrode with rabbit IgG sandwich immunoassay on the oxidized polyaniline form was much larger than on the reduced polyaniline form under the same circumstances. However, the peak current from reduced polyaniline films was still slightly larger than the baseline signal (polyaniline on bare gold directly in our electrolyte without modification). The very small signal for an electrode with reduced polyaniline may due to the presence of some oxidized polyaniline as a result of exposing the electrode to ambient after reducing it under -200 mV potential and nonspecific adsorption of antibody on polyaniline surface. The results indicate that antibodies only attach to the oxidized polyaniline film modified electrode and can thus be

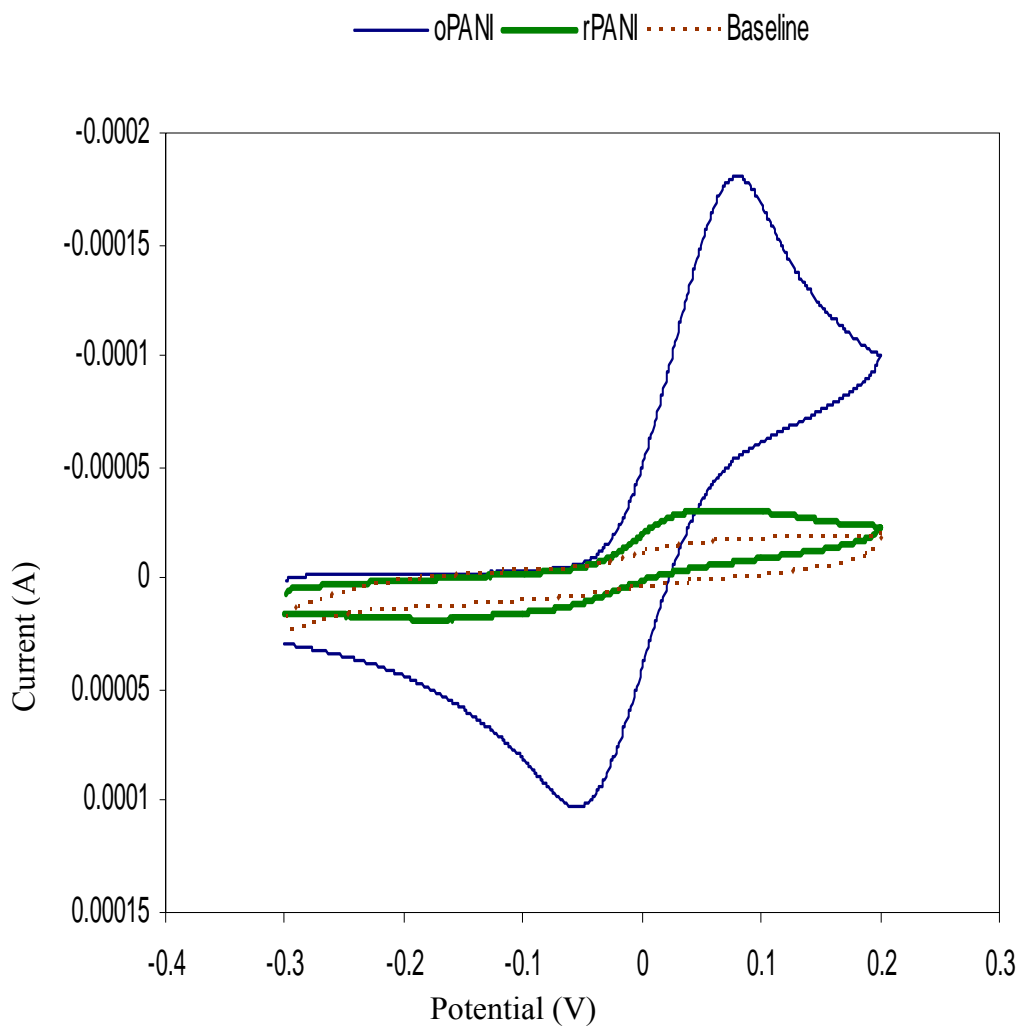


Figure 2.2 Cyclic voltammograms of Rabbit sandwich assay on oxidized (blue solid line), reduced polyaniline modified gold electrodes (green solid line) and baseline caused by pAPP non-enzymatic hydrolysis (brown dashed line). (Scan rate=100 mV/s, C_{pAPP} =4mM, and incubation time=30 min)

used as the immunosensor to detect specific antigens. However, reduced polyaniline film cannot produce a good signal for immuno-sandwich assays. Therefore, the leucoemeraldine form of polyaniline is not a good substrate for the immunosensor. It seems reasonable to suggest that antibodies nucleophilically attack the quinoid ring of the emeraldine form of polyaniline. As the leucoemeraldine form contains no quinoid rings, there is no reaction between the reduced polyaniline and the antibodies.

2.3.2.2 Cross reaction of Anti-rabbit IgG and Anti-Sheep IgG

Three types of oxidized polyaniline electrodes were used in this research. One electrode was modified by a sheep IgG sandwich assay (sIgGsw), and the second by a rabbit IgG sandwich assay (rIgGsw). For the third electrode, after the anti-sheep IgG had been laid down on the surface the electrode was reacted with rabbit IgG. Finally, this electrode was immersed into labeled anti-rabbit IgG solution for half an hour. This sample is referred to as the sAb-rAg-rAb* electrode. In Figure 2.3, cyclic voltammograms of 4-aminophenol are shown for these three kinds of immunoassay. Both the anti-rabbit and anti-sheep IgG sandwich assays on oxidized polyaniline film exhibited very good cyclic voltammetry signals, with peak currents of about 10^{-4} A for oxidation of 4-aminophenol. This indicates that anti-sheep IgG have attached to the oxidized polyaniline as well as anti-rabbit IgG and this sandwich assay can therefore also be used to detect sheep IgG. However, although the anti-sheep IgG did attach successfully to the oxidized polyaniline film, only a very small signal was obtained for the rabbit IgG (Figure 2.3). According to Figures 2.2 and 2.3, both anti-rabbit IgG and anti-sheep IgG can be immobilized on an oxidized polyaniline surface and anti-sheep IgG has no reaction with rabbit IgG. It therefore seems likely that the weak signal might be due to non-specific

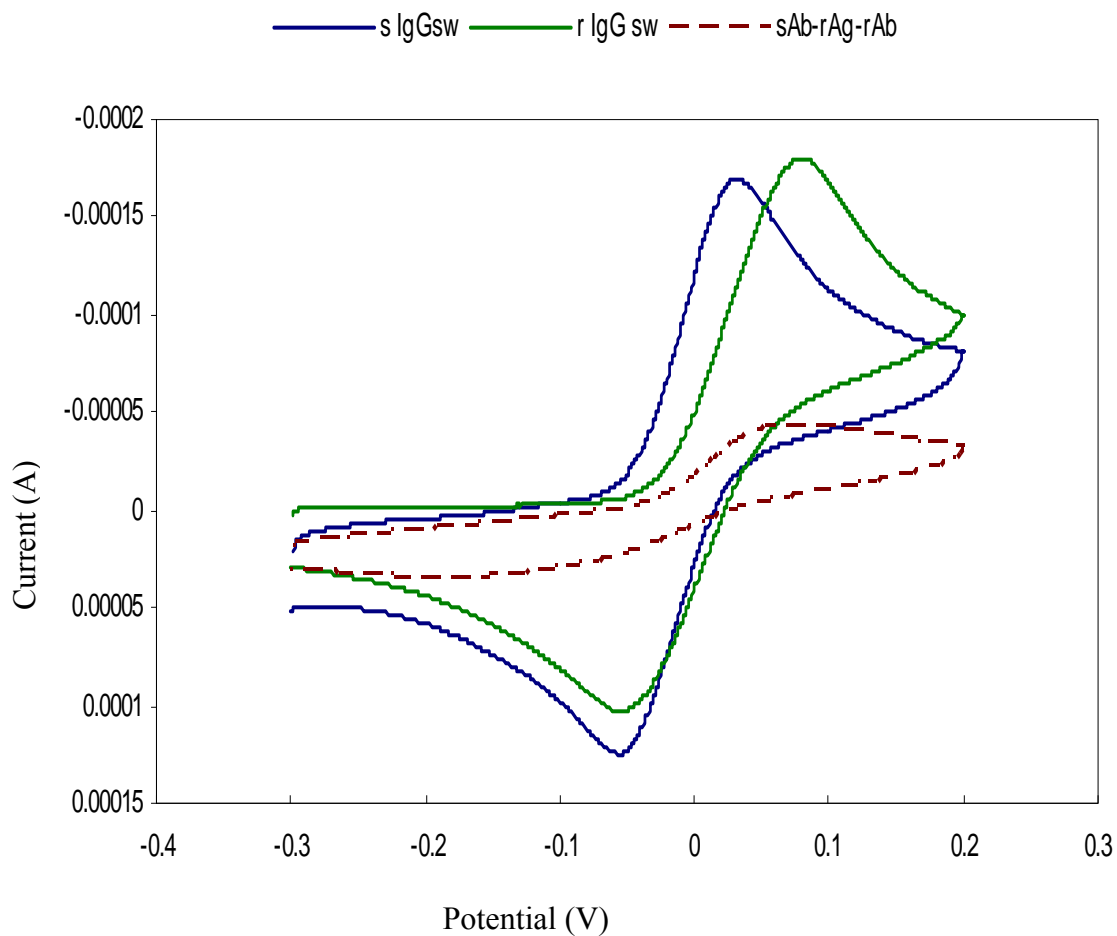


Figure 2.3. Cyclic voltammograms of Rabbit, Sheep IgG sandwich assay and cross reaction between Rabbit and Sheep IgG on oxidized polyaniline modified gold electrodes. (Experimental condition as in figure 2.2)

adsorption of labeled anti-rabbit IgG on the oxidized polyaniline film. Figures 2.2 and 2.3 suggest that both rabbit and sheep IgG can be qualitatively and quantitatively analyzed simultaneously in a mixed solution of sheep IgG and rabbit IgG mixed solution if two electrode arrays modified with different antibodies are used.

Attempts were also made to construct a sheep IgG sandwich assay on reduced polyaniline, along with a rabbit IgG sandwich assay. Figure 2.4 shows that the reduced polyaniline does not react with anti-sheep IgG, however, since only a negligible peak current for the 4-aminophenol electrochemical reaction on the electrode was produced. This result is similar to that for the rabbit IgG reaction on reduced polyaniline and provides further evidence that reduced polyaniline does not react with antibodies. Here, the polyaniline film was first reduced under -200 mV and then immersed into anti-sheep IgG, after which the electrode was oxidized under 600 mV potential in 0.5 M H_2SO_4 solution and then modified with rabbit IgG sandwich assay. The resulting cyclic voltammogram is given in Figure 2.4. The peak current of 4-aminophenol produced on this electrode is almost the same as that on the electrode with the rabbit sandwich assay directly prepared on oxidized polyaniline film, also shown in Figure 2.4. This result indicates that immersing reduced polyaniline film with sheep IgG beforehand did not affect the performance of the immunosensor if it is to be reused as the electrode surface for a rabbit IgG immunoassay after reoxidation of the polyaniline.

Figure 2.4 further proves that only oxidized polyaniline can react with antibodies. Consequently, according to these data it would be possible to design an array of cantilevers or microelectrodes that can detect different proteins by controlling the chemical state of polyaniline at the same time. For example, some cantilever or

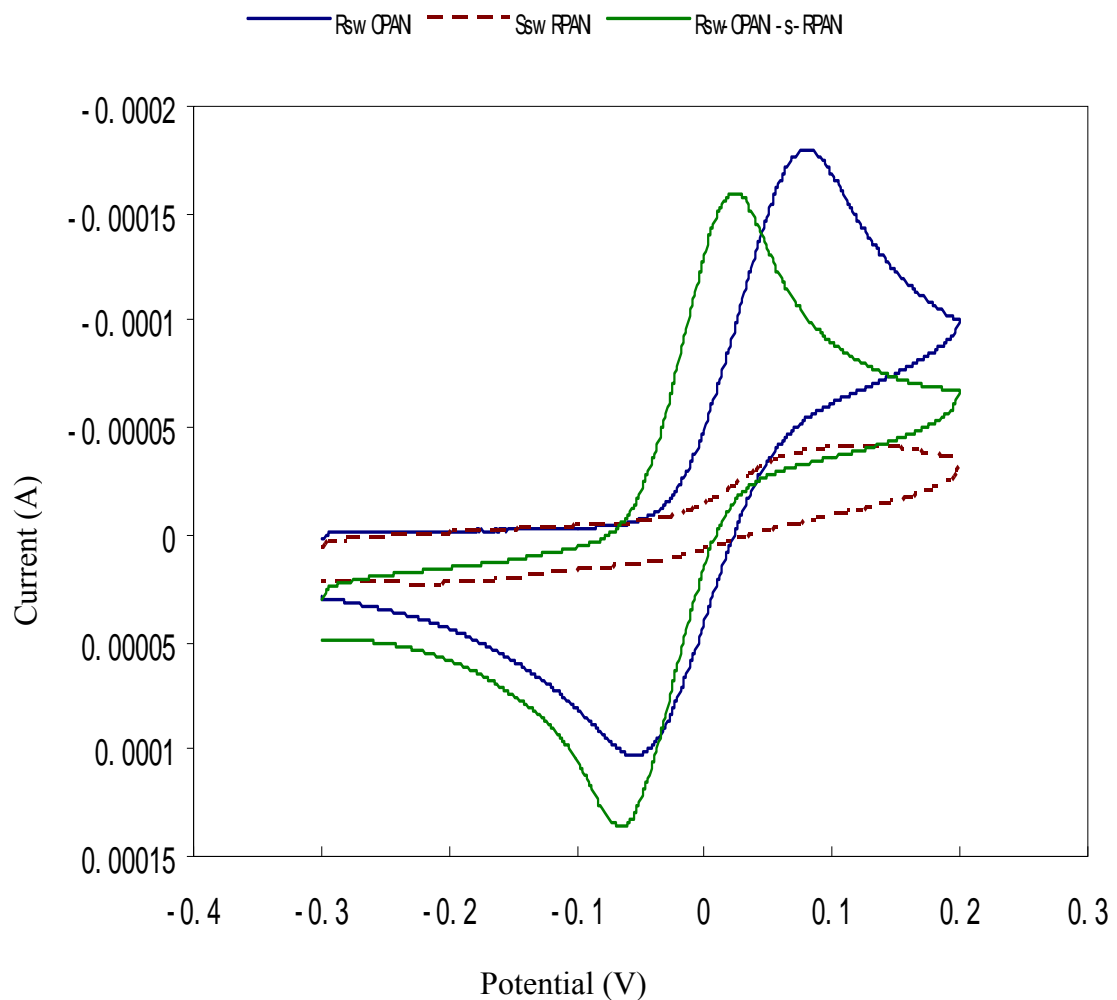


Figure 2.4 Cyclic voltammogram of the electrodes with Rabbit IgG sandwich assay on oxidized polyaniline (blue line); Sheep IgG sandwich assay on reduced polyaniline (brown dashed line); and Rabbit IgG sandwich assay prepared by first reducing polyaniline at -200 mV for 5 min, followed by immersion in anti-Sheep IgG, oxidizing the polyaniline on the electrode and then modifying it with anti-rabbit IgG. (Experimental condition as in figure 2.2)

microelectrode arrays can be deposited with oxidized polyaniline film, while others are deposited with reduced polyaniline film. After immersion in anti-rabbit IgG solution, the oxidized polyaniline samples will have been modified with anti-rabbit IgG while the reduced polyaniline film has not attached any antibodies. The reduced polyaniline on the unmodified cantilevers or microelectrodes can then be reoxidized by applying a 600 mV potential in 0.5 M H₂SO₄. Now, the anti-sheep IgG can be immobilized on these cantilevers or microelectrodes with oxidized polyaniline, thus producing an array of cantilevers or microelectrodes that have been modified with two different antibodies (anti-rabbit IgG and anti-sheep IgG) in order to detect rabbit IgG and sheep IgG at the same time.

2.3.2.3 Reactivity of Fab Fragment of anti-rabbit IgG

For most applications, a critical consideration for antibody immobilization is the orientation of the antibody binding site with respect to the surface. In order to improve the activity of the immobilized antibodies, several groups have focused on the covalent attachment of F(ab)₂ fragments of IgG to thiol reactive linker modified substrates through a native thiol group on the antibody that is structurally opposite to the antigen-binding site³³⁻³⁶. It is known that the F(ab)₂ fragments retain their immunoreactivity.

Han et al. have suggested that small nucleophilic molecules, such as amines and thiols, can form covalent bonds to the polyaniline backbone⁵⁻⁷. We have demonstrated that butanethiol can covalently attach onto oxidized polyaniline backbone by MALDI-MS data. The F(ab) fragment of the antibody has a thiol group at the end, therefore we propose that using the F(ab)₂ fragment of the antibody could result in a better orientation of the antibody on the polyaniline film than is possible using the whole monoclonal

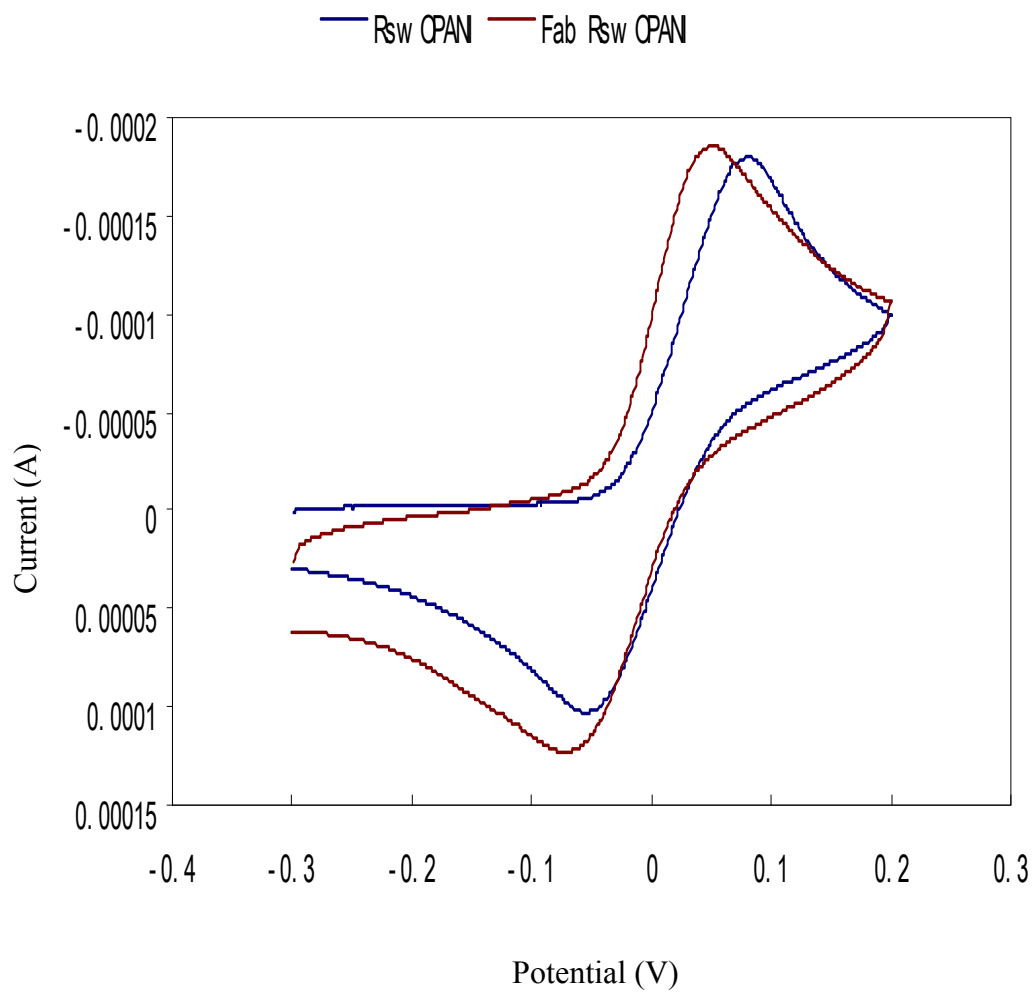


Figure 2.5 Cyclic voltammogram for the electrode with monoclonal anti-rabbit IgG sandwich assay and F(ab) fragment of anti-rabbit IgG sandwich assay on oxidized polyaniline film (Experimental condition as in figure 2.2)

antibody. The effect of using the F(ab)₂ fragment of anti-rabbit IgG for this immunoassay instead of monoclonal anti-rabbit IgG is shown in Figure 2.5. According to the figure, the oxidation peak of 4-aminophenol at 0.1 V on the surface of the F(ab)₂ fragment anti-rabbit IgG sandwich assay modified electrode is a little stronger than that obtained for the whole monoclonal anti-rabbit IgG sandwich assay. This small enhancement of the oxidation peak may indicate a little better orientation of F(ab)₂ fragment antibody on the oxidized polyaniline, although it may arise only as a result of experimental error. The data indicates that using F(ab)₂ fragments of the antibody produces little improvement in the level of sensor activity. The reason for this is not clear based on the current data.

2.3.2.4 The influence of 11-mercapto-1-undecanol on the interaction between antibodies and oxidized polyaniline

Anti-sheep IgG should have absolutely no reaction with rabbit IgG. However, Figure 2.3 c reveals a small signal in the cyclic voltammogram for the electrode with cross sandwich assay (sAb-rAg-rAb^{*}). This small signal might result from the non-specific adsorption of rabbit IgG and enzyme labeled rabbit IgG on the polymer film.

In order to eliminate this non-specific adsorption, we immersed the electrode in 0.1 mM 11-mercapto-1-undecanol in buffer solution after modifying the electrode with monoclonal anti-rabbit IgG. The electrode was then reacted with rabbit IgG, followed by enzyme-labeled anti-rabbit IgG. This treatment decreased the cyclic voltammetry signal on this electrode dramatically compared to those electrodes on which the rabbit IgG sandwich assay directly prepared on the oxidized polyaniline film (Figure 2.6), possibly because the 11-mercapto-1-undecanol reacted with polyaniline and replaced the anti-rabbit IgG on the polyaniline film.

To test whether 11-mercapto-1-undecanol reacts more readily with oxidized polyaniline than monoclonal anti-rabbit IgG, 11-mercapto-1-undecanol was reacted first with an oxidized polyaniline film on a gold electrode and then the sandwich assay was prepared on the electrode. The oxidized peak for PAP generated on this electrode was much smaller than on the electrode with the rabbit sandwich assay directly prepared on oxidized polyaniline. These results indicate that the reactivity of oxidized polyaniline film with anti-rabbit IgG decreases dramatically after reacting the electrode with 11-mercapto-1-undecanol. Consequently, 11-mercapto-1-undecanol cannot be used to reduce non-specific adsorption as it deactivated the polyaniline and made it much less reactive with protein.

Exchanging the monoclonal anti-rabbit IgG for the F(ab)₂ fragment of anti rabbit IgG and repeating the experiment revealed very different results, however. Even treating the F(ab)₂ fragment anti-rabbit IgG modified electrode with 11-mercapto-1-undecanol before reacting it with antigens (rabbit IgG) decreased the peak current in the cyclic voltammogram only slightly compared to the corresponding sandwich assay directly on polyaniline film (Fig 2.7). 11-mercapto-1-undecanol clearly did not deactivate the reaction of polyaniline with the F(ab) fragment of anti-rabbit IgG. The small decrease in the signal may result from the elimination of non-specific adsorption. Han et al.⁵ have shown that alkanethiols such as dodecane-1-thiol and butane-1-thiol react with polyaniline at a much higher rate (*ca.* 1000 times faster) than amines. We therefore propose that monoclonal antibodies reacted with oxidized polyaniline through nucleophilic amine groups to form covalent bonds. It is also possible that the interactions between monoclonal antibodies and polyaniline are electrostatic. This interaction is weak

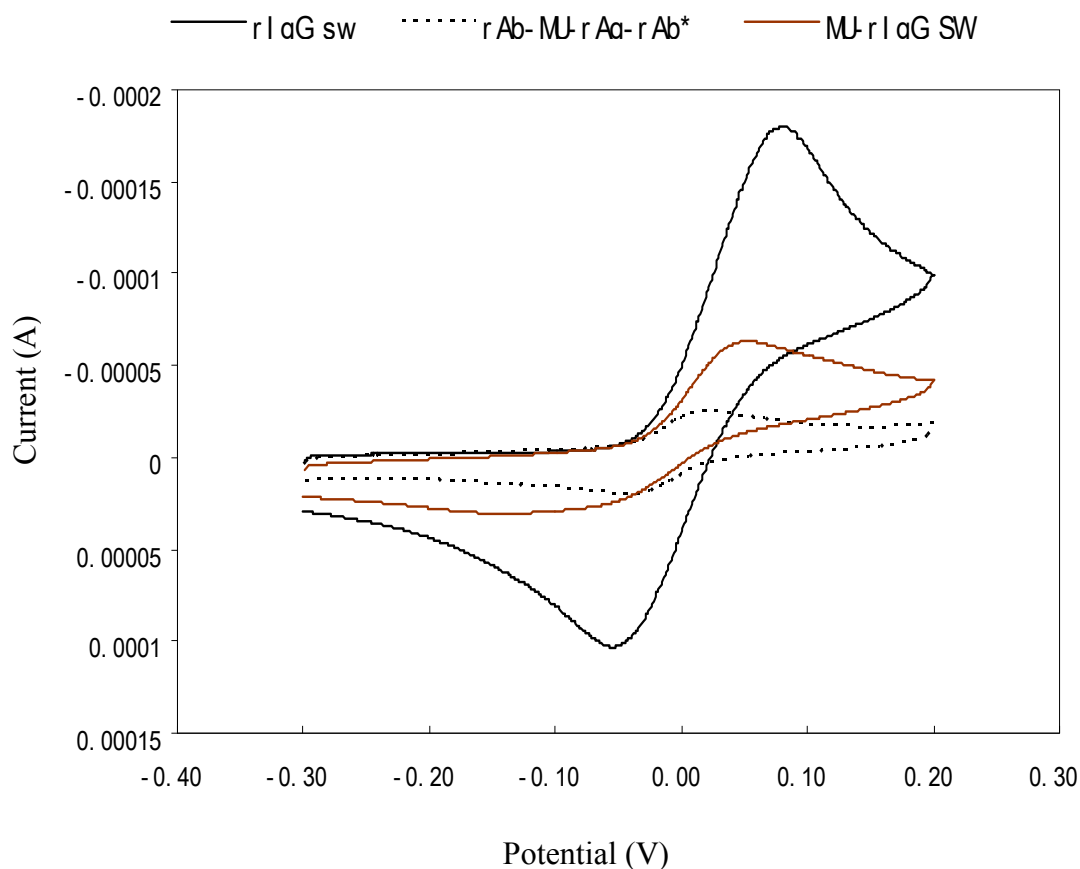


Figure 2.6 Cyclic voltammograms on the electrode with the following modifications: monoclonal anti-rabbit IgG sandwich assay (black solid line); rabbit anti IgG on oxidized polyaniline surface followed by immersion in 1mM 11mercapto-1-undecanol solution in buffer A for 1 hr, then reaction with rabbit IgG and finally labeled rabbit anti IgG (black dashed line); immersion of the electrode with polyaniline film into 1mM 11mercapto-1-undecanol solution in buffer A for 1 hr followed by soaking in rabbit anti IgG solution for 1 hr, reaction with rabbit IgG and finally labeled rabbit anti-IgG consequently (solid brown line). (Experimental condition as in figure 2.2)

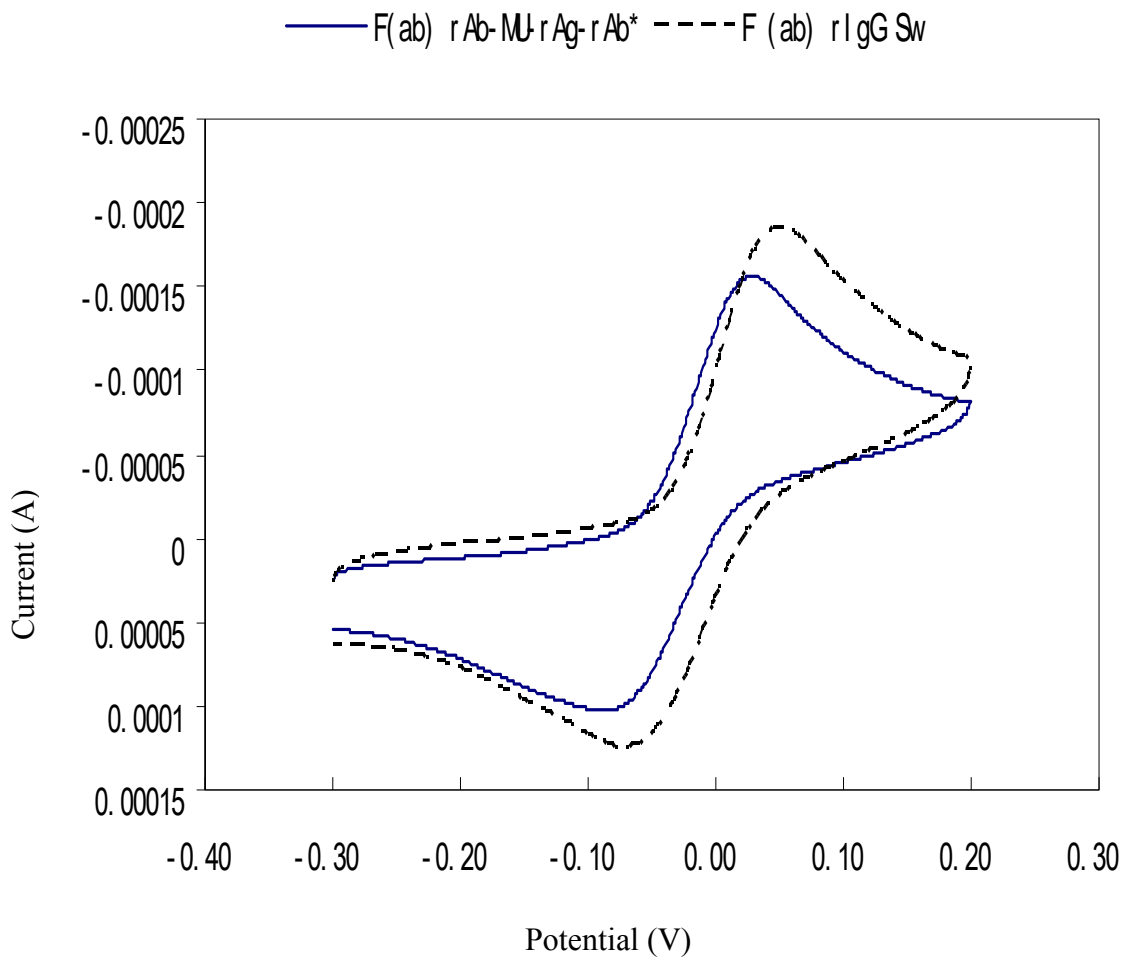
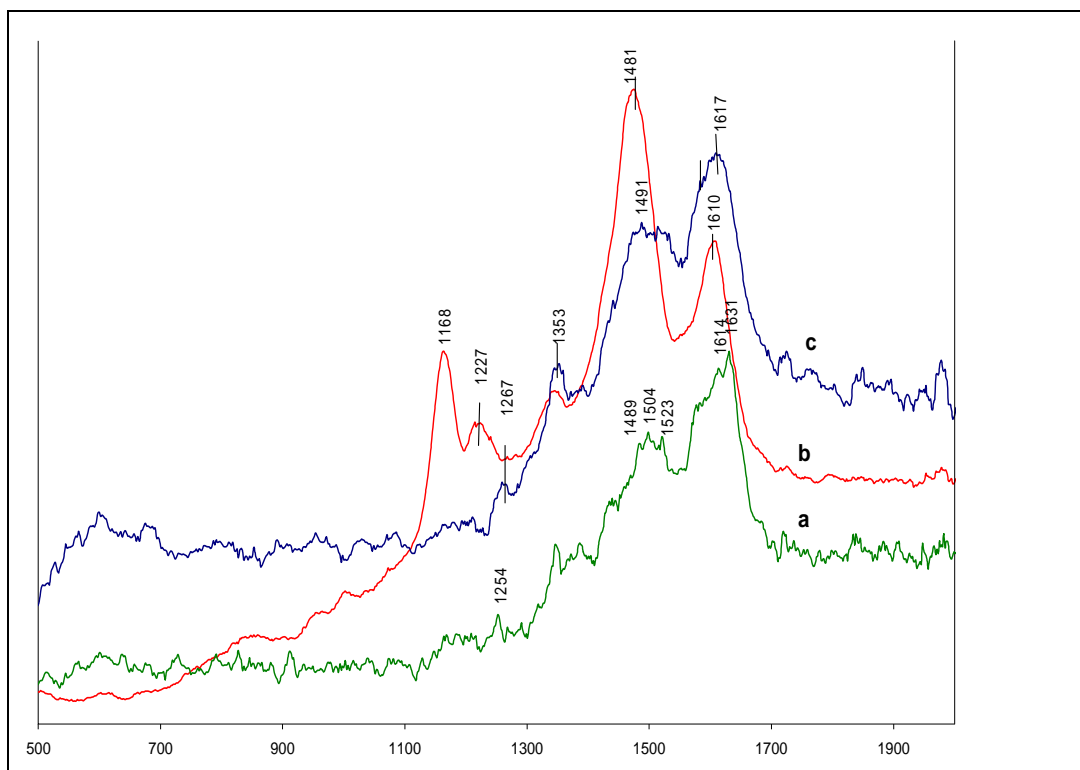


Figure 2.7 Cyclic voltammogram for the electrode with F(ab) fragment of anti-rabbit IgG sandwich assay on oxidized polyaniline film (black dashed line) and electrode obtained by modifying first with rabbit anti IgG (Fab fragment) on oxidized polyaniline surface followed by immersion in 1mM 11-mercapto-1-undecanol solution in buffer A for 1 hr, reaction with rabbit IgG and finally labeled anti-rabbit IgG. (Experimental condition as in figure 2.2)

and antibodies are easily replaced by the thiol group on 11-mercapto-1-undecanol. However, the F(ab)₂ fragment antibody also has a thiol group at the end which could nucleophilically attack the polyaniline backbone to form a covalent bond, preventing the F(ab) fragment of the antibody from being replaced by 11-mercapto-1-undecanol and allowing the immunoassay to retain its sensitivity, as shown in Figure 2.7.

2.3.3. Surface Enhanced Raman Spectroscopy (SERS)

The Raman spectra of an oxidized polyaniline film formed from the reaction between oxidized polyaniline and anti-rabbit IgG F(ab)₂ fragments, and reduced polyaniline film are presented in Figure 2.8 and the corresponding Raman peak assignments are displayed in Table 2.2. It is clear from this figure that the Raman spectra change dramatically as a result of modifying the oxidized polyaniline electrode with F(ab)₂ fragment anti-rabbit IgG. After reaction with the antibody, the Raman spectrum of the oxidized polyaniline film is transformed, becoming close to the spectrum of the reduced polyaniline film. The peak at 1163 cm⁻¹, which corresponds to the quinoid ring C-H in-plane bending ring¹⁷⁻¹⁹, and the peak at 1227 cm⁻¹, which corresponds to the C-N stretch both disappear after the oxidized polyaniline has reacted with the antibody. The most intense peak of the spectrum recorded for polyaniline film treated at 600 mV appears at about 1490 cm⁻¹. The intensity of the peaks at 1490-1500 cm⁻¹, which are assigned to the C=N stretching + C-C stretch + C-H bending on the quinoid ring, decreased compared to the peaks at 1610-1630 cm⁻¹, which are ascribed to the C-C stretch + C-H bending on the benzenoid ring¹⁹. This evidence indicates that the emeraldine form of polyaniline was reduced after immersion into a solution of F(ab)₂ antibody fragments.



Wave number (cm^{-1})

Figure 2.8 Raman spectrum of a) reduced polyaniline film; b) oxidized polyaniline film and (c) polyaniline film after the oxidized form has reacted with F(ab) fragments of Rabbit IgG. The excitation wavelength is 632.5 nm. (Collection time =20 s)

Table 2.2 Assignment of Raman peaks of Polyaniline

<i>Wave Numbers (cm⁻¹)</i>	<i>Assignment</i>
1615-1615	Benzoid ring, C-C stretching, C-H bending
1585-1595	Quinoid ring, C=C stretching
1560-1550	Benzoid ring, C-C stretching
1486-1500	Quinoid ring, C=N stretching C-C stretching
1415-1425	Quinoid ring, C-C stretching
1213-1225	Quinoid ring, C-N stretching
1160-1165	Quinoid ring, In-plane C-H bending

2.4. Discussion

All the cyclic voltammetry results and Raman results reported here indicate that antibodies can be reacted with oxidized polyaniline to produce a good immunosensor that can be used to detect the corresponding antigen. From previous data obtained by our group, an oxidization potential applied on polyaniline films at 600 mV, produced the largest peak current for PAP. Above 600 mV, polyaniline is easily degraded. Therefore, 600 mV was chosen as the oxidation potential for this study. Table 2.3 shows the oxidized peak current for PAPP enzymatic hydrolysis on electrodes with different modifications. The peak currents for electrodes with sandwich assays on oxidized polyaniline are 1.5×10^{-4} - 1.8×10^{-4} A. However, the peak currents for electrodes with sandwich assays on the reduced polyaniline form are 2.4×10^{-5} - 4.8×10^{-5} almost an order of magnitude smaller than for the oxidized polyaniline form.

Although antibodies may attach to an oxidized polyaniline surface through electrostatic interaction, Han et al.⁵⁻⁷ reported that the quinonimine units present in PANI may be attacked by nucleophiles. MALDI-MS data indicate that oxidized PANI reacts with butanethiol in aqueous solution to form a new polyaniline format and SERS data suggests that F(ab) antibody fragments reduce the emeraldine form of polyaniline into the leucoemeraldine form. Although there is no direct evidence to prove whole monoclonal antibodies can nucleophilically attack the quinonimine units of oxidized polyaniline, it can be proved that F(ab)₂ antibody fragments can attach to the polyaniline backbone through nucleophilic reaction to form covalent bonds using cyclic voltammetry, surface enhanced Raman and MALDI-MS data. According to the cyclic voltammetry results, it is also

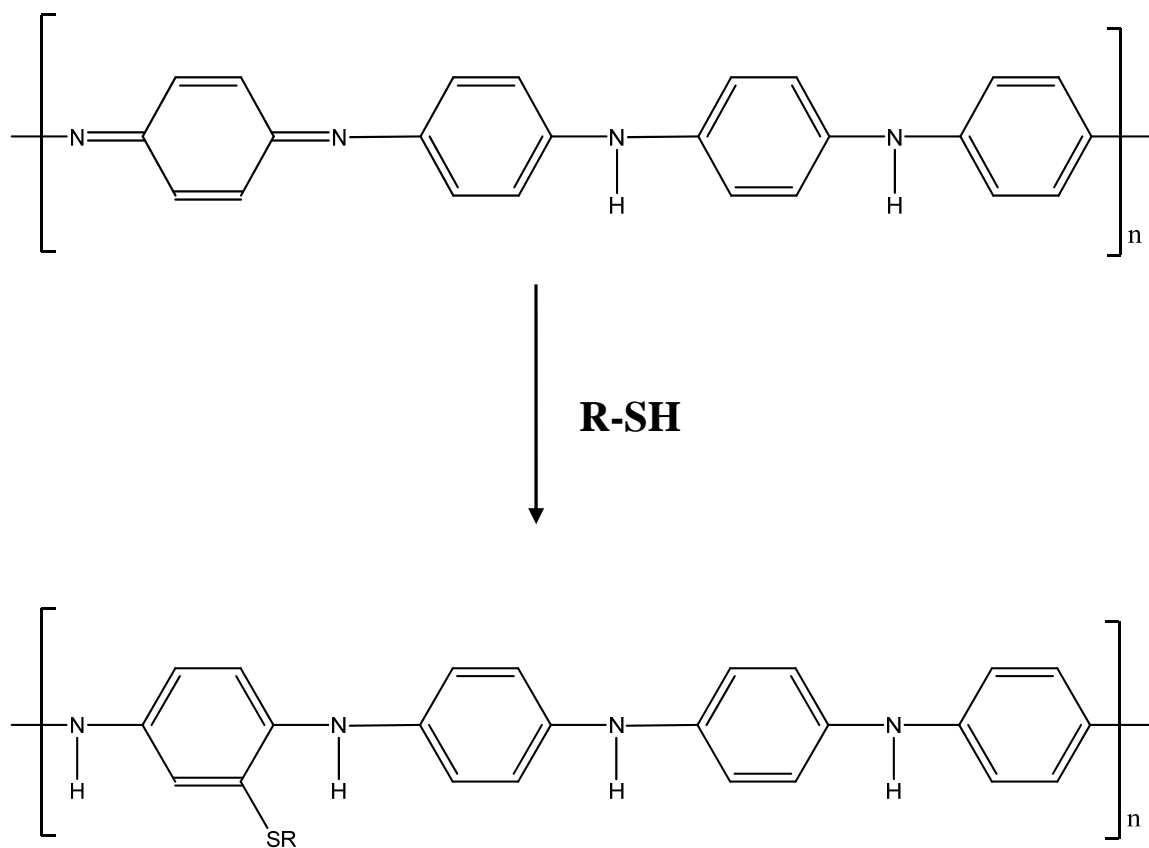
possible that nucleophiles such as the amine group in monoclonal antibodies attacks the quinonimine units in oxidized polyaniline.

Raman spectroscopy has provided evidence that the polyaniline prepared at 600 mV exists as the oxidized form containing much more quinonimine units, and is therefore more susceptible to nucleophilic attack than polyaniline prepared at -200 mV. After immersing the oxidized polyaniline into F(ab)₂ fragment antibody solution, the Raman spectrum changed, with a stronger signal for benzenoid rings and weaker quinonimine signals, indicating that the polyaniline was reduced by F(ab)₂ fragment anti-rabbit IgG. Weak Raman peaks at 1490-1510 cm⁻¹ in the reduced form polyaniline film, which are assigned to the C=N stretching + C-C stretch +C-H bending modes on the quinoid ring, may have resulted from exposing the electrode to water for a short time when rinsing, thus oxidizing a very small part of the polyaniline. After exposing the electrode in air for two hours, the polyaniline film with anti-rabbit IgG was found to be reoxidized. Moreover, the anti-rabbit IgG attached on the benzenoid ring might induce a change in the geometry of the polyaniline. As Figure 2.9 reveals, exposing the polyaniline film with anti-rabbit IgG to water for 2 hours causes the strong peak at 1167 to reappear and the resulting spectrum (Figure 2.9 c) is close to that of the emeraldine form (Figure 2.9 a). This indicates that the functionalized polyaniline was reoxidized by exposing the electrode to water. In Figure 2.9, the intensity of the peak at 1347 cm⁻¹ for the ν_s (C~N⁺) vibration after reoxidizing the antibody functionalized polyaniline is broader and much more significant than the peak from the original oxidized polyaniline. It had previously been reported that peaks in 1300-1400 cm⁻¹ region are associated with the ν_s (C~N⁺) vibration, where ~ denotes the bond intermediate between the single and double bond, and this vibrational mode is affected by

Table 2.3 Oxidized peak current for PAPP enzymatic hydrolysis on electrodes with different modifications

Electrode modification	Ip (peak current of CV) / A
Baseline (gold foil)	4.90E-06
rIgG sw on RPANI	2.40E-05
rIgG sw on OPANI	1.76E-04
sIgG sw on RPANI	2.90E-05
sIgG sw on OPANI	1.60E-04
cross reaction sAIgG-rIgG-rAIgG* on OPANI	3.70E-05
RPANI-sAIgG-OPANI-rAIgG-rIgG-rAIgG*	1.50E-04
Fab rIgG sw on OPANI	1.83E-04
rAIgG-SHOH-rIgG-rAIgG*	4.80E-05
SHOH-rAIgG-rIgG-rAIgG*	1.50E-05
FabrAIgG-SHOH-rIgG-rAIgG*	1.47E-04

rIgG: rabbit IgG, sIgG: sheep IgG, rAIgG: anti-rabbit IgG, sAIgG: anti-sheep IgG, FabrAIgG: anti-rabbit IgG sandwich assay, rAIgG*: Labeled anti-rabbit IgG, sAIgG: labeled anti-sheep IgG, OPANI: Oxidized polyaniline, RPANI: Reduced polyaniline, sw: sandwich assay, SHOH: 11-mercapto-1-undecanol



Scheme 2.4 Model of the attachment of an antibody to the emeraldine state of polyaniline

the ring sulfonation^{18,37}. As we expected, the polyaniline ring was functionalized by the antibody in our work, just as for ring sulfonation, and consequently the high intensity and broader peak might be due to an interaction between the antibody on the ring and the highly protonated emeraldine form of polyaniline (a bipolaron or two polarons) produced after exposing the functionalized polyaniline in the water for 2 hours. Moreover, the higher frequency peaks in the 1490-1510 cm^{-1} region assigned to the C=N stretching + C-C stretch + C-H bending on the quinoid ring appeared on the antibody modified polyaniline rather than on the oxidized polyaniline without modification. It has been suggested that the higher frequency in this region might be associated with more localized polaronic sites^{18,38}. Yue et al.³⁹ reported increased charge localization for ca. 50% ring-sulfonated polyaniline compared with emeraldine hydrochloride salt using XPS analysis and assumed that the hydrogen bonding or electrostatic interaction between the SO_3^{2-} group and positively charged nitrogen sites were responsible for this localization. Proteins contain many hydrogen bonds and negative charges, which may cause the peak shift in the region of 1490-1510 cm^{-1} in the on Raman spectra of polyaniline discussed above, since hydrogen bonds and/or the electrostatic interaction between the negative charge on antibodies and positively charged nitrogen could increase the charge localization.

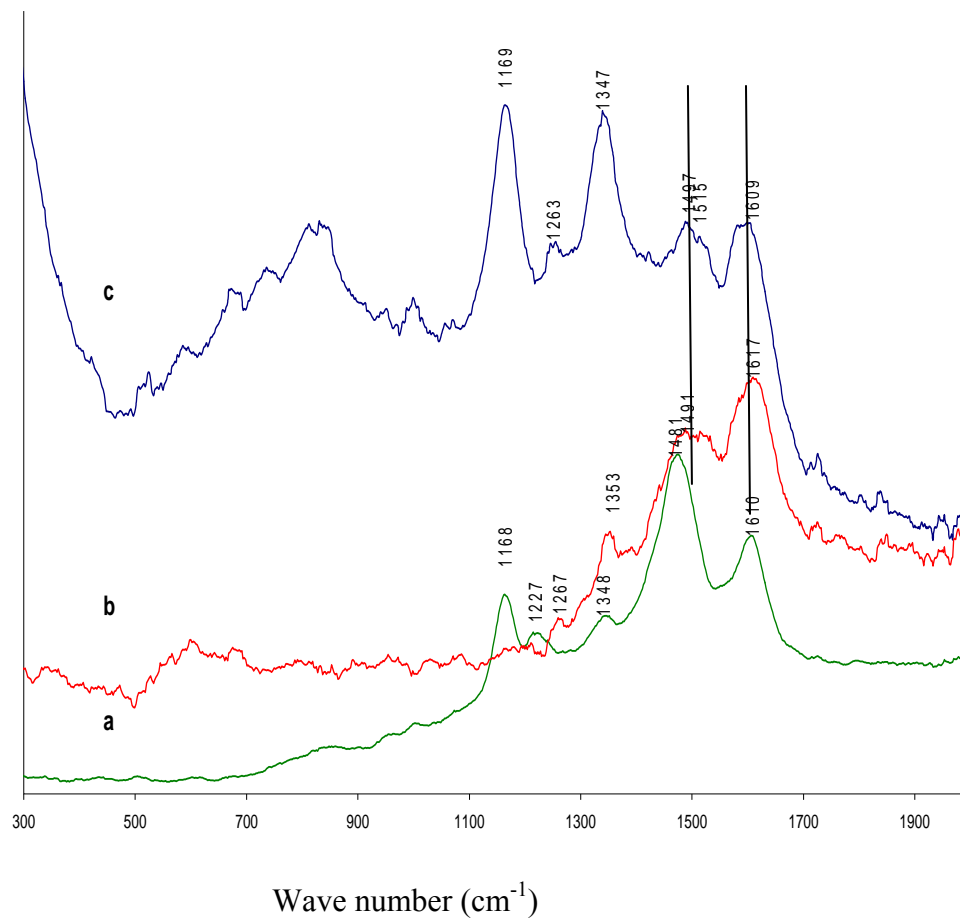


Figure 2.9 Raman spectra of oxidized polyaniline film (a); polyaniline film after oxidized form reacting with F(ab) fragment of Rabbit IgG (b); and polyaniline film after oxidized form reacting with F(ab) fragment of Rabbit IgG and then exposure to water for 2 hours (c) . The excitation wavelength is 632.5 nm. (Collection time =20 s)

2.5. Conclusions and future application

Electrochemical studies have shown that only oxidized forms of polyaniline can react with anti-rabbit IgG and anti-sheep IgG to form a good immunosensor. It is proposed that the antibody could be nucleophilically attached to the polyaniline quinoid ring by an amino group or thiol group. Zhou and co-workers analyzed cytochrome *C* on a polyaniline modified gold electrode¹² and found the polyaniline film was reduced by the thiol group on cytochrome *C* and a sulfide bond to the polyaniline backbone was formed. In the work reported here, F(ab)₂ fragments of anti-rabbit IgG were immobilized on support matrices and cyclic voltammetry results obtained for the 4-aminophenol electrochemical reaction ($I_p = 1.83 \times 10^{-4}$), which was found to be similar to that obtained on a monoclonal anti-rabbit IgG immobilized surface ($I_p = 1.76 \times 10^{-4}$). According to the results shown in Figures 2.6 and 2.7, there was a significant difference in the influence of 11-mercapto-1-undecanol on the activity of sensors with sensing elements of monoclonal anti-rabbit IgG or F(ab)₂ fragments of anti-rabbit IgG. This result might be because monoclonal anti-rabbit IgG is coupled with the surface of polyanilines via nucleophilic amine groups on lysine, which is outside the protein. As for F(ab) fragment of protein, the thiol groups are located at the ends of the protein molecule and it can therefore react with oxidized polyaniline via a sulfide bond to form the corresponding derived polyaniline backbone. It has been proposed that 11-mercapto-1-undecanol could replace the monoclonal antibody since the sulfide bond is likely to be stronger than the amide bond to the polyaniline. However, it could not replace the F(ab) fragment of the antibody because F(ab) fragments are also connected to polyaniline by sulfide bonds.

The Raman spectra collected for this study also provided evidence that the emeraldine form of polyaniline is converted into the leucoemeraldine form after reaction with F(ab)₂ fragment antibody solution. In the proposed application, an array of cantilever biosensors or microelectrode immunosensors can be designed to detect a panel of target antigens by modifying each cantilever or microelectrode with a different antibody and controlling the chemical state of polyaniline film on the surface of substrate, as shown in Figure 2.10.

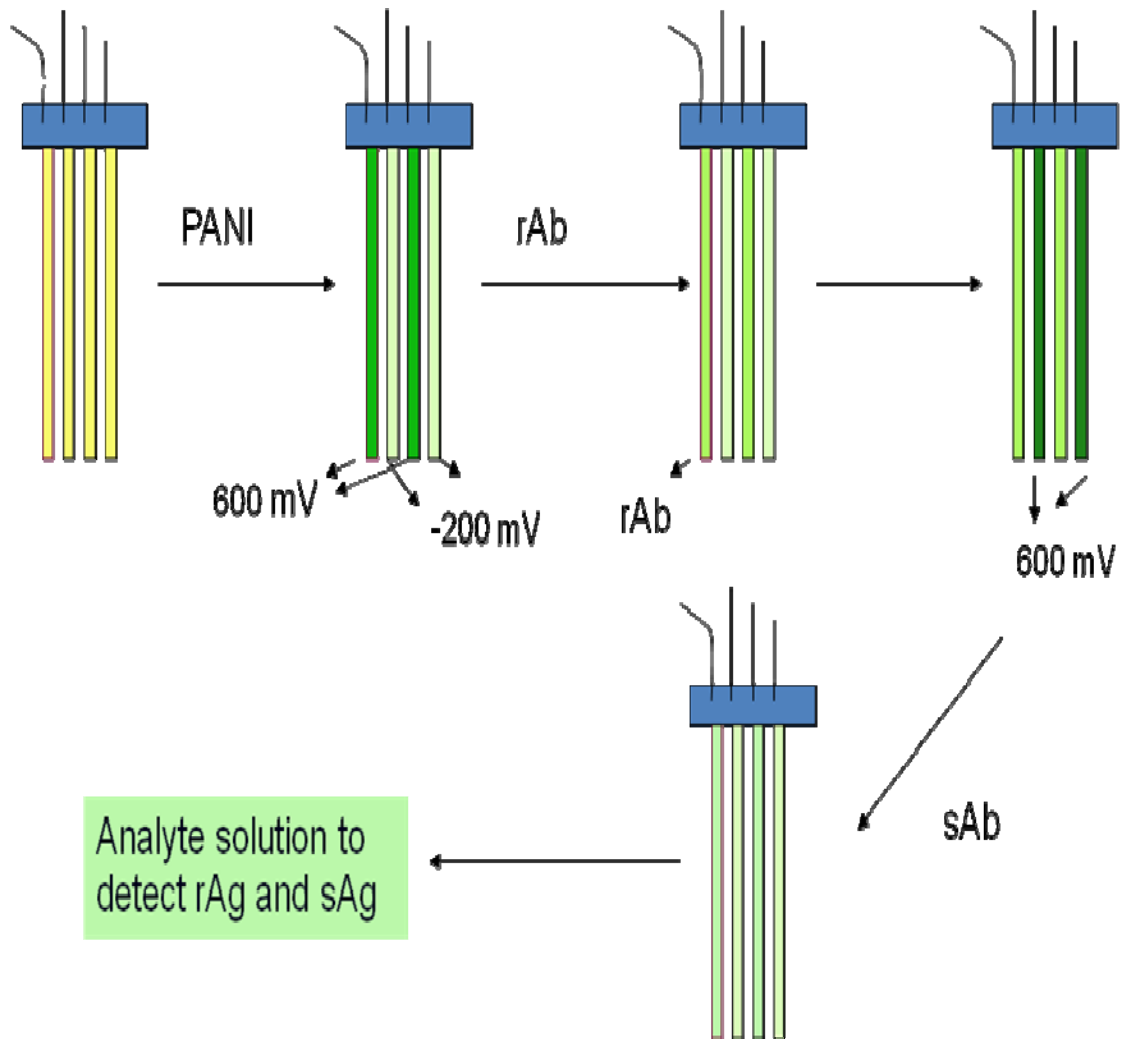


Figure 2.10 Proposed application of immunosensor array prepared on polyaniline film

References

1. Nalwa, H. S., *Handbook of Organic Conductive Molecules and Polymers*. John Wiley & Sons: Chichester and New York, 1997; Vol. 1-4.
2. Genies, E. M.; Boyle, A.; Lapkowski, M.; Tsintavis, C., *Syn. Met.* **1990**, 36, 139.
3. Mazur, M.; Krysinski, P., *J. Phys. Chem. B* **2002**, 106, 10349.
4. Chandrakanthi, N.; Careem, M. A., *Polym. Bull. (Berlin)* **2000**, 45, 113.
5. Han, C. C.; Jeng, R., *Chem. Commun.* **1997**, 553.
6. Han, C. C.; Hseih, W. D.; Yeh, J. Y.; Hong, S. P., *Chem. Mater.* **1999**, 11, 480.
7. Han, C. C.; Hong, S. P.; Yang, K. F.; Bai, M. Y.; Lu, C. H.; Huang, C. S., *Macromolecules* **2001**, 34, 587.
8. Amanda, J. H.; Richard, P. V., *Anal. Bioanal. Chem.* **2004**, 379, 920.
9. Haehner, G. M.; Spencer, N. D., *Tribology Lett.* **1997**, 3, 359.
10. Aguilar, Z. P.; Vandaveer, W. R.; Fritsch, I., *Anal. Chem.* **2002**, 74, 3321.
11. Treloar, P. H.; Nkohkwo, A. T.; Kane, J. W., *Electroanal.* **1994**, 6, 561.
12. Zhou, Y. X.; Yu, B.; Levon, K., 1, *Syn. Met.* **2003**, 142, 137.
13. McCreery, R. L., *Raman spectroscopy for chemical analysis*. In John Wiley & Sons: New York, 2000; p 420.
14. Haynes, C. L.; Van Duyne, R. P., *J. Phys. Chem. B* **2003**, 107, 7426.
15. McFarland, A. D.; Young, M. A.; Dieringer, J. A.; Van Duyne, R. P., *J. Phys. Chem. B* **2005**, 109, 11279.
16. Medyantseva, E. P.; Khaldeeva, E. V.; Budnikov, G. K., *Journal of Analytical Chemistry* **2001**, 56, 886.
17. Arsov, L. D.; Plieth, W.; Kobmehl, G., *J. Solid State Electrochem.* **1998**, 2, 355.

18. Niaura, G.; Mazeikiene, R.; Malinauskas, A., *Syn. Met.* **2004**, 145, 105.
19. Baibaric, M.; Cochet, M.; Lapkowski, M.; Mihut, L.; Lefrant, S.; Baltog, I., *Syn. Met.* **1998**, 96, 63.
20. Karas, M.; Bachmann, D.; Bahr, U.; Hillenkamp, F., *Int. J. Mass Spectrom. Ion Processes* **1987**, 78, 53.
21. Karas, M.; Hillenkamp, F., *Anal. Chem.* **1988**, 60, 2301.
22. Zhang, J.; Cass, A. E. G., *Analytica Chimica Acta.* **2000**, 408, 241.
23. Liu, Y.; Hsu, T.; Tsa, J., *J. Phys. Chem. C* **2007**, 111, 10570.
24. Liu, Y.; Wang, C.; Tsai, C., *Electrochem. Commun.* **2005**, 7, 1345.
25. Przybilla, L.; Brand, J. D.; Yoshimura, K.; Rader, H. J.; Mullen, K., *Anal. Chem.* **2000**, 72, 4591.
26. Trimpin, S.; Rouhanipour, A.; Az, R.; Rader, H. J.; Mullen, K., *Rapid Commun. Mass Spectrom.* **2001**, 15, 1364.
27. Trimpin, S.; Grimsdale, A. C.; Rader, H. J.; Mullen, K., *Anal. Chem.* **2002**, 74, 3777.
28. Dolan, A. R.; Wood, T. D., *Synth. Met.* **2004**, 143, 243.
29. Ruan, C.; Li, Y., *Talanta* **2001**, 54, 1095.
30. Li, F. Electrochemical studies of underpotential deposition with surface plasmon resonance and enzyme immunoassay Auburn University, Auburn, 2004.
31. Huang, W.; Hua, W.; Song, J., *Talanta* **2003**, 61, 411.
32. Schwarz, J.; Wolfram, O. n.; Heiner, K.; Frank, S.; Horst, H., *Electrochim. Acta* **2003**, 48, 2479.
33. Wimalasena, R. L.; Wilson, G. S., *J. Chromatogr.* **1991**, 572, 85.

34. Spitznagel, T. M.; Jacobs, J. W.; Clark, D. S., *Enzyme Microb. Technol.* **1993**, 15, 916.
35. Lu, B.; Xie, J.; Lu, C.; Wu, C.; Wei, Y., *Anal. Chem.* **1995**, 67, 83.
36. Alarie, J. P.; Sepaniak, M. J.; Vo-Dinh, T., *Anal. Chim. Acta.* **1990**, 229, 169.
37. Boyer, M. I.; Quillard, S.; Louarn, G.; Froyer, G.; Lefrant, S., *J. Phys. Chem. B* **2000**, 104, 8952.
38. Folch, S.; Gruger, A.; Régis, A.; Colomban, P., *Syn. Met.* **1996**, 81, 221.
39. Yue, J.; Epstein, A. J., *Macromolecules (Washington, DC, United States)* **1991**, 24, 4441.

CHAPTER 3

PREPARATION AND CHARACTERIZATION OF COVALENTLY LINKED BACTERIOPHAGE-NANOPARTICLE NETWORKS

3.1. Introduction

The use of biomolecules for material fabrication has become very popular in recent years¹⁻³. Hybrid nanomaterials composed of both nanoparticles and biomolecules can combine the highly selective catalytic and recognition properties of biomaterials, for example proteins/enzymes and DNA, with the electronic, photonic, and catalytic features of nanoparticles (NPs). Therefore, the conjugation of nanoparticles and other nano objects (e.g. nanorods and carbon nanotubes) with biomolecules is an attractive area of research within nanobiotechnology⁴⁻⁶.

A substantial body of prior research has focused on the delivery of macromolecules and small particles through the vasculature of malignant tumors. It has been demonstrated that macromolecules and small particles in the 60–400 nm size range will extravasate and accumulate in tumors⁷⁻¹¹ via a passive mechanism referred to as the ‘enhanced permeability and retention’ (EPR) effect^{12, 13}. Biomolecules in particular are fascinating macromolecular structures in terms of their unique recognition, transport, and catalytic properties. Various nanoparticles have already been applied as targeted biomarkers and drug-delivery agents to tumors in the analysis and medical treatment of cancers^{14, 15}.

Consequently, the conjugation of gold nanoparticles and biomolecules could provide new ways to incorporate electronic or optical transduction of biological phenomena and lead to the development of novel biosensors.

The unique optical or electronic properties of metal or semiconductor nanoparticles are of key importance for the development of high-throughput techniques for the parallel analysis of numerous components in samples. For example, Au NPs (20 nm) have been modified with shells of bovine serum albumin (BSA) conjugated to various cellular targeting peptides in order to provide functional nanoparticles capable of penetrating the biological membrane and targeting the cell nuclei¹⁴.

A wide range of antibody-based biosensors, cell targeting and drug delivery approaches have been developed since the advent of monoclonal antibodies¹⁶. Monoclonal antibodies and derived single-chain antibodies can now be used to deliver potent cytotoxic components to cancer cells that, once bound, internalize and kill the target cell^{17,18}. However, although antibodies frequently have the desired sensitivity and selectivity, there can be problems with antibody reagents. In some cases, antibodies may be unobtainable due to the non-antigenic nature of the analyte, or the target of interest may need to be analyzed in a sample matrix that is not compatible with the antibody function. Filamentous bacteriophages (phages) are the workhorse of antibody engineering and are gaining increasing importance in nanobiotechnology¹⁹. Filamentous bacteriophages are expected to have a significantly larger drug-carrying capacity than a monoclonal antibody since the pIII minor capsid protein in the phage can be easily engineered to display ligand peptides that will bind to and modify the behavior of target cells in selected tissues²⁰⁻²⁴. With up to 10^{12} unique members, phage-display libraries

provide a vast pool of candidate receptors for essentially any target, including small molecules, DNA, RNA, and proteins.

Biomolecules can be conjugated with gold nanoparticles through both electrostatic binding and covalent coupling. For example, gold and silver nanoparticles produced by citrate reduction have been functionalized with immunoglobulin G (IgG) molecules at pH values that lie slightly above the isoelectric point of the citrate ligand²⁵, allowing effective binding between the positively charged amino acid side chains of the protein and the negatively charged citrate groups of the colloids.

Non-covalent adsorption methods (such as electrostatic binding) are most frequently employed for the immobilization of biomolecules onto particles. However, proteins can easily be lost from the surface and are prone to denaturation, thereby losing activity. The vast number of surface modification and coupling chemistries that have been exploited to covalently bind these molecules has been well documented²⁶. By covalently attaching proteins to particle surfaces, the problems of instability, reversibility or inactivation can be overcome.

In the research reported here, we conjugated gold nanoparticles with a bacteriophage through covalent bonding. TEM, UV-VIS, and SERS techniques were used to prove that the resulting bacteriophage and gold nanoparticles had been successfully joined through a covalent bond. SEM and SERS revealed that the gold nanoparticles and filamentous bacteriophage conjugate were indeed biocompatible and that the bacteriophage's cell-targeting properties were preserved.

3.2. Experimental

3.2.1 Materials and reagents

Tetrachloroauric acid (HAuCl₄) and sodium borohydride (NaBH₄) were purchased from Sigma-Aldrich. Potassium phosphate monobasic (KH₂PO₄), potassium phosphate dibasic (K₂HPO₄), potassium ferricyanide (K₃Fe(CN)₆), sodium perchlorate (NaClO₄) and EDTA were purchased from Fisher-Scientific. 2-Iminothiolane was obtained from Pierce Biotechnology Co. All were used as received.

Wild-type bacteriophage fd8-1 with a concentration of 1x10¹² cfu and fd bacteriophage E2 with a concentration of 1x10¹² cfu were provided by I-Huan Chen from Dr. James Barbaree's group in the Department of Biological Science at Auburn University. The phage propagation procedures were as previously described in Sorokulova et al.²⁷. *E.coli* solution with a concentration of 1x10⁹ cfu was prepared by Yuhong Wang from Dr. Tuang-shi Huang's group in the Department of Nutrition and Food Science at Auburn University.

3.2.2 Sample preparation

Uncapped gold nanoparticles were prepared by reduction of HAuCl₄ using NaBH₄ as the reducing agent^{28,29}. 0.1 M NaBH₄ was prepared and kept in ice bath for 30 minutes, after which 0.6 ml of the NaBH₄ was added to 20ml of 2.5 x 10⁻⁴ M freshly prepared HAuCl₄ solution. The resulting solution was stirred for 20 minutes and then aged for one day at room temperature. The gold nanoparticle colloidal suspension produced is stable for several weeks.

The 2-IT solution was freshly prepared for every use since it is not stable in either air or aqueous solution. The solution concentration was 1 mM in 0.1M phosphate buffer with 2mM EDTA. Phosphate buffer was prepared using potassium phosphate monobasic (KH_2PO_4), and potassium phosphate dibasic (K_2HPO_4). The pH of the buffer was 7.

3.2.3 Cyclic Voltammetry

All cyclic voltammetry experiments were performed in custom built single compartment Teflon cells (ca. 20 ml total volume) using a BAS-Epsilon workstation. A standard three-electrode configuration was used in which the Au wire was the working electrode, a Pt wire was the counter electrode and Ag|AgCl was the reference electrode. 1 mM $\text{K}_3\text{Fe}(\text{CN})_6$, 0.1 M NaClO_4 aqueous solution was used as the electrolyte. Before and after transferring the sample, the solution was thoroughly degassed with ultrapure Ar and isolated from air with a blanket of Ar during experiments. The scan rate was 100 mV/s .

3.2.4 AFM

AFM samples were prepared on a gold film generated by sputter coating gold onto a freshly cleaved mica surface. First, 1000 μl 1×10^{12} bacteriophage in phosphate buffer solution was mixed with 70 μl 1mM 2-IT for 30 minutes, then one drop solution placed on the surface of the gold film and the sample left undisturbed in the refrigerator for 1 day. The sample was then rinsed using distilled water and dried under nitrogen gas. AFM was performed using a Park Scientific Instruments Autoprobe CP scanning probe microscope in tapping mode. The tips used were obtained from Digital Instruments, Inc. and had a force constant of 0.12 N/m. All images were acquired with a 100 μm Scanner Master in air at room temperature. The images obtained were analyzed with PSI ProScan 1.5 data analysis software.

3.2.5 TEM

Copper mesh grids previously coated with Formvar and evaporated with carbon were floated on drops of solution for about 20 minutes. Liquid was removed from the grid by carefully touching the edge of the grid onto filter paper. The grids were not allowed to dry completely at any point during the following procedure. The grids were floated on drops of 1% ammonium molybdate in distilled water (pH 7.0) for 60 sec, after which excess fluid was removed and the grids allowed to dry overnight. TEM images were captured by a transmission electron microscope (Zeiss EM 10 TEM) at an operating voltage of 60 kV. Au nanoparticle size was determined by averaging particle sizes within representative TEM fields. TEM images were analyzed using image J software.

3.2.6 UV-VIS

UV-visible spectra for gold nanoparticles, 2-IT and the reaction between IT and the amine group were obtained by measuring the absorbance of 2-IT in a reaction solution of bacteriophage/lysine and IT in 0.1 M potassium phosphate buffer (pH 7.0) with 2 mM EDTA solution using a UV-visible spectrophotometer (Cary 50 Bio, Varian).

3.2.7 Raman

Samples for Raman spectroscopy were prepared by dripping the sample onto a gold film sputter coated on a freshly cleaved mica surface. The samples were kept in the refrigerator at 4°C for a day and then rinsed using distilled water five times and dried under nitrogen. Raman spectra were obtained using a Renishaw Invia Raman microscope spectrometer equipped with a Leica DMLB microscope. A NIR diode laser with a wavelength of 785 nm wavelength was used in this experiment.

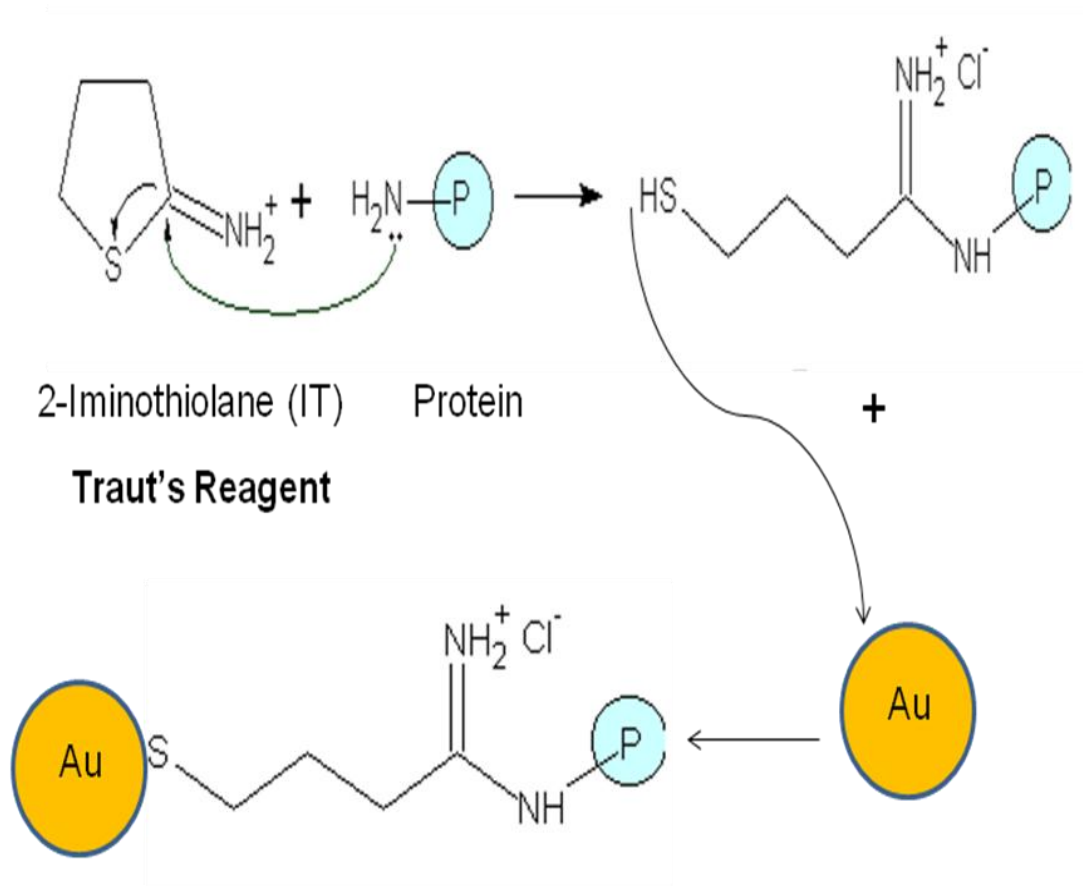
3.2.8 SEM

Scanning electron microscopy (SEM) was used to physically characterize the filamentous bacteriophage. The phage sample was prepared using the same method as for the AFM sample. 10 μ l of the salmonella spore provided by Dr. Barbaree's group with a concentration of 10^5 cfu was dripped onto the surface of the film. The sample was then incubated at room temperature for about 2 hours and washed using distilled water five times. Finally, the sample was dried under nitrogen gas. The sample was exposed to 2% osmium tetroxide (OsO₄) vapor for one hour as an SEM stain for fixing the spores. Following the exposure to OsO₄, it was mounted on an aluminum stub and sputtered with a thin layer of gold using a PELCO sputter coater from Ted Pella, Inc. (Redding, CA) in order to provide a conductive surface for SEM examinations. All SEM micrographs were taken using either a Zeiss DSM 940 SEM (Thornwood, NY) or a JEOL7000F field emission SEM at 20kV.

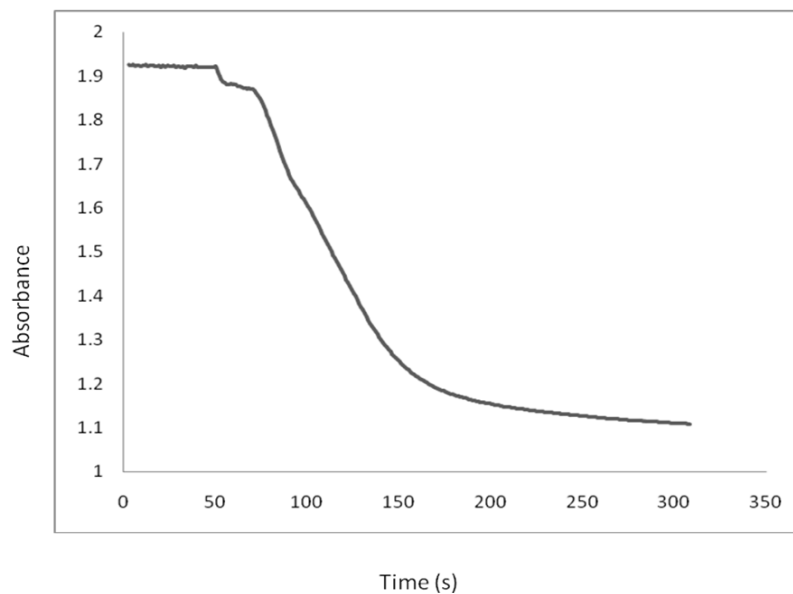
3.3 Results and Discussion

3.3.1 Results for reaction between 2-Iminothiolane and lysine or bacteriophage

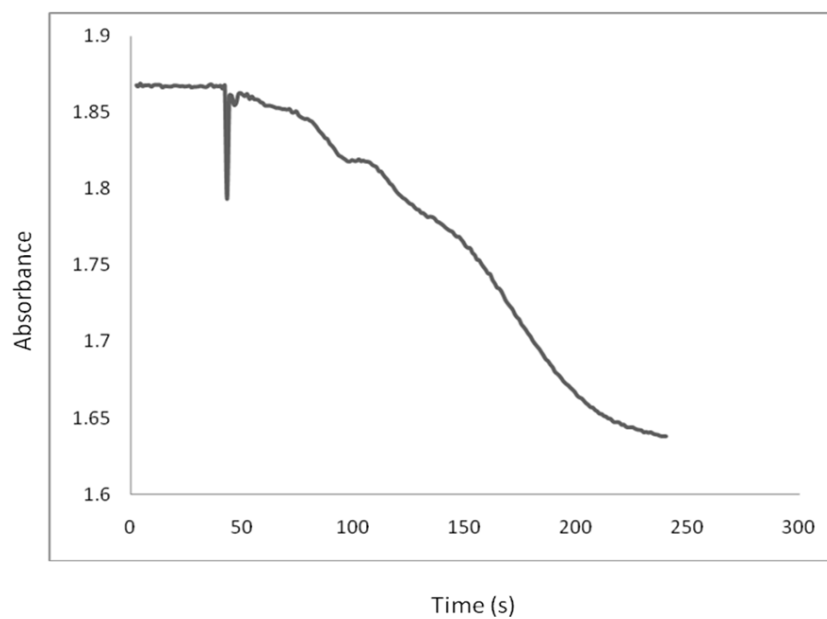
2-Iminothiolane (2-IT), popularly known as Traut's reagent, was used as a crosslinker to attach gold nanoparticles to the bacteriophage through covalent bonding. 2-IT reacts spontaneously and efficiently with primary amines at pH 7-9³⁰. Primary amine groups from lysine residues on the surface of a protein can be converted to thiol functional groups in a simple one step reaction with 2-IT, giving the protein a high affinity for Au surfaces. The reaction between 2-IT and proteins and the formation of a protein-gold nanoparticle assembly via the thiol functional group are illustrated in Figure 3.1. It has been suggested that a layer of thiolated protein G on an Au surface using 2-IT



Scheme 3.1 Thiolation reaction on the protein surface of protein via Traut's reagent, and the reaction of gold nanoparticles and protein



a



b

Figure 3.1 Change of UV-Vis absorbance at 268 nm as a function of reaction time due to adding (a) lysine or (b) fd bacteriophage into 1 mM 2-IT solution

provides a promising and attractive means of immobilizing a capture antibody in electrochemical immunosensors³¹.

Here, UV-VIS absorbance was used to characterize the reaction between bacteriophage or lysine and 2-IT. The UV/Vis spectrometer was zeroed on a 1.00 mL cuvette filled with the same solution of 0.1 M phosphate buffer with 2mM EDTA at pH 7.0 that was used as a solvent for the 2-IT reagent solution. The blank solution was removed and 980 μ l of 1mM 2-IT solution was added to the cuvette. The absorbance spectra at 268 nm were monitored as the reaction progressed (Figure 3.1 a and b). The absorbance before the addition of lysine was found to be about 1.92. When 20 μ l of 0.5 mM lysine in 0.1 M PBS buffer was added rapidly, the absorbance at 268 nm dropped from 1.9 to 1.1 in 4 minutes, indicating that the concentration of 2-IT reduced dramatically as the 2-IT reacted with lysine. A similar result was obtained for the reaction between 2-IT and the bacteriophage when 20 μ l 10^{12} cfu bacteriophage was added into 980 μ l of 1mM 2-IT solution, where the absorbance dropped from 1.86 to 1.64 in 4 minutes. This data provides evidence that the crosslinker (2-IT) used in this project can react with filamentous bacteriophage. The reactions between 2-IT and both lysine and the bacteriophage proceeded very rapidly.

Cyclic voltammetry also confirmed that the 2-IT reacted with the bacteriophage. It is well known that $K_3Fe(CN)_6$ has a very good reversible cyclic voltammetry signal on a clean gold signal. In our research, we also found a good CV signal for ferricyanide on a naked gold surface. The same gold electrode was removed from the ferricyanide solution and immersed into thiolated bacteriophage solution for 1 day. The data are shown in Figure 3.2, which compares the electrochemical activity of ferricyanide on a naked gold

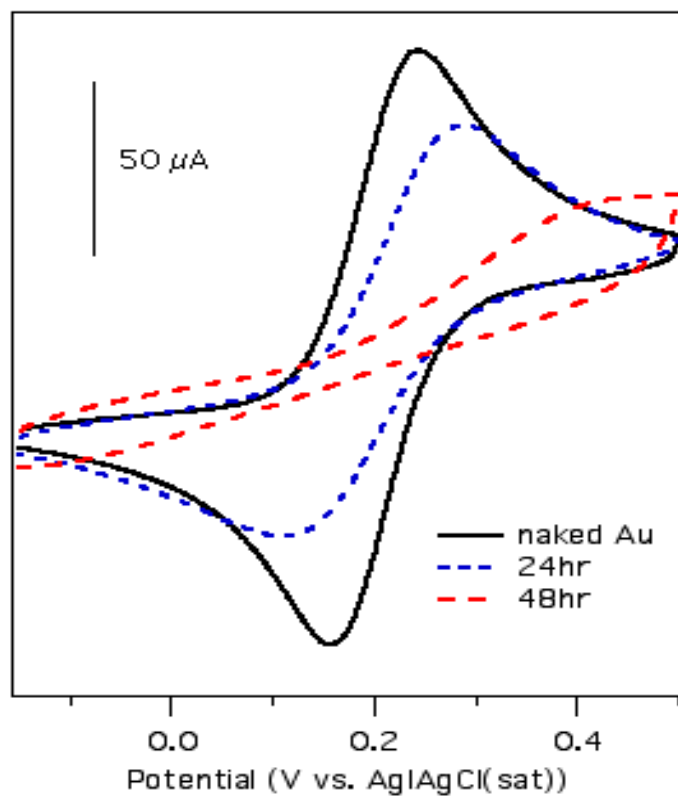
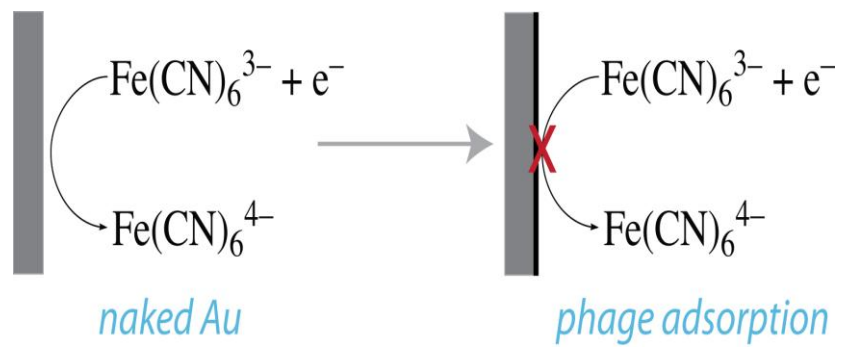


Figure 3.2 Blocked electrochemical reaction on an IT reacted bacteriophage modified gold electrode. (Area~1 cm²)

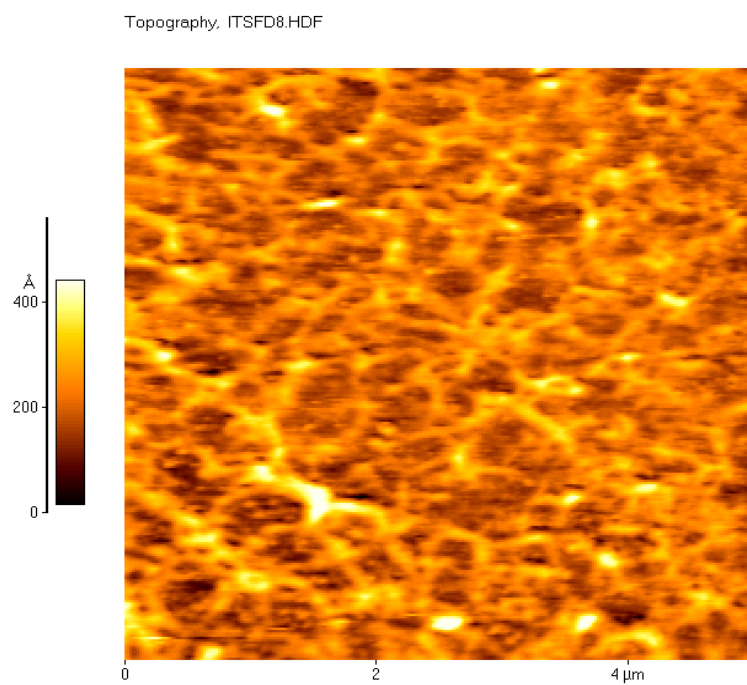


Figure 3.3 Tapping mode AFM image of IT reacted bacteriophage modified gold surface

electrode and a bacteriophage modified gold electrode. The cyclic voltammetry data show that the oxidation and reduction peak current of ferricyanide decreased markedly after the electrode had been immersing in IT reacted bacteriophage solution for 1 day. After the electrode was immersed in the solution for 2 days, the peak current of ferricyanide had dropped almost to zero. This is because the thiol (-SH) groups are produced on the surface of the bacteriophage when 2-IT reacts with the primary amine group of lysine. Thiol groups can react with a clean gold surface to form a strong covalent bond. The presence of a uniform, tight and non-conducted layer of bacteriophage on the gold makes the gold electrode less conductive or non-conductive, thus blocking the electrochemical reaction of ferricyanide on the electrode surface and reducing the CV signal for ferricyanide.

AFM imaging (Figure 3.3) also confirmed the formation of a bacteriophage film on the gold surface. 10 μ l 2-IT reacted bacteriophage was dropped on the gold surface, which was sputter coated on mica for 1 day and then rinsed and dried. As the figure shows, the bacteriophage formed a uniform network on the gold surface. The AFM image thus indicates that the bacteriophage interacts strongly with the gold surface.

3.3.2 Formation of gold nanoparticles

When sodium borohydride was added to tetrachlorauric acid solution rapidly and stirred for 20 minutes, the color of the solution changed from yellow through purple to a final color of red pink, indicating the formation of gold nanoparticles. UV-Vis irradiation is a useful technique for metal nanoparticle characterization as their surface plasmon absorbance lies in the visible range. Surface plasmon resonance (SPR) excites collective oscillations of the electrons on the surface of the gold nanoparticles, whose particle size

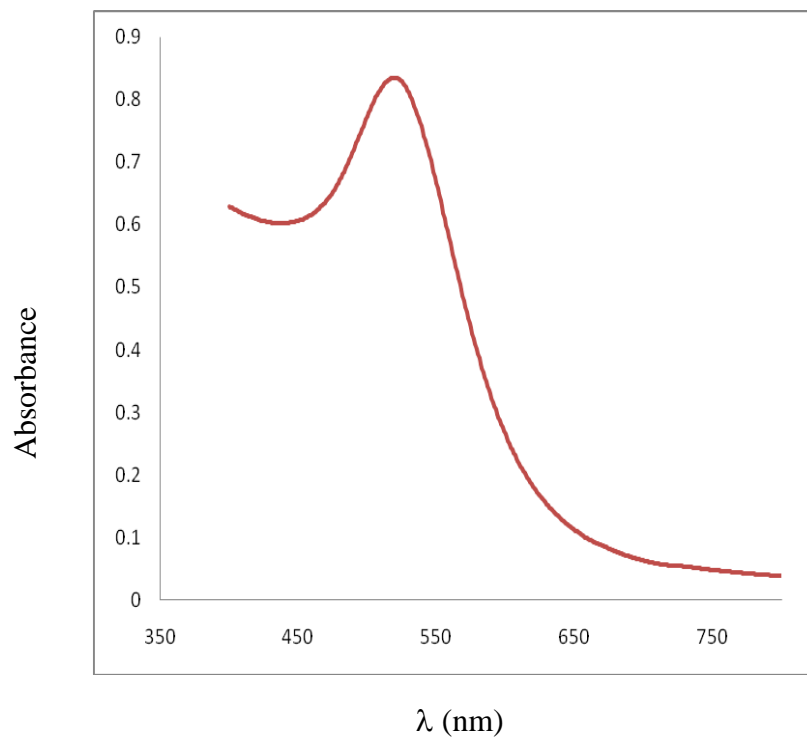
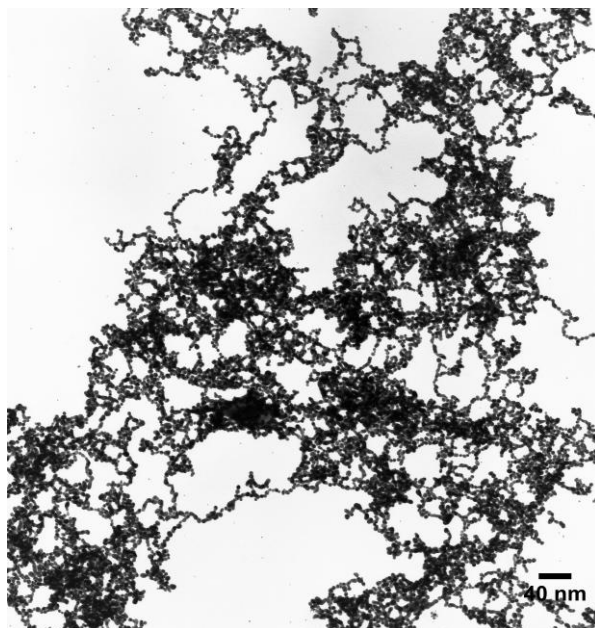
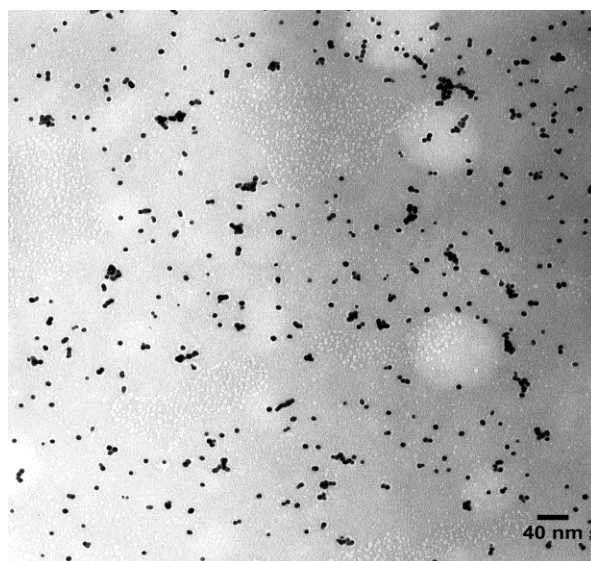


Figure 3.4 UV-Vis spectrum of 100 times diluted originally prepared gold colloid solution



a



b

Figure 3.5 TEM of gold colloid with concentration (a) as originally prepared and (b) 100 times diluted

is of the order of 1/10 wavelength of incident light, upon irradiation with visible light³². Consequently, gold nanoparticles exhibit strong adsorption of electromagnetic waves in the visible range. Haiss et al.³³ reported that gold particles with diameters in the range 2.5-100 nm have UV-Vis peaks between 520 nm-580 nm. Here, UV-Vis was used to prove that gold nanoparticles had been produced through measuring the UV absorbance of the gold colloid solution after ageing the solution of gold nanoparticles for three days. Distilled water was used as a blank solution. It has been reported that borohydridereduced gold nanoparticles have an average size of 5 nm and their absorption maximum is at about 520 nm²⁹. In our UV-Vis data, the original solution was diluted by 100 times. The resulting UV-Vis spectrum is shown in Figure 3.4. There is a UV adsorption maximum for gold nanoparticles at 524 nm (λ_{\max}), which indicates stable gold nanoparticles have indeed been synthesized. According to Mie's theory³⁴, the surface plasmon resonance and the plasmon bandwidth depend on the size of the metallic particles in the solution, with the peak value representing the size of the gold nanoparticles in the solution. The λ_{\max} in our data is consistent with the reported surface plasmon absorption peak for gold nanoparticles in the 3-20 nm size range^{33, 35}. It is important to note, however, that the λ_{\max} also depends on other factors, such as the dielectric constant of the surrounding medium and the inter-particles size, so the UV-Vis data cannot provide more precise size information for the gold particles. The formation of gold nanoparticles was also confirmed by transmission electron microscopy (TEM) and the size of the nanoparticles was measured.

Figure 3.5 shows TEM micrographs of the gold nanoparticles in the original solution and in the same solution diluted 100 times, with the gold nanoparticles appearing as black

dots. The TEM results confirm that gold nanoparticles were successfully synthesized and that the average diameter of the nanoparticles was about 10 nm.

3.3.3 TEM results for gold-bacteriophage conjugate formation

According to the proposed mechanism for gold-bacteriophage conjugate formation, the sulfhydryl (-SH) group produced by the reaction between 2-IT and the bacteriophage will form a covalent bond with the gold nanoparticles. The observation of experiment shows the gold colloid solution was converted to a red solid suspension after adding 500 μl of the gold colloid solution into a thiolated bacteriophage solution prepared by mixing 70 μl 1 mM 2-IT solution into 1000 μl 1×10^{12} bacteriophage solution for 1 hour. This phenomenon suggests that a reaction takes place between the thiolated bacteriophage and the gold nanoparticles.

TEM data (Figure 3.6 a, b) illustrate that gold nanoparticles indeed bond to the bacteriophage. The TEM data reveal that the size of the nanoparticles is much larger than those of the originally synthesized gold nanoparticles, with the average size increasing from less than 10 nm to 36 nm. The size of nanoparticles is also very uniform, ranging only from about 30 to 40 nm. However, many factors, including the nature and concentration of the reducing agent, the ratio of metal salt to capping agent, and the temperature, pH, and ionic strength, can all be used to control the size and shape of the nanoparticles formed. For example, the original pH value of the gold colloid solution used here was 5, which increased as a result of adding the bacteriophage solution with pH 7. The pH value is known to affect the size of gold nanoparticles^{36, 37} and Au nanoparticles can be made to agglomerate by varying the solution's ionic conditions, especially for electrostatic stabilized nanoparticles. Adding the thiolated bacteriophage

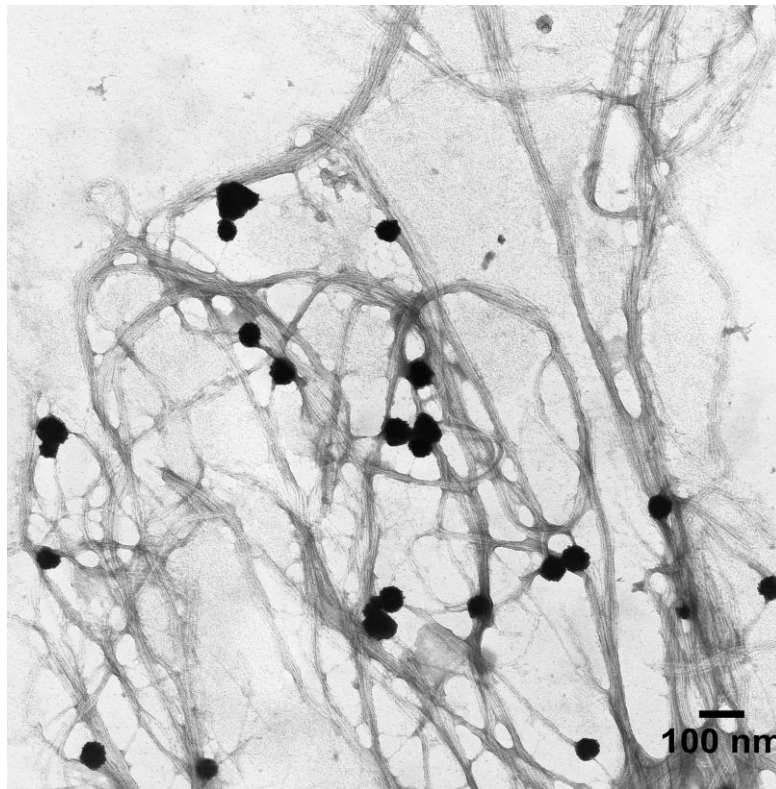


Figure 3.6 a TEM image of bacteriophage conjugate (100 μ l gold colloid +35 μ l 1mM IT reacted with 500 μ l 10^{12} cfu bacteriophage).

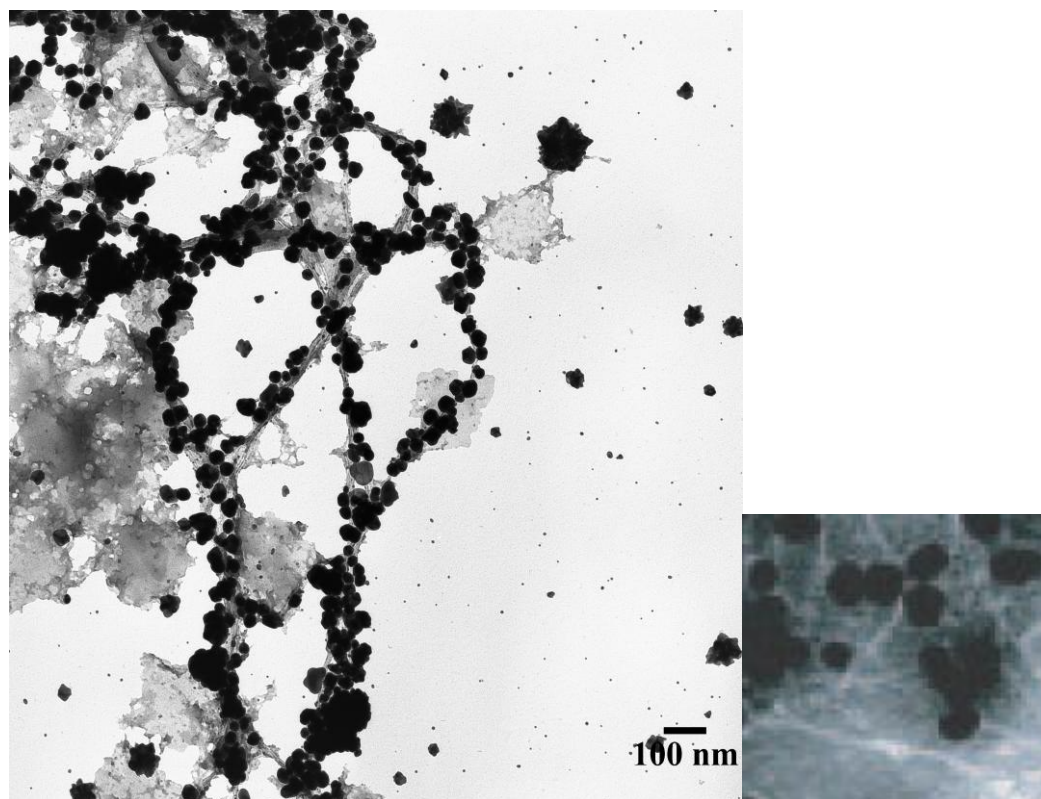


Figure 3.6 b TEM image of bacteriophage conjugate (500 μl gold colloid +35 μl 1mM IT reacted with 500 μl 10^{12} cfu bacteriophage) and c TEM image of Au-phage network through electrostatic interaction (ref 43).

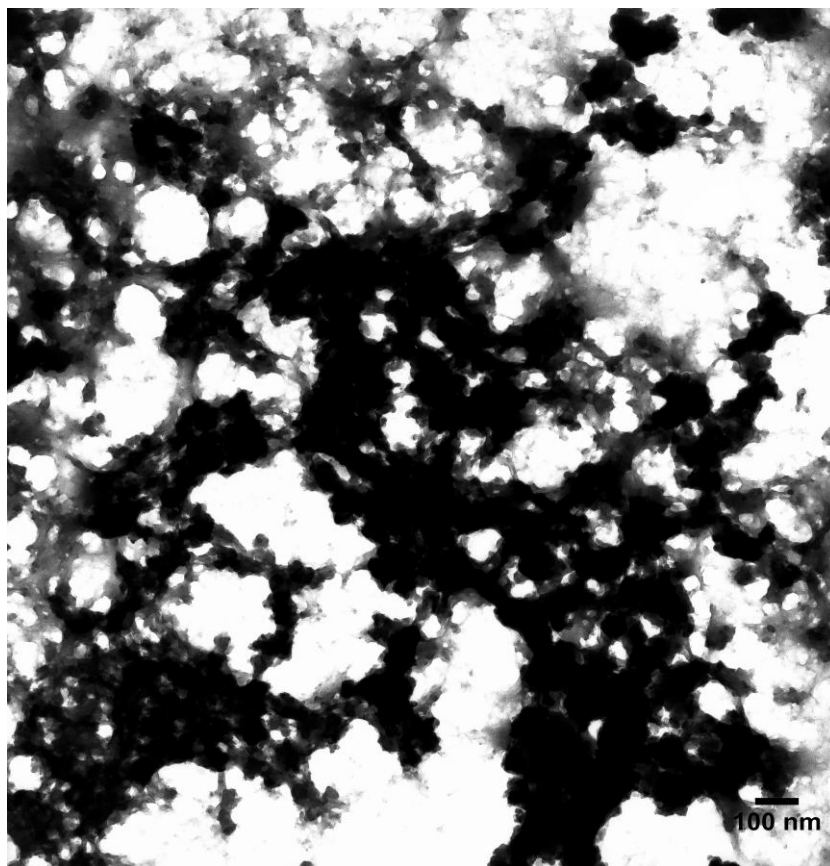
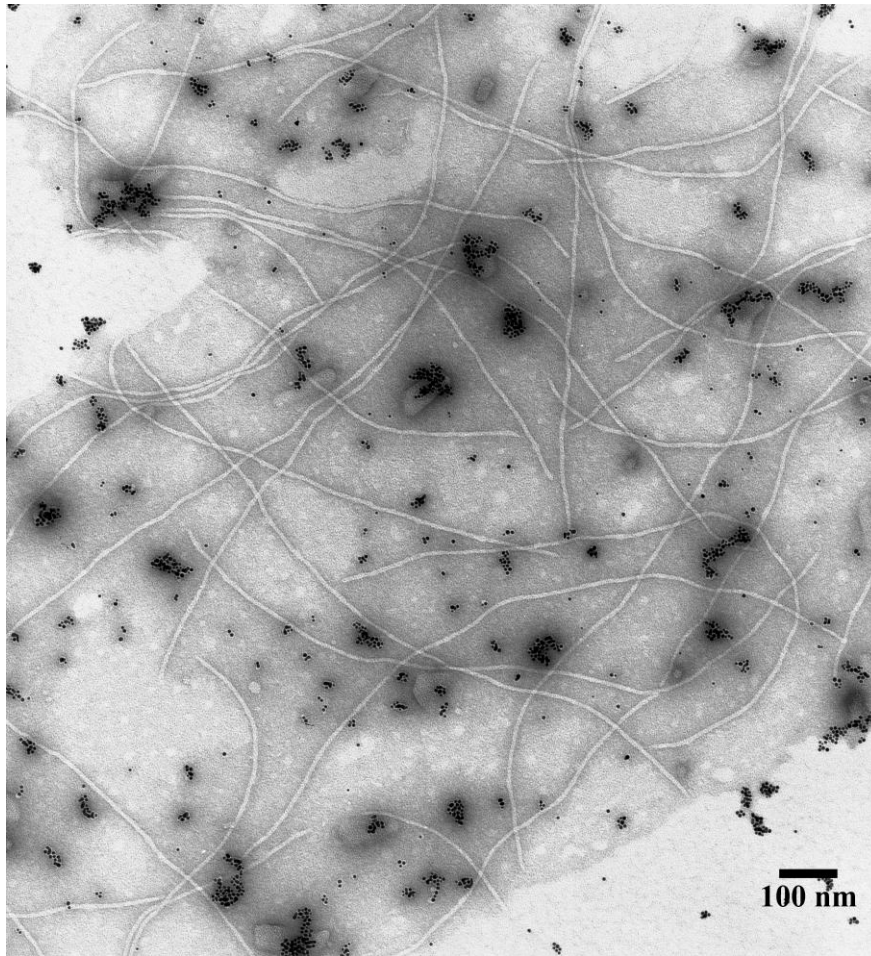


Figure 3.6 d TEM image of bacteriophage conjugate (700 μl gold colloid + 200 μl 1 mM IT reacted with 500 μl 10^{12} cfu bacteriophage solution).



e

Figure 3.6 e TEM image of bacteriophage conjugate (70 μ l phosphate buffer +1000 μ l bacteriophage solution + 500 μ l gold colloid solution).

solution to the solution of gold nanoparticles raises the ionic strength and pH of the medium containing the gold nanoparticles³⁸⁻⁴⁰, and gold colloids aggregate more readily as the electrostatic repulsive force is balanced out by the high ionic strength.

The other possible explanation for this phenomenon is that the bacteriophage acts as a stabilizer when it reacts with gold nanoparticles. The phenomenon of aggregation or flocculation of the particles in gold colloid solution upon the addition of a “cross-linking” agent is well documented^{41, 42}. In our research, thiolated bacteriophages act as the crosslinking agent, therefore nanoparticles agglomerate while the bacteriophage is bundled together. However, the actual mechanism by which nanoparticles grow in bacteriophage solution reacted with 2-iminothilane is not clear based on our present data.

Figure 3.6 a and b show TEM images of samples with different volumes of gold nanoparticles added into solutions prepared by mixing 35 μ l 1mM 2-IT solution with 500 μ l 10^{12} cfu bacteriophage solution for 1 hr. In Figure 3.6 a, 100 μ l gold nanoparticle colloid solution was added to IT reacted bacteriophage solution and the final sample was aged for 1 day in the refrigerator. The TEM data reveals that almost every gold nanoparticle is connected to a bacteriophage. Since one particle can bind several bacteriophages, this could lead to bacteriophages being bundled together and the consequent aggregation of gold nanoparticles. In Figure 3.6 b, 500 μ l gold nanoparticles was added to IT reacted phage solution and once again the entire bacteriophage surface was occupied by gold nanoparticles, with the gold nanoparticles being distributed on the bacteriophage surface evenly. This differs from the TEM image, shown in Figure 3.6 c, of the sample reported previously by Souza et al.⁴³, who found the distribution of the gold nanoparticles on the bacteriophage surface to be random when conjugated together

through the electrostatic interaction. Our TEM data suggests, therefore, that 2-iminothiolane reacts with the primary amine group of lysine on the bacteriophage surface and these amine groups on all the surface PVIII proteins have the same ability as 2-IT to produce the sulfhydryl (-SH) group that can form covalent bonds with gold nanoparticles.

Since 2-IT produces sulfhydryl functional groups capable of interacting strongly with the gold surface, the concentration of 2-IT also has an effect on the conjugate of bacteriophage and nanoparticles. In Figure 3.6 d, 200 μl 1 mM IT was added to 500 μl 10^{12} cfu bacteriophage solution and then incubated for 1 hour at room temperature. After incubation, the 2-IT reacted bacteriophage solution was mixed with 700 μl gold nanoparticle colloid and kept in the refrigerator for 1 day. The large amount of IT added to the bacteriophage solution resulted in more thiolation on the surface bacteriophage and a subsequent increase in gold nanoparticle and bacteriophage agglomeration because of the interaction between nanoparticles and bacteriophages through covalent bonding. The TEM image shows an extensive black network in which gold nanoparticles and bacteriophages cannot be identified clearly. This network might have been formed as a result of the gold nanoparticles aggregating tightly on the surface due to the greater availability of sulfhydryl groups compared to the samples in Figure 3.6 a and b. Figure 3.7 d indicates that the volume ratio of 2-IT added to react with bacteriophage is the main determinant of the aggregation characteristics of gold nanoparticles and bacteriophage. It thus seems likely that 2-IT is the main driver for the conjugation of the gold nanoparticles and bacteriophages here. This suggests that the interaction between gold nanoparticles and bacteriophages is covalently bonded through the sulfhydryl (-SH)

groups produced from the reaction between IT and bacteriophage. To confirm that bacteriophages conjugate with gold nanoparticles in the presence of 2-iminothiolane by covalent bonding rather than electrostatic interaction, 70 μl phosphate buffer and 1000 μl bacteriophage solution was mixed with 500 μl gold colloid solution for 1 day. The TEM data shown in Figure 3.6 e reveal both black dots of Au nanoparticles and long, white, filamentous phage structures in the same picture. Here, few of the gold nanoparticles were connected with bacteriophages and the bacteriophages were not bundled together. Figure 3.6 e illustrates that the gold nanoparticles prepared for this study can make no connections with the bacteriophage in the absence of 2-IT. The average size of the gold nanoparticles is still about 10nm, similar to those in the original gold nanoparticle solution. The size of the gold nanoparticles therefore did not increase as a result of mixing 2-IT reacted bacteriophage and gold nanoparticles together. This data suggests that agglomeration of the gold nanoparticles and bundling of the bacteriophages mainly results from the reaction between bacteriophages and gold nanoparticles through the sulfhydryl bond. Higher pH and stronger ionic strength lead only to small aggregations of gold nanoparticles.

3.3.4. SERS results for formation of gold nanoparticles-bacteriophage conjugate

To confirm that gold nanoparticles and bacteriophage have indeed been conjugated together, Raman spectroscopy was applied to test the surface enhanced effect of gold nanoparticles on the Raman signal of fd bacteriophage. Raman spectra of three different samples are illustrated in Figure 3.7. The spectrum with the purple line is for the sample prepared by mixing 500 μl gold nanoparticles with 2-IT reacted bacteriophage solution (35 μl 2-IT solution + 500 μl bacteriophage solution). This spectrum exhibits a very good

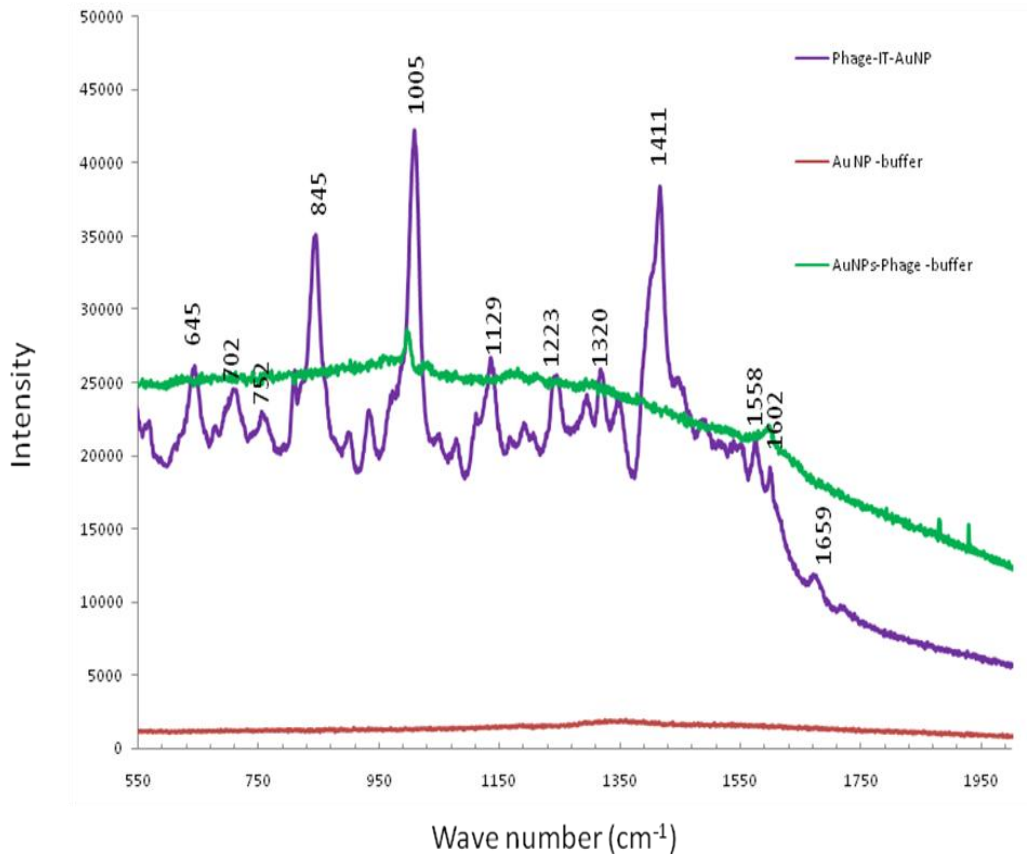


Figure 3.7 Raman spectra of gold nanoparticles conjugated with bacteriophage through 2-IT (phage-IT-AuNP), gold nanoparticles and phosphate buffer (AuNP-buffer) and bacteriophage, buffer and gold nanoparticles mixture (AuNP-phage-buffer). (Collection time =15 s)

signal for the bacteriophage and is dominated by the peak corresponding to the amino acid containing phenyl groups such as phenylalanine (1005 cm^{-1}), tyrosine (845 cm^{-1}), and tryptophan (748 cm^{-1} , 1320 cm^{-1}), as well as C-H vibrations ($1410\text{-}1460\text{ cm}^{-1}$)⁴⁴⁻⁴⁶. Peaks at 1411 cm^{-1} correspond to His Asp, Glu and Lys proteins. There are additional Raman peaks corresponding to the Amide I ($1660\text{-}1670\text{ cm}^{-1}$) and Amide III ($1200\text{-}1300\text{ cm}^{-1}$) vibrations.

The assignment of Raman peaks to fd bacteriophage are summarized in Table 3.1. However, mixing $500\text{ }\mu\text{l}$ gold nanoparticles with $535\text{ }\mu\text{l}$ of the phosphate buffer used to prepare both the IT and bacteriophage solutions produced no Raman peaks, shown by the red line in Figure 3.8. The result for this control experiment suggests that the gold nanoparticles and buffer solution used here do not produce specific Raman signals. Another control experiment was done with a sample prepared by mixing $500\text{ }\mu\text{l}$ gold nanoparticles solution with $35\text{ }\mu\text{l}$ phosphate buffer and $500\text{ }\mu\text{l}$ bacteriophage solutions. The Raman spectrum of this sample is shown as the green line in Figure 3.9. The spectrum has only weak peaks from the phenylalanine at 1005 cm^{-1} and 1602 cm^{-1} . Other peaks which should appear in spectrum of fd bacteriophage are too weak to be identified in this data. These results indicate that the gold nanoparticles-bacteriophage system cannot generate good Raman signal without 2-IT as a crosslinker, and further confirms that IT plays a key role in building the gold nanoparticles-bacteriophage network.

Differences in the intensity and resolution of the Raman signals in the blue and green spectra can be explained by the surface enhancement effect of the gold nanoparticles for the bacteriophage. Gold nanoparticles are a good substrate for surface enhanced Raman spectroscopy. In order to obtain a good SERS signal, analyte molecules must reside

Table 3.1. Assignment of spectral regions of fd bacteriophage

Raman peak region (cm ⁻¹)	Assignment
645	C-C twist tyrosine
840-860	Tyrosine, phenylalanine ring stretching
1000-1010	Phenylalanine ring stretching
1200-1300	Amide III Vibrations
1330-1350	Tryptophan ring stretching
1410-1460	C-H vibrations, Tryptophan ring stretching
1558	Tryptophan ring stretching
1602	Tryptophan, phenylalanine ring stretching
1650	Amide I

within the enhanced electromagnetic fields generated when the localized surface plasmon resonance on gold nanoparticles is excited by a laser. Therefore, the distance between analytes and rough metal surface is very important in analytical applications of SERS. SERS signals decay rapidly as a function of distance⁴⁷⁻⁵⁰. According to the work of Sun et al., the characteristic distance at which SERS signals decrease by half is about 7 Å⁴⁷. Theoretical calculations for well-characterized nanoparticles suggest that surface enhanced field from nanostructure surfaces degrade exponentially, with a characteristic decay length of about 2 nm⁵¹. This explains the TEM data shown in Figure 3.8 e: since most gold nanoparticles failed to attach to the bacteriophage surface and the distance between the gold nanoparticles (rough metal surface) and bacteriophage (analyte) was not close enough to give good surface enhancement, the green spectrum in Figure 3.8 could not display good Raman peaks for bacteriophage. However, when 2-IT reacted bacteriophage was conjugated with gold nanoparticles, the short distance between the gold nanoparticles (substrate) and bacteriophage (analyte) (Figure 3.8 a and b) resulted in a very good Raman signal for the bacteriophage, shown as the blue spectrum in Figure 3.8. The Raman data therefore suggest that the gold nanoparticles and bacteriophage indeed conjugate together through covalent bonding, with a resulting short distance between analytes and rough substrate and a consequent strong SERS signal.

3.3.5 Bioactivity of bacteriophage in networks

To test the activity of 2-IT reacted bacteriophage, scanning electron microscopy was used to observe the binding of salmonella to the immobilized 2-IT reacted fd phage E2 directly. Bacteriophage fd E2 is the engineered fd8-l phage which has a specific attachment to *Salmonella typhimurium*⁵². In this test, a thin gold film on a mica surface

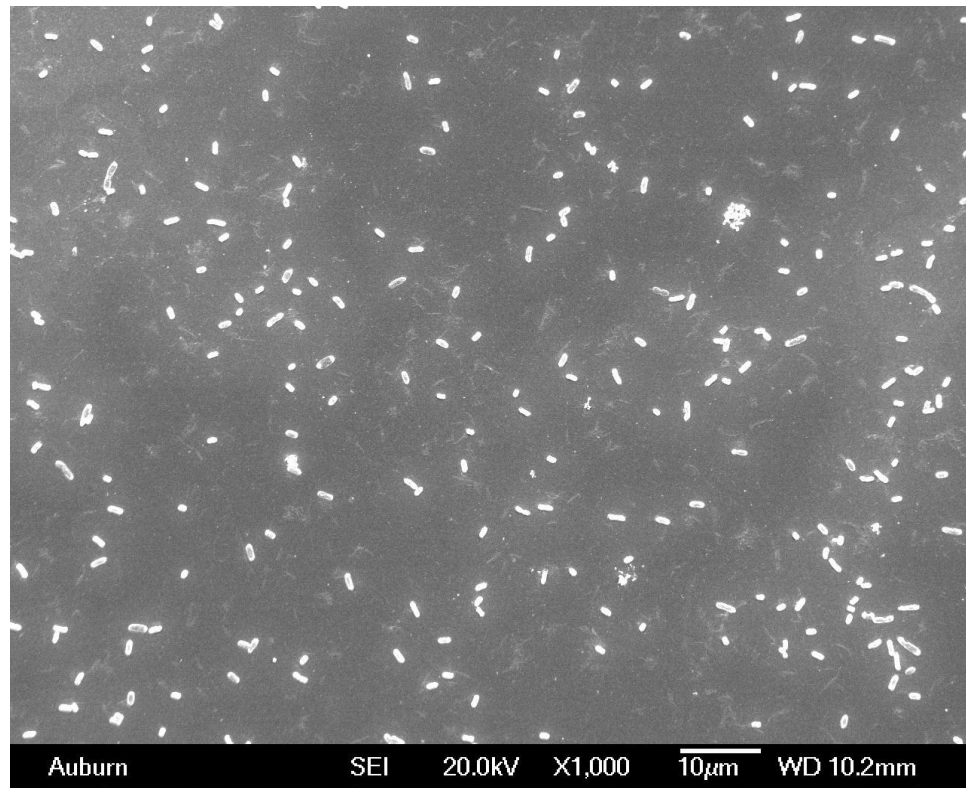


Figure 3.8 SEM image of *Salmonella typhimurium*-bacteriophage E2 infection

was coated with the thiolated bacteriophage E2. The film was soaked in a suspension of salmonella cells (10^5 cfu) for 30 mins, washed five times, and examined in the scanning electron microscope. We observed specific binding of bacterial cells to the immobilized phage (Figure 3.8) and confirmed that the ability of bacteriophage E2 to absorb *Salmonella typhimurium* spores is preserved after reacting with 2-IT.

Raman spectroscopy was also applied to test the bacteriophage activity for reactions with *Escherichia coli* (*E. coli*). Here, *E. coli* (BD2399) with a concentration of 10^9 cfu in distilled water was used. In Figure 3.9, the green line represents the spectrum for *E. coli* only. The sample was prepared by the following procedure. *E. coli* solution was dropped on a gold film sputter coated on a mica substrate and one drop of gold colloid solution was mixed with the *E. coli* solution. This surface was dried spontaneously in the refrigerator and measure by RS without further cleaning. Gold colloid solution was used for surface enhancement in this experiment. The Raman spectrum of the *E. coli* is expected to consist of bands corresponding to lipids, proteins and DNA. Peak assignment of the bacterial cells is reported in Table 3.2. Peaks at $1550-1610\text{ cm}^{-1}$ are due to the C=C stretching of Tyr, Trp and Phe on the protein. Peaks at $1655-1680$ are assigned to the stretching vibration of C-O or the stretching vibration C-N in the amide I groups⁵³. Peaks at $1420-1480\text{ cm}^{-1}$ are attributed to C-H deformation in lipid groups, proteins, and adenine and guanine in DNA groups⁵³. The band at $1220-1284\text{ cm}^{-1}$ corresponds to amide III vibrations and the C-H bend in lipids. The Raman spectra recorded in our work generally agreed with the spectra reported by Naja et al.⁵⁴. Differences are ascribed to the different sample preparation methods used and the analysis inducing conformational alterations of the cellular proteins and changes in their

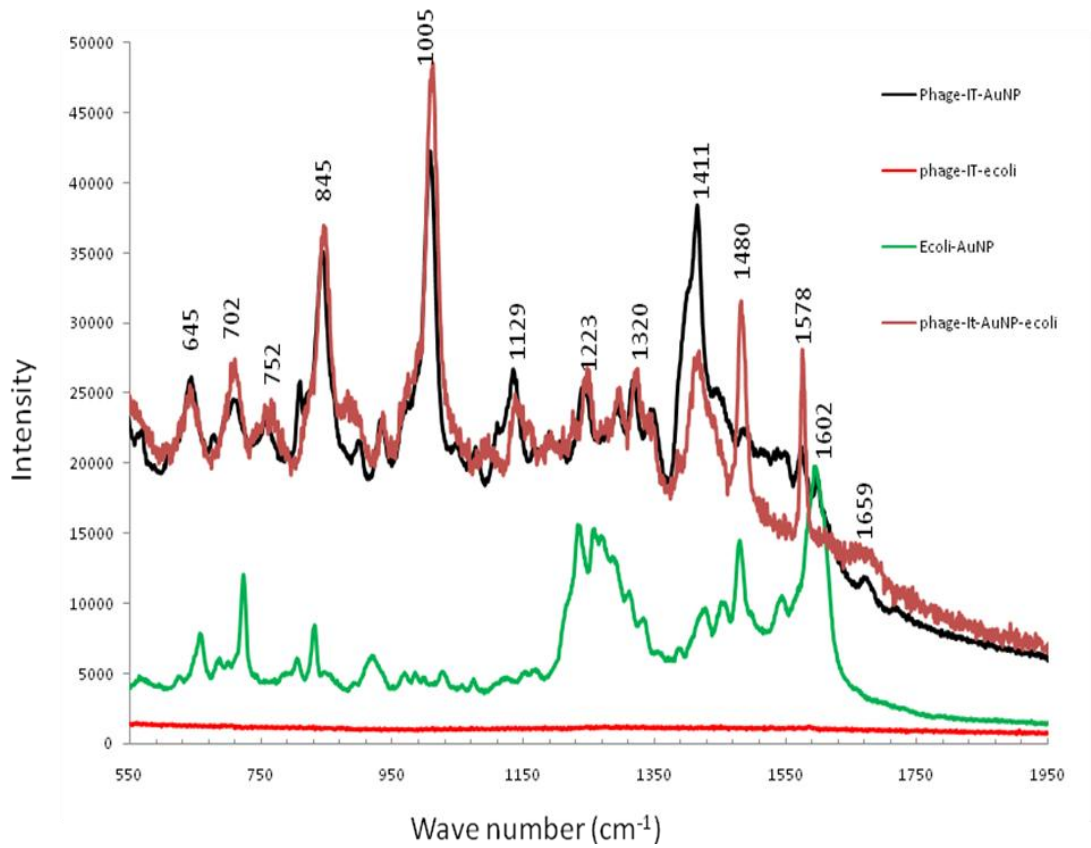


Figure 3.9 Raman spectra of bacteriophage-*E. coli* infection (Phage-IT-AuNP: gold bacteriophage-nanoparticles conjugated using IT; Phage-IT-e coli: *E. coli* infection of IT reacted bacteriophage ; Ecoli-AuNP: mixture of *E. coli* solution and gold colloid solution; Phage-IT-AuNP-e coli: *E. coli* infection of gold bacteriophage-nanoparticles conjugated using IT). (Collection time =15 s)

Raman spectra⁵⁵. The prevalence of protein features can be explained by the 55% dry weight of protein in the *E. coli* composition. Proteins occupy the surface of bacteria, only a short distance from the nanoparticles, and therefore produce good surface enhancement effects and a correspondingly strong Raman signal.

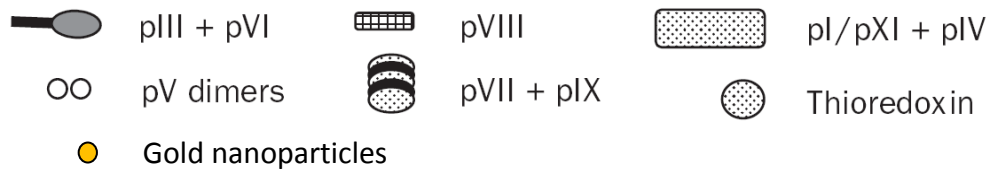
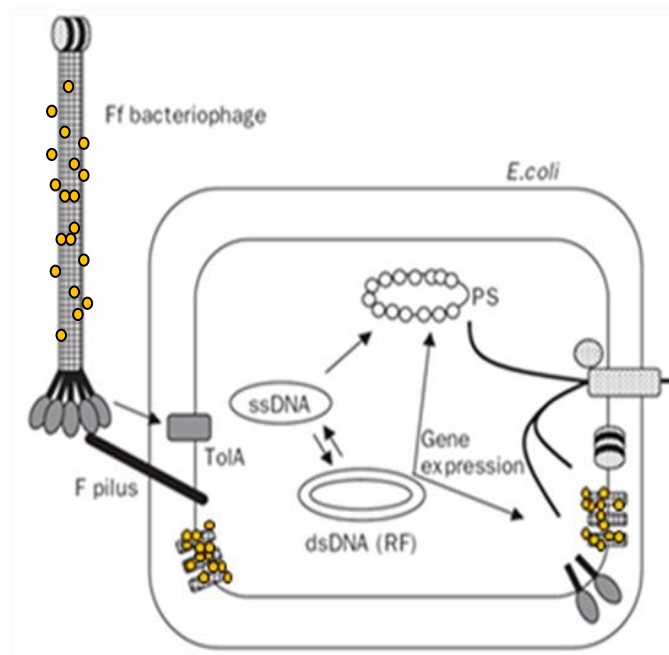
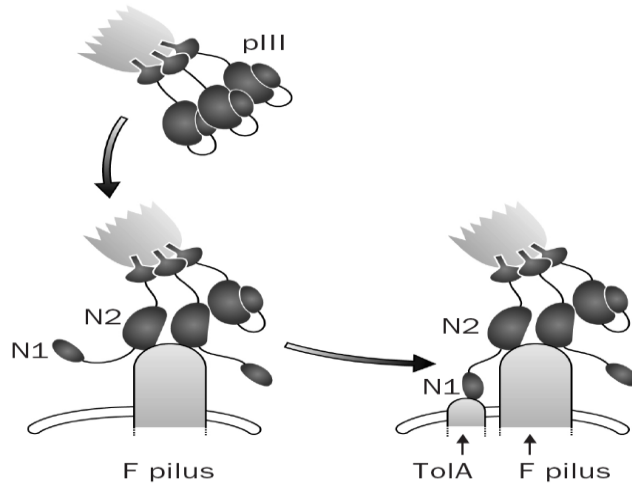
The thiolated bacteriophage was immobilized on the gold surface and reacted with *E. coli* solution. The sample was cleaned with distilled water several times and dried under nitrogen. The Raman spectrum of this sample is shown as the red line in Figure 3.11. There was no Raman signal seen from either the bacteriophage or *E. coli* since there was no surface enhancement effect in this sample.

Next the gold nanoparticle-bacteriophage network's ability to detect *E. coli* using Raman spectroscopy was tested. A freshly prepared assembly of gold nanoparticles and bacteriophage was immobilized on the gold film and then reacted with the *E. coli* solution. The sensor surface was then rinsed with distilled water several times and dried under nitrogen. The resulting Raman spectrum is shown as a brown line in Figure 3.9. Comparing this spectrum to the bacteriophage spectrum previously obtained (the black spectrum in Figure 3.9 revealed two new strong peaks at 1480 cm^{-1} and 1578 cm^{-1} . Peaks at 1578 cm^{-1} are thought to be due to guanine and adenine nucleic acids in DNA and the peaks at 1480 cm^{-1} correspond to nucleic acids, lipids and proteins.

DNA structures generally reside inside cells and it is therefore not easy to obtain a signal from nucleic acids by SERS since gold nanoparticles attach to the bacteriophage surface. It is possible that *E. coli* infection makes bacteriophages conjugated with gold nanoparticles intrude into the inside of *E. coli* cells, thus producing strong signals from both the DNA and membrane. In Scheme 3.2, phage-*E. coli* infection⁵⁶ is initiated by the

Table 3.2 Raman assignment of spectral regions of bacterial cells^{53-55, 57}

Peaks in spectra (cm ⁻¹)	DNA	protein	lipid
640		Tyr/c-s stretching	
702		C-S stretching	
845	OPO stretch	Tyr-hydrogen bonding of the phenolic hydroxyl group	C1-C3 head group stretching
1005		Phe ring stretching	
1129		Amide vibration, C-N stretching	(C-C) _{ip} stretching (all- <i>trans</i>)
1200-1300	T(δ C6H+C2N3) C(δ C6H+C4N4')	Amide III vibration	1295-1305 (CH ₂) twisting deformation 1250-1280 (=CH) _{ip} in plane olefinic hydrogen bend
1320	1340: A (-N7C5+C8N7)	CH bending	
1411*		His Asp, Glu, Lys	
1480*	Guanine vibration (1489 strong)	1450 (weak) CH, CH ₂ , CH ₃ bending	1420-1480 CH ₂ bending and twisting
1578*	G(C4N3+C5C4+N7C5) vibration A(C5C4-C4N3)	1582, 1553, Trp vibration, amide II Asp, Glu carboxylate stretching	
1602		C=C ring stretching (Phe, Tyr, Trp)	
1659	1650, T(C5C4-C4O)	Amide I stretching Amide I vibration C-O stretching, C-N stretching	1640-1680, (C=C) olefinic stretching



Scheme 3.2 Mechanism of *E. coli*-bacteriophage infection (ref 56)

binding of the N2 domain of pIII to the tip of the F pilus, which is believed to be present in two to three copies per cell. The binding of N2 to the tip of the F pilus releases the N1 domain, which then becomes free to interact with the C-terminal domain of TolA (TolAIII), also referred as the coreceptor. Through the action of TolA, the major capsid protein, pVIII, and probably also the pVII and pIX minor coat proteins depolymerize and become integrated into the host inner membrane as the single-stranded DNA enters the cytoplasm. Once in the *E. coli* membrane, pVIII proteins of the infecting phage join the pool of newly synthesized pVIII, and are assembled to newly formed particles. According to this mechanism of infection, the covalently conjugated gold nanoparticles that entered the *E. coli* cell with the bacteriophage thus produce good surface enhanced Raman signals for the lipids and proteins on the membrane of the bacterial cell and DNA, since gold nanoparticles are integrated into the inner membrane with depolymerized pVIII and are physically very close to both the inner membrane and plasmids of the bacterium. Therefore, the strong peaks at 1578 cm^{-1} may be due to the protein's amino acid Trp on the membrane and the DNA of plasmids in the cells, and the peaks at 1480 cm^{-1} should correspond to the lipid of the membrane and the DNA in *E. coli* cells after *E. coli* infection. It is also possible that the 1578 cm^{-1} peak may be attributed to C=C ring stretching (Phe, Tyr, Trp) on the *E. coli* cell membrane, which should be from $1550\text{-}1610\text{ cm}^{-1}$ in the original *E. coli* cell (green spectra). Both the peak shift and peak width change after infection with bacteriophage, which could be due to conformation changes in the cell during the infection process. These Raman results therefore indicate that pIII proteins on the bacteriophage of the conjugate prepared for this study retain their infection activity.

3.4 Conclusions and potential applications

This chapter reports the successful effort to synthesize bacteriophage and gold networks through covalent bonding using 2-iminothiolane as the crosslinker and provides evidence to suggest that these networks are biocompatible and preserve the biorecognition activity of the pIII protein. By carefully engineering the pIII protein of the bacteriophage, the networks generated can be used for cell-targeting and biosensor applications. Figure 3.10 shows an example of a potential application for the new gold nanoparticles-bacteriophage network described in this chapter. The networks must first be immobilized on the gold surface using their sulfhydryl group. By taking advantage of gold's optical properties⁵⁸⁻⁶⁰, targets that specifically attach to the engineered bacteriophage can be detected using fluorescence microscopy, near-infrared (NIR) spectroscopy and surface-enhanced Raman scattering (SERS) spectroscopy.

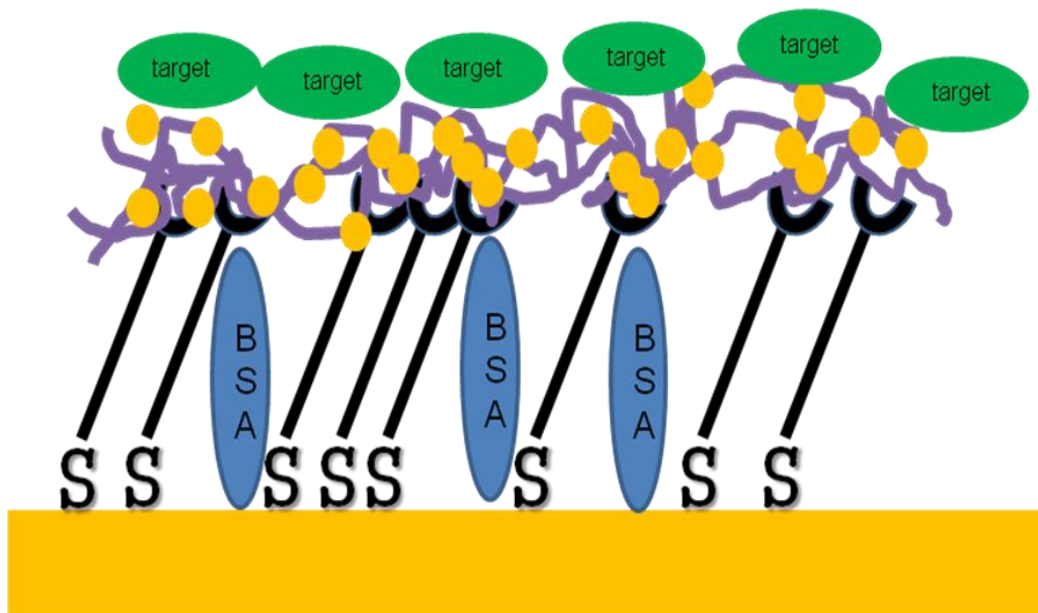


Figure 3.10 Proposed sensor application of the gold nanoparticles-bacteriophage network described in this chapter

References

1. Niemeyer, C. M., *Angew. Chem., Int. Ed.* **2001**, 40, 4128.
2. Bittner, A. M., *Naturwissenschaften* **2005**, 92, 51.
3. Ball, P., *Nanotechnology* **2005**, 16, R1.
4. Niemeyer, C. M., *Angew. Chem.* **2001**, 113, 4254.
5. Csaki, A.; Maubach, G.; Born, D.; Reichert, J.; Fritzsche, W., *Single Mol.* **2002**, 3, 275.
6. Penn, S. G.; Hey, L.; Natan, M. J., *Curr. Opin. Chem. Biol.* **2003**, 7, 609.
7. Kong, G.; Braun, R. D.; Dewhirst, M. W., *Cancer Res.* **2000**, 60, 4440.
8. Ishida, O.; Maruyama, K.; Sasaki, K.; Iwatsuru, M., *Int. J. Pharm.* **1999**, 190, 49.
9. Litzinger, D. C.; Buiting, A. M.; van Rooijen, N.; Huang, L., *Biochim. Biophys. Acta* **1994**, 1190, 99.
10. Yuan, F.; Leunig, M.; Huang, S. K.; Berk, D. A.; Papahadjopoulos, D.; Jain, R. K., *Cancer Res.* **1994**, 54, 3352.
11. Hobbs, S. K.; Monsky, W. L.; Yuan, F.; Roberts, W. G.; Griffith, L.; Torchilin, V. P.; Jain, R. K., *Proc. Natl. Acad. Sci.* **1998**, 95, 4607.
12. Maeda, H., *Adv. Enzyme Regul.* **2001**, 41, 189.
13. Maeda, H.; Fang, J.; Inutsuka, T.; Kitamoto, Y., *Int. Immunopharmacol.* **2003**, 3, 319.
14. Tkachenko, A. G.; Xie, H.; Coleman, D.; Glomm, W.; Ryan, J.; Anderson, M. F.; Franzen, S.; Feldheim, D. L., *J. Am. Chem. Soc.* **2003**, 125, 4700.
15. Brigger, I.; Dubernet, C.; Couvreur, P., *Adv. Drug Delivery Rev.* **2002**, 54, 631.

16. Kohler, G.; Milstein, C., *Nature* **1975**, 256, 495.
17. Kreitman, R. J., *Curr. Opin. Immunol.* **1999**, 11, 570.
18. Trail, P. A.; King, H. D.; Dubowchik, G. M., *Cancer Immunol. Immunother.* **2003**, 52, 328.
19. Sarikaya, M.; Tamerler, C.; Jen, A. K.; Schulten, K.; Baneyx, F., *Nat. Mater.* **2003**, 2, 577.
20. Giordano, R. J.; Cardo-Vila, M.; Lahdenranta, J.; Pasqualini, R.; Arap, W., *Nat. Med.* **2001**, 7, 1249.
21. Trepel, M.; Arap, W.; Pasqualini, R., *Curr. Opin. Chem. Biol.* **2002**, 6, 399.
22. Barbas, C. F.; Burton, D. R.; Scott, J. K.; Silverman, G. J., *Phage Display, A Laboratory Manual*. Woodbury, NY, 2001.
23. Kolonin, M. G.; Saha, P. K.; Chan, L.; Pasqualini, R.; Arap, W., *Nat. Med.* **2004**, 10, 625.
24. Arap, W.; Kolonin, M. G.; Trepel, M.; Lahdenranta, J.; Cardo-Vila, M.; Giordano, R. J.; Mintz, P. J.; Ardel, P. U.; Yao, V. J.; Vidal, C. I., *Nat. Med.* **2002**, 8, 121.
25. Shenton, W.; Davis, S. A.; Mann, S., *Adv. Mater.* **1999**, 11, 449.
26. Hermanson, G. T.; Mallia, A. K.; Smith, P. K., *Immobilized Affinity Ligand Techniques*, Academic: London, 1992.
27. Sorokulova, I. B.; Olsen, E. V.; Chen, I.-H.; Fiebold, B.; Barbareeb, J. M.; Vodyanoyc, V. J.; Chind, B. A.; Petrenkoa, V. A., *Journal of Microbiological Methods* **2005**, 63, 55.
28. Reddy, V. R.; Currao, A.; Calzaferri, G., *Journal of Physics: Conference Series* **2007**, 61, (960).

29. Frens, G., *Nature Phys. Sci.* **1971**, 20, 241.
30. Traut, R. R.; Bollen, A.; Sun, T.-T.; Hershey, J. W. B.; Sundberg, J.; Pierce, L. R., *Biochem.* **1973**, 12, 3266.
31. Fowler, J. M.; Stuart, M. C.; Wang, D. K. Y., *Anal. Chem.* **2007**, 79, 350.
32. Link, S.; El-Sayed, M. A., *Annu. Rev. Phys. Chem.* **2003**, 54, 331.
33. Haiss, W.; Thanh, N. T. K.; Aveyard, J.; Fernig, D. G., *Anal. Chem.* **2007**, 79, 4215.
34. Mie, G., *Contributions to the optics of turbid media, particularly of colloidal metal solutions-Translation*. National Translation Center: Chicago, 1978.
35. Hornyak, G. L.; Patrissi, C. J.; Oberhauser, E. B.; Martin, C. R.; Valmalette, J. C.; Lemaire, L.; Dutta, J.; Hofmann, H., *Nanostructured Materials* **1997**, 9, 571.
36. Armendariz, V.; Herrera, I.; Peralta-Videa, J. R.; Jose-Yacaman, M.; Troiani, H.; Santiago, P.; Gardea-Torresdey, J. L., *Journal of Nanoparticle Research* **2004**, 6, 377.
37. Shipway, A. N.; Lahav, M.; Gabai, R.; Willner, I., *Langmuir* **2000**, 16, 8789.
38. Sokolov, K.; Follen, M.; Aaron, J.; Pavlova, I.; Malpica, A.; Lotan, R.; Richards-Kortum, R., *Cancer Res.* **2003**, 63, 1999.
39. Paciotti, G.; Myer, L.; Weinreich, D.; Goia, D.; Pavel, N.; McLaughlin, R.; Tamarkin, L., *Drug Deliv* **2004**, 11, 169.
40. Sakura, T.; Nagasaki, Y., *Colloid Polym Sci* **2007**, 285, 1407.
41. Grabar, K. C.; Freeman, R. G.; Hommer, M. B.; Natan, M. J., *Anal. Chem.* **1995**, 67, 735.
42. Shipway, A. N.; Lahav, M.; Gabai, R.; Willner, I., *Langmuir* **2000**, 16, 8789.

43. Souza, G. R.; Christianson, D. R.; Staquicini, F. I.; Ozawa*, M. G.; Snyder, E. Y.; Sidman, R. L.; Miller, J. H.; Arap, W.; Pasqualini, R., *Proceedings of National Academy of Sciences of the United States of America* **2006**, 103, 1215.
44. Overman, S. A.; Bondre, P.; Maiti, N. C.; Thomas, G. J., *Biochemistry* **2005**, 44, 3091.
45. Overman, S. A.; Kristensen, D. M.; Bondre, P.; Hewitt, B.; Thomas, G. J., **2004**, 43, 13129.
46. Overman, S. A.; Thomas, G. J., *Biochemistry* **1995**, (34), 5440.
47. Ye, Q.; Fang, J.; Sun, L., *J. Phys. Chem. B* **1997**, 101, 8221.
48. Murray, C. A.; Allara, D. L.; Rhinewine, M., *Phys. Rev. Lett.* **1981**, 46, 57.
49. Murray, C. A.; Allara, D. L., *J. Chem. Phys.* **1982**, 76, 1290.
50. Macdonald, I. D. G.; Smith, W. E., *Langmuir* **1996**, 12, 706.
51. Haynes, L. C.; McFarland, D. A.; Duyne, R. P., *Anal. Chem.* **2005**, 339A.
52. Sorokulovaa, I. B.; Olsenb, E. V.; Chen, I. H.; Fiebord, B.; Barbaree, J. M.; Vodyanoyc, V. J.; Chind, B. A.; Petrenko, V. A., *Journal of Microbiological Methods* **2005**, 63, 55.
53. Notingher, L., *Sensors* **2007**, 7, 1343.
54. Naja, G.; Bouvrette, P.; Hrapovic, S.; Luong, J. H. T., *Analyst* **2007**, 132, 679.
55. Sengupta, A.; Mujacic, M.; Davis, E. J., *Anal Bioanal Chem* **2006**, 386, 1379.
56. Russel, M.; Lowman, H. B.; Clackson, T., Introduction to phage biology and phage display. In 2005; p 1.
57. Gremlich, H.-U.; Yan, B., *Infrared and Raman Spectroscopy of Biological Materials*. Marcel Dekker Inc.: New York, 2000; p 329.

58. Souza, G. R.; Miller, J. H., *J. Am. Chem. Soc.* **2001**, 123, 6734.
59. Yguerabide, J.; Yguerabide, E. E., *Anal. Biochem.* **1998**, 262, 157.
60. Mirkin, C. A.; Letsinger, R. L.; Mucic, R. C.; Storhoff, J. J., *Nature* **1996**, 382, 607.

CHAPTER 4

PREPARATION AND CHARACTERIZATION OF

POLYOXOMETALATE/PROTEIN ULTRATHIN FILMS GROWN

ON ELECTRODE SURFACES USING LAYER-BY-LAYER

ASSEMBLY

Reproduced with permission from [*Langmuir* **2008**, *24*, 3584-3589.] Copyright [2008]

American Chemical Society

4.1. Introduction

In addition to yielding fundamental insights into biological electron transfer processes, the use of redox enzymes to interface with external solid electrodes has many potential applications, such as amperometric biosensors and biofuel cells¹⁻⁷. Over the past years, a wide variety of experimental strategies⁸⁻¹⁰ have been investigated to establish reliable electrical communication between enzymes and electrodes, including layer-by-layer (LbL) deposition, the direct modification of enzymes with electron relays, and the reconstitution of apo-flavoenzymes (i.e., glucose oxidase) on self-assembled monolayers.

The immobilization of redox proteins such as cytochrome *c* (*cyt c*) onto electrode surfaces through LbL deposition has been highly successful in practice¹¹⁻¹⁹. Owing to their multiple charges and flexible backbones, polyelectrolytes are often the material of choice in forming LbL thin films. While the multiple charges collectively enforce strong

binding between the polymer molecule and the oppositely charged surface, the flexible polymer chain can easily adjust to the local surface structure and charge distribution. Nevertheless, several LbL film preparation schemes exist where metal and inorganic nanoparticles are used instead of polyelectrolytes. For example, He *et al.* demonstrated an LbL formation of hemoglobin multilayer film using 35-nm SiO₂ nanoparticles²⁰. Polyoxometalates (POMs), a large family of charged, nanoscopic inorganic clusters, are attractive materials for electrode modification because of their reversible redox behavior, good chemical stability and electronic conductivity²¹⁻²⁹. We expect POMs to be excellent counter ions for LBL deposition because of their relatively high surface charge and their versatile self-assembly capabilities³⁰. Compared to previously used nanoparticles, POMs are at least an order of magnitude smaller in size and should form more conformal films. Moreover, these inorganic nanoclusters themselves show electrocatalytic activity (e.g., for reduction of hydrogen peroxide²⁶, nitrogen monoxide²⁸, iodate²⁹), a characteristic worth exploring in designing new LbL-based films.

Herein, we report on the preparation and characterization of LbL assembled ultrathin films containing model proteins and POMs. We show that stable, electrochemically well-behaved protein-containing films can be reproducibly prepared using nanoscopic (~ 1 nm) POMs as the counter ion. This approach departs from the majority of previously reported LbL procedures³¹⁻³⁴ in which polyelectrolyte counter ions are generally employed. Cyclic voltammetry, UV-vis spectroscopy and atomic force microscopy (AFM) are used to characterize films formed using *cyt c* and P₂W₁₈O₆₂⁶⁻, a Dawson-type POM. The electron transfer of these films as a function of film thickness is systematically analyzed. Finally, the use of these films to catalyze hydrogen peroxide reduction is shown.

This work was performed in collaboration with Dr. Kai Jiang, a member of Dr. Wei Zhan's group. I was responsible for conducting the image scanning required by the project.

4.2. Experimental Section

4.2.1. Reagents.

Cytochrome c (M.W. 12300) and myoglobin (M.W. 16900) from horse heart were obtained from Sigma. Tris(2,2'-bipyridyl)dichlororuthenium(II) hexahydrate ($\text{Ru}(\text{bpy})_3\text{Cl}_2 \cdot 6\text{H}_2\text{O}$, 99.95%) was from Aldrich. Hydrogen peroxide (H_2O_2 , 30%), potassium dihydrogen phosphate (KH_2PO_4), dipotassium phosphate (K_2HPO_4) and potassium chloride (KCl) were from Fisher Scientific. Phosphate buffer saline (PBS, 0.01 M at pH = 7.4) was prepared by dissolving suitable amounts of KH_2PO_4 and K_2HPO_4 in water. All solutions employed in these experiments were prepared using 18.2 M Ω •cm deionized water (Millipore). Polyoxometalates, including $\text{K}_6\text{P}_2\text{W}_{18}\text{O}_{62}$ and $\text{K}_{12}\text{H}_2\text{P}_2\text{W}_{12}\text{O}_{48}$, were synthesized following reported procedures³⁵.

4.2.2. Film assembly

Prior to film assembly, the glassy carbon electrode (Bioanalytical Systems, diameter: 3 mm) was polished with 1.0, 0.3, 0.05 μm alumina slurries to a mirror-like finish. The electrode was then sonicated in 1:1 (w/w) HNO_3 aqueous solution, ethanol and water, each step for 5 min, and polarized at 1.2 V (vs. Ag/AgCl) for 5 min in 0.5 M NaOH aqueous solution with a Pt wire counter electrode. This treatment renders the electrode negatively charged. The electrode was then immersed in a 5 mg/mL $\text{Ru}(\text{bpy})_3\text{Cl}_2 \cdot 6\text{H}_2\text{O}$ aqueous solution for 1 h, resulting a positively charged, $\text{Ru}(\text{bpy})_3^{2+}$ layer on the surface. Finally, the positively charged electrode was immersed into corresponding POM (0.2

mM) and protein solutions (1 mg/mL) for 15 min for each adsorption step. Between each step, the modified electrode was rinsed with deionized water and dried in a stream of flowing nitrogen. The POM/Ru(bpy)₃²⁺ layered films were prepared similarly except that the *cyt c* solution was replaced by a 5 mg/mL Ru(bpy)₃Cl₂ aqueous solution²¹. For consistency, all the films used in this study are terminated by a POM layer.

The ultrathin POM/protein LbL films can also be prepared under electrochemical conditions. Initially, the glassy carbon electrode was polished, rinsed and polarized as described above. Then, it was subjected to potential scan between -0.8 and 0 V (vs. Ag/AgCl) at 0.1 V/s for 400 cycles in 5 mg/mL Ru(bpy)₃Cl₂ aqueous solution. This Ru(bpy)₃²⁺ modified electrode was then scanned in a POM solution (0.2 mM) (0.2 - 0.9 V vs. Ag/AgCl) and followed by *cyt c* solution (0.05 mg/mL in 0.05 M H₂SO₄; -0.55 - 0.05 V vs. Ag/AgCl), each for 100 cycles.

Glass substrates (Corning 7409) for UV-vis measurements (0.6 × 2 cm², 1 mm thick) were sonicated in Micro-90 washing solution (International Products Co.) for 1 h and then in a cleaning solution (60% ethanol + 39% water + 1% NaOH, w/w) for 30 min at 50 °C, and finally rinsed by water. Slides subjected to this treatment have a negatively charged surface. A positively charged Ru(bpy)₃²⁺ monolayer was then formed on the glass surface by immersing the slides into Ru(bpy)₃²⁺ solution for 1 h. The {P₂W₁₈O₆₂⁶⁻/*cyt c*}_n layers were assembled by immersing the slides into the corresponding solutions for 15 min.³

4.2.3. UV-vis Spectroscopy

All measurements were carried out using a UV-visible spectrophotometer (Cary 50 Bio, Varian).

4.2.4. AFM Measurements

AFM measurements to determine film thickness were performed using protein/POM films formed on mica. To facilitate the LbL assembly process on these substrates, freshly cleaved mica specimens were first immersed in a 5 mg/mL Ru(bpy)₃Cl₂ aqueous solution overnight to accumulate positive charges on surface. After thoroughly rinsing the mica samples with DI water, POM/protein films were assembled using the same static dipping procedure we used for glassy carbon electrodes. Patterning of LbL films on mica substrates was realized by a lithography-based lift-off procedure reported previously³⁶.

All AFM experiments were performed using a Park Scientific Instruments Autoprobe CP scanning probe microscope in tapping mode. The tips used were obtained from Digital Instruments, Inc. with a force constant of 0.12N/m. The samples were scanned at approximately 1Hz on a 100 μm piezoelectric scanner. The scan sizes and other experimental details are provided in the figure captions.

4.2.5. Electrochemistry

A CHI 910B bipotentiostat (CH Instruments, Austin, TX) and a three-electrode cell were used for the electrochemical film preparation and characterization. A Ag/AgCl reference electrode and a platinum wire counter electrode were employed throughout the experiment. Throughout the experiment, all the tested solutions were bubbled with Ar for at least 25 min to remove oxygen.

4.3. Results and Discussion

4.3.1 Film Assembly

We found that the initial electrode cleanness and overall surface charge is crucial for the successful formation of robust protein/POM LbL multilayers. After pretreatment, the

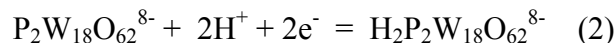
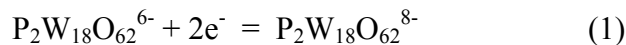
glassy carbon electrode was coated with a $\text{Ru}(\text{bpy})_3^{2+}$ layer so that the electrode surface became positively charged and thus electrostatically attractive to POMs. From there, multiple protein/POM layers could be built by either static dipping or electrochemical scanning in the appropriate adsorbate-containing solutions. In the case of static dipping, a 15-min immersion was found to be sufficient to achieve nearly complete monolayer coverage on the electrode. On the other hand, we found that electrochemical cycling could produce LbL films routinely, but the amounts of protein and POM immobilized often varied from run to run. While in the following we focus our discussion on $\text{P}_2\text{W}_{18}\text{O}_{62}^{6-}/\text{cyt } c$ films formed on glassy carbon, we have had similar success in preparing LbL films using different proteins and POMs, and using substrates such as gold and mica.

4.3.2. Characterization of LbL films

The growth of $\{\text{POM}/\text{protein}\}_n$ films on glassy carbon electrodes was monitored using cyclic voltammetry in 0.1 M H_2SO_4 solution, since, as expected for Wells-Dawson anions, the POM modified electrodes only showed well-behaved, reversible redox waves under acidic aqueous conditions³⁷. Representative cyclic voltammograms of $\{\text{P}_2\text{W}_{18}\text{O}_{62}^{6-}/\text{cyt } c\}_n$ films are shown in Figure 1a. Three pairs of reversible redox peaks with $E_{1/2}$ values at about 0 V (A/A'), -0.20 V (B_1/B_1') and -0.43 V (B_2/B_2'), respectively, are observed between -0.5 V and +0.2 V. In addition, the peak current associated with each of the three waves increases linearly as the number of deposited layers increases.

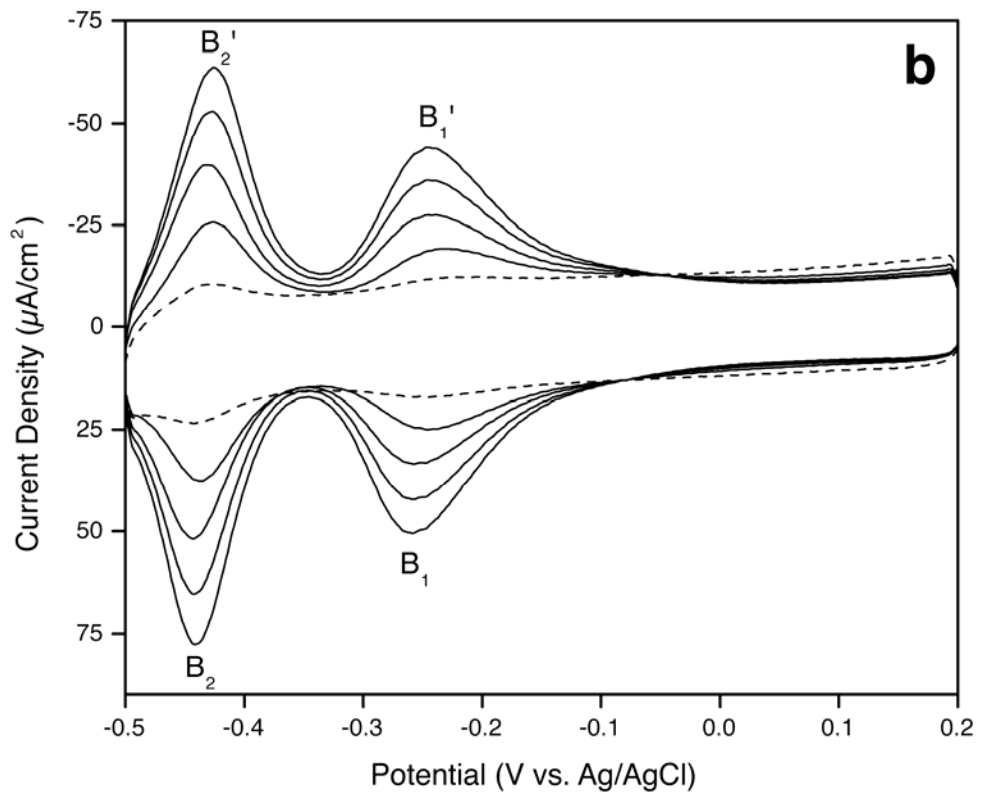
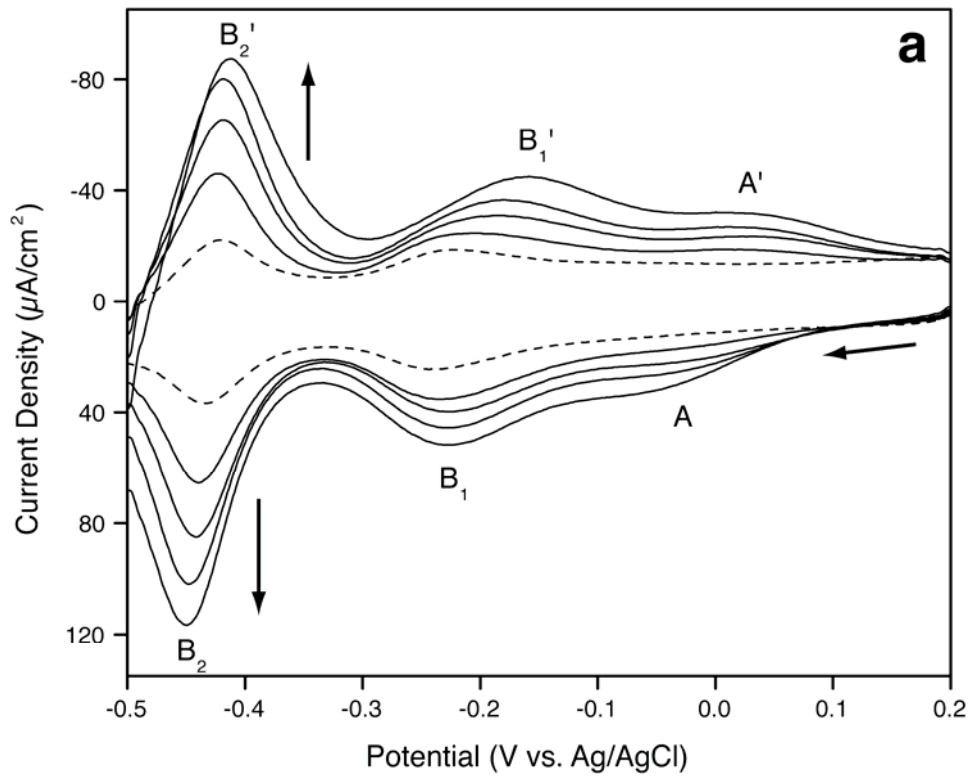
To assign the electrochemical processes associated with each voltammetric wave, a blank film was prepared in which *cyt c* was replaced with $\text{Ru}(\text{bpy})_3^{2+}$ (as before, $\text{P}_2\text{W}_{18}\text{O}_{62}^{6-}$ was the counter ion). Because $\text{Ru}(\text{bpy})_3^{2+}$ does not undergo electrochemical reactions in the potential region used for these measurements, all of the redox features

observed from the blank film could be assigned to the POM. As shown in Figure 1b, two pairs of reversible waves are seen (B_1/B_1' and B_2/B_2'). The reductive voltammetry of the Wells-Dawson POMs series in acidic aqueous media is well-studied; typically, four reversible waves between 0 V and -0.750 V are observed. The first two waves are one-electron reductions and the second two waves are two-electron/two-proton reductions. In the case of both the $\{P_2W_{18}O_{62}^{6-}/cyt\ c\}_n$ and $\{P_2W_{18}O_{62}^{6-}/Ru(bpy)_3^{2+}\}_n$ films studied here, it appears that the first wave (B_1) is a two-electron wave. This behavior has been reported before: at extremely low pH values, in the case of transition metal substituted Wells-Dawson compounds, and in $P_2W_{18}O_{62}^{6-}/poly(1-naphthol)$ films³⁸. Based on these considerations, the electrochemical processes associated with peaks B_1/B_1' and B_2/B_2' can be described by the following reactions²³:



The amount of $P_2W_{18}O_{62}^{6-}$ immobilized in each layer was calculated from the integrated charges of wave B_2 or B_2' to be $1.5 - 1.6 \times 10^{-10}$ mol/cm², which corresponds to a nearly full monolayer coverage²¹.

Figure 1c is an overlay of CVs obtained from $\{P_2W_{18}O_{62}^{6-}/cyt\ c\}_2$ and $\{P_2W_{18}O_{62}^{6-}/Ru(bpy)_3^{2+}\}_4$ films. On the basis of this data, we assign the couple (A/A') around 0 V to the direct reduction (oxidation) of *cyt c*. It should be noted that the formal potential of *cyt c* in the $\{P_2W_{18}O_{62}^{6-}/cyt\ c\}_2$ film is shifted to somewhat more negative values than what is typically observed for *cyt c* in solution or in uncharged monolayer films³⁹. The interaction of *cyt c* with the negatively charged POM would be expected to stabilize the oxidized form of the protein and cause $E_{1/2}$ to shift to more negative values, consistent



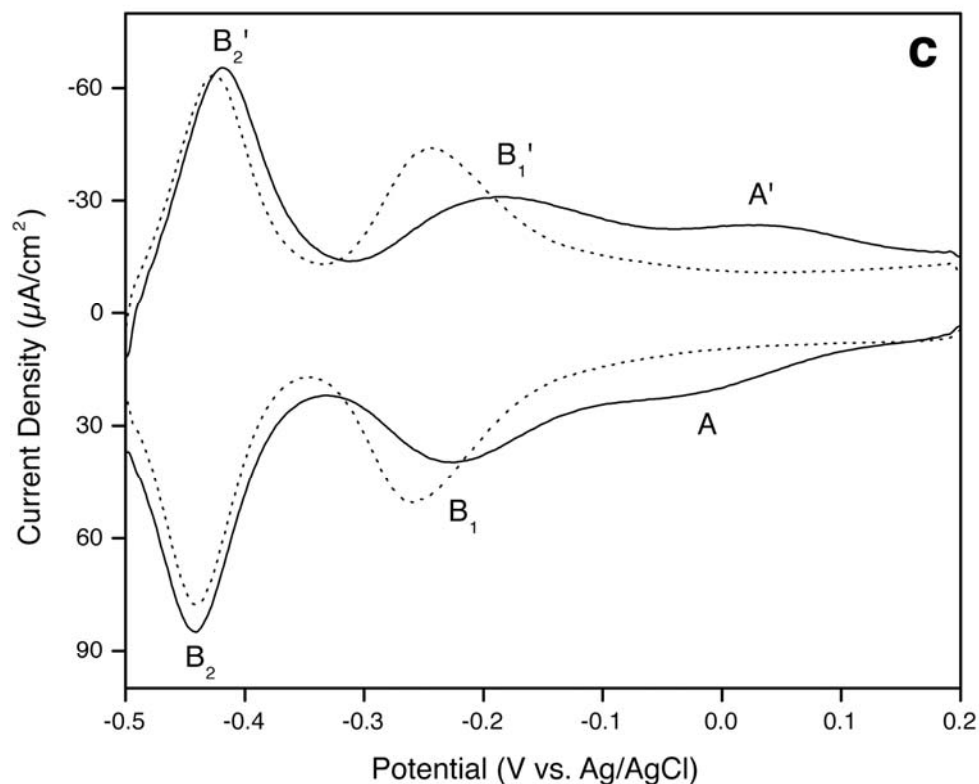
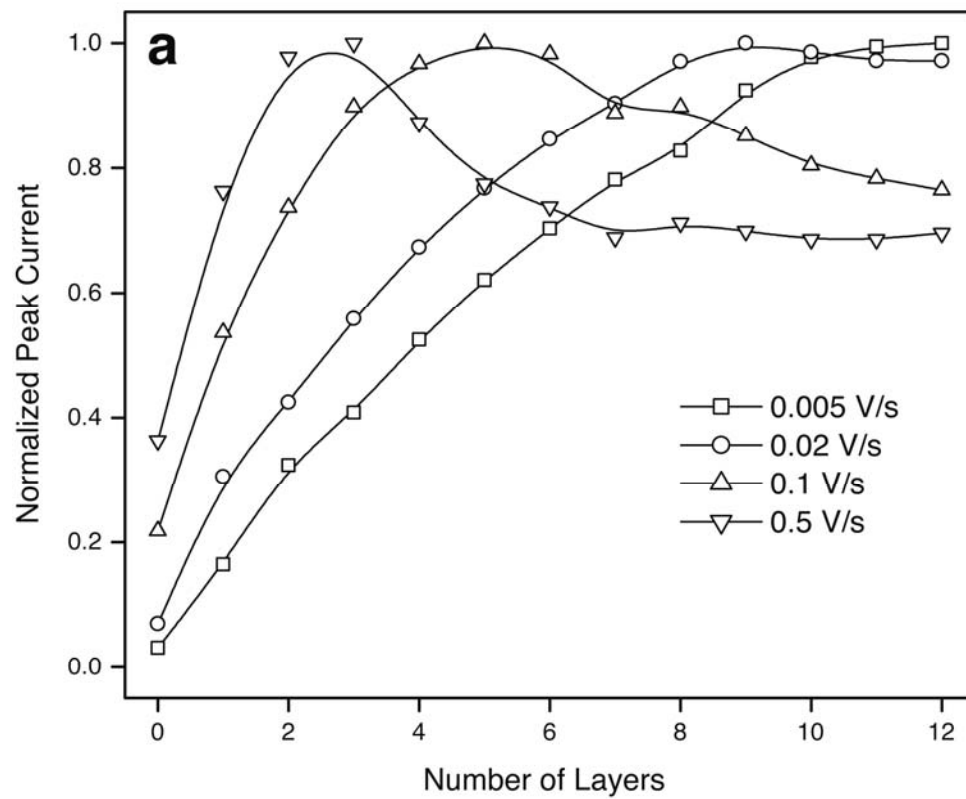


Figure 4.1. Layer-by-layer formation of $P_2W_{18}O_{62}^{6-}$ and *cyt c* (or $Ru(bpy)_3^{2+}$) thin films characterized by cyclic voltammetry (CV). The multilayered films were formed by alternately dipping a glassy carbon electrode (GCE) in respective POM and protein (or $Ru(bpy)_3^{2+}$) solutions. The first layer (dash line) of $P_2W_{18}O_{62}^{6-}$ was electrostatically attracted onto the electrode surface by a pre-adsorbed $Ru(bpy)_3^{2+}$ layer. See Experimental section. Supporting electrolyte: 0.1 M H_2SO_4 aqueous solution; scan rate: 0.1 V/s. (a) $\{P_2W_{18}O_{62}^{6-}/cyt c\}_n$, $n = 1-4$; (b) $\{P_2W_{18}O_{62}^{6-}/Ru(bpy)_3^{2+}\}_n$, $n = 1-4$; (c) Comparison of $\{P_2W_{18}O_{62}^{6-}/cyt c\}_2$ and $\{P_2W_{18}O_{62}^{6-}/Ru(bpy)_3^{2+}\}_4$ (dot line).

with the observed positive shift of $E_{1/2}$. Also evident in the $\{P_2W_{18}O_{62}^{6-}/cyt\ c\}_n$ films is that the peak splitting becomes greater as the number of layers increases, which could arise from a modified electronic microenvironment as a result of the interaction between $P_2W_{18}O_{62}^{6-}$ and *cyt c*. Nevertheless, the integrated charges of wave $B_1(B_1')$ remain comparable between the two films, indicating that the additional peaks ($A(A')$) are indeed due to *cyt c* redox processes.

Voltammetric measurements carried out on $\{P_2W_{18}O_{62}^{6-}/Ru(bpy)_3^{2+}\}_n$ films at different scan rates reveal that the POM peak currents are proportional to the scan rate up to 0.5 V/s at $n = 8$, consistent with the electrochemical behavior expected from a surface-confined species⁴⁰. In contrast, the scan rate dependence we observed in the case of $\{P_2W_{18}O_{62}^{6-}/cyt\ c\}_n$ films appears more complex. Figure 2a shows how the normalized peak current of B_2' changes with the number of $P_2W_{18}O_{62}^{6-}/cyt\ c$ multilayers at different scan rates. For the four different scan rates tested (0.5, 0.1, 0.02, and 0.005 V/s), the maximum peak current occurs at layer numbers of $n = 3, 5, 9,$ and 12 , respectively. At relatively high scan rates, the peak currents first decrease beyond the maximum and then level off, suggesting that the scan rate has exceeded the rate of electron transfer through the multilayer¹⁵. If this is true, then measurements at low scan rates should approach the ideal linear dependence of peak current on scan rate. Indeed, when the scan rate is lowered to 0.005 V/s, all 12 layers are electrochemically accessible (Figure 2b). More quantitative measurements on charge transport through these films will be discussed in the next section.

UV-vis absorption spectroscopy was also used to characterize the formation of $\{P_2W_{18}O_{62}^{6-}/cyt\ c\}_n$ films, since *cyt c* has an intense Soret band at around 409 nm



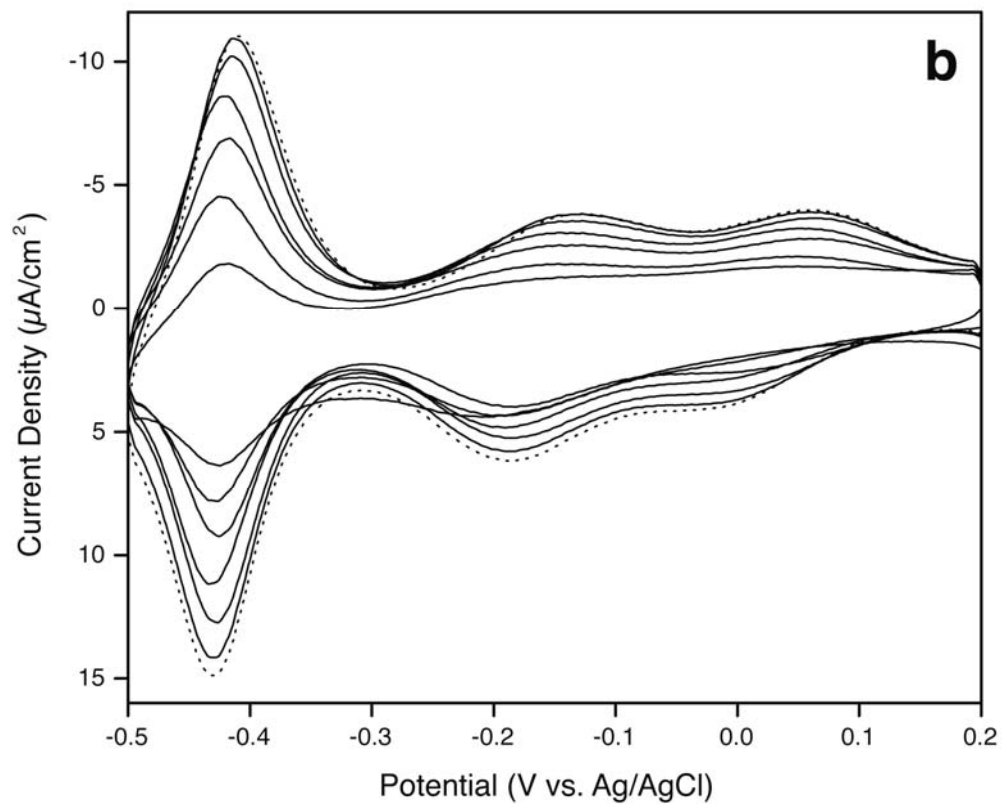


Figure 4.2. Electrochemical responses of a $\{P_2W_{18}O_{62}^{6-}/cyt\ c\}_n$ film under different CV scan rate. (a) Normalized peak (B_2' as in Figure 1a) current of $\{P_2W_{18}O_{62}^{6-}/cyt\ c\}_n$ ($n = 1-12$) at different scan rate; (b) Cyclic voltammograms of $\{P_2W_{18}O_{62}^{6-}/cyt\ c\}_n$ at 0.005 V/s (solid line: $n = 1, 3, 5, 7, 9$ and 11; dot line: $n = 12$).

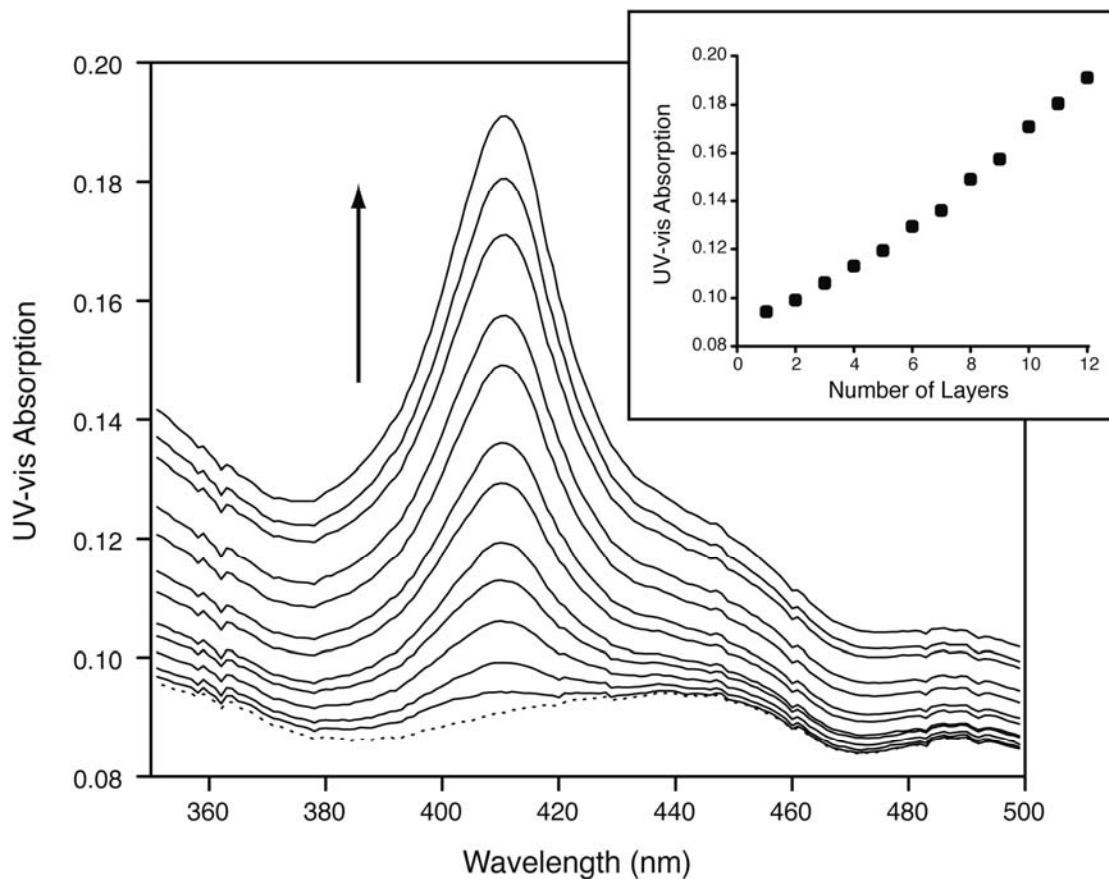


Figure 4.3. UV-vis absorption spectra of $\{P_2W_{18}O_{62}^{6-}/cyt\ c\}_n$ ultrathin film layer-by-layer assembled on a glass slide. dotted line: blank; solid lines show stepwise growth of $\{P_2W_{18}O_{62}^{6-}/cyt\ c\}_n$ on both sides of glass slide, $n = 1-12$; the arrow indicates the film growth direction. Inset: layer-by-layer growth of *cyt c* absorption at 409 nm.

(Figure 3). The increase of absorption at 409 nm was found to be directly proportional to the number of layers deposited and is consistent with our cyclic voltammetry results. Moreover, the well-defined band shapes of the UV-vis spectra suggest that the ternary structure of *cyt c* has not been significantly perturbed during the LbL assembly process. From the increase in absorption, the average coverage of *cyt c* in each layer is calculated to be close to one monolayer, that is, $\sim 2.2 \times 10^{-11}$ mol/cm²⁴⁰⁻⁴². The inset to Figure 3 shows a plot of absorption peak intensity as a function of layer number. Interestingly, there is a small but noticeable increase in the slope of this graph after about the fifth layer. Similar behavior has been observed in the case of polymer-based LbL films³¹.

4.3.3. AFM characterization of {P₂W₁₈O₆₂⁶⁻/*cyt c*}_n films.

Owing to the intrinsic negative surface charge, mica surfaces are ideal for forming POM/*cyt c* LbL films. Combining LbL assembly and a previously published microfabrication technique³⁶, we were able to fabricate simple patterned LbL films and measure the film thickness directly using atomic force microscopy to profile lithographically defined step edges. A typical AFM image of {P₂W₁₈O₆₂⁶⁻/*cyt c*}₁₀ film near one such step edge is shown in Fig. 4. The upper left portion of the image shows an exposed region of the bare mica substrate, while the more textured region in the lower part of the image reveals the topography of the LbL film. The linear features that can be seen near the step edge are film defects and do not correspond to individual monolayer steps. In this image, a step height of ~ 40 nm was obtained when the tip was scanned from the mica substrate to the patterned film. This result is in excellent agreement with the physical dimensions of the POM (~ 1 nm) and protein ($\sim 3 \times 3 \times 4$ nm) used, as well as the number of film layers prepared.

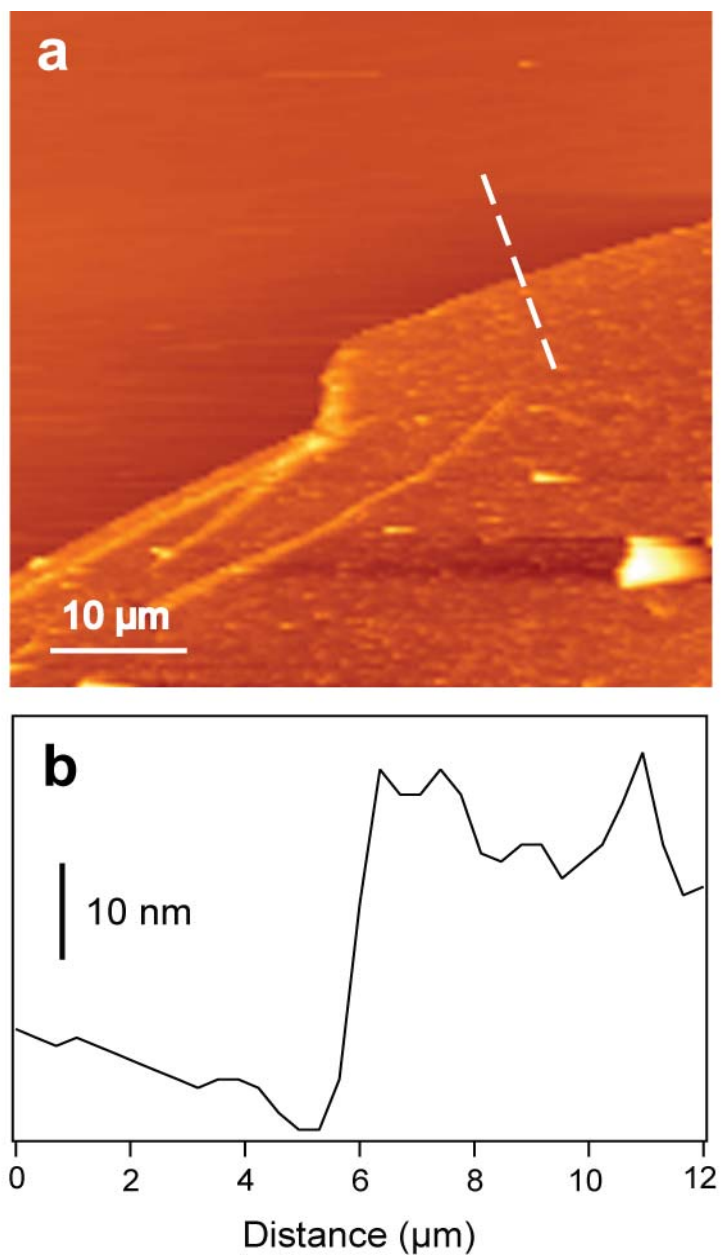


Figure 4.4. Determination of LbL film thickness using AFM. (a) Tapping mode AFM imaging was used to profile lithographically defined patterns in LbL films. An area of the patterned film containing regions of bare mica as well as a $\{P_2W_{18}O_{62}^{6-}/cyt\ c\}_{10}$ film is shown (b). The height profile as measured along the dashed line in the image a.

4.3.4. Effect of film thickness on overall electron transfer rate.

Following Laviron's approach⁴³, we examined the effect of LbL film thickness on the electron transfer rate by studying the redox peak splitting as a function of the scan rate. For this purpose, we chose the second reduction/oxidation peak of $P_2W_{18}^{6-}$ (B_2/B_2') because it is well resolved in cyclic voltammetry. In this analysis, cathodic and anodic peak potentials are plotted as a function of the logarithm of the scan rate, and the limiting slope of the resulting plots at high scan rate is used to determine k°_{app} . Typical Laviron plots are shown in Figure 5. Table 1 shows the $P_2W_{18}^{6-}$ rate constant for films of different thickness assuming $\alpha = 0.5$. Clearly, the electron transfer slows down as the film becomes thicker in both preparations; in particular, the rate decrease is faster for $\{Ru(bpy)_3^{2+}/cyt\ c\}_n$ films as a result of larger building block (*cyt c* vs. $Ru(bpy)_3^{2+}$) and thus thicker films.

4.3.5. Electrocatalysis of hydrogen peroxide reduction using $\{P_2W_{18}O_{62}^{6-}/cyt\ c\}_n$ films.

An important application of electroactive LbL films is their electrocatalysis, as hybrid films prepared in this manner can dramatically enhance the reduction/oxidation of many species that otherwise only display sluggish electrochemical behavior. We chose to test the electrocatalytic reduction of hydrogen peroxide using our films because *cyt c* is known to be catalytically active for H_2O_2 reduction^{44, 45}. As shown in Fig. 6a, the film containing both $P_2W_{18}O_{62}^{6-}$ and *cyt c* enhance the electro-reduction of H_2O_2 by greater than 10 fold as compared to that from a film having $P_2W_{18}O_{62}^{6-}$ only. In addition, if $\{P_2W_{18}O_{62}^{6-}/cyt\ c\}_n$ films are used, the reduction current actually decreases as the number of layers grows. These results indicate that the catalytic activity of the films is dominated by the contribution of *cyt c*. Using films containing a single layer of $P_2W_{18}O_{62}^{6-}$ and *cyt c*,

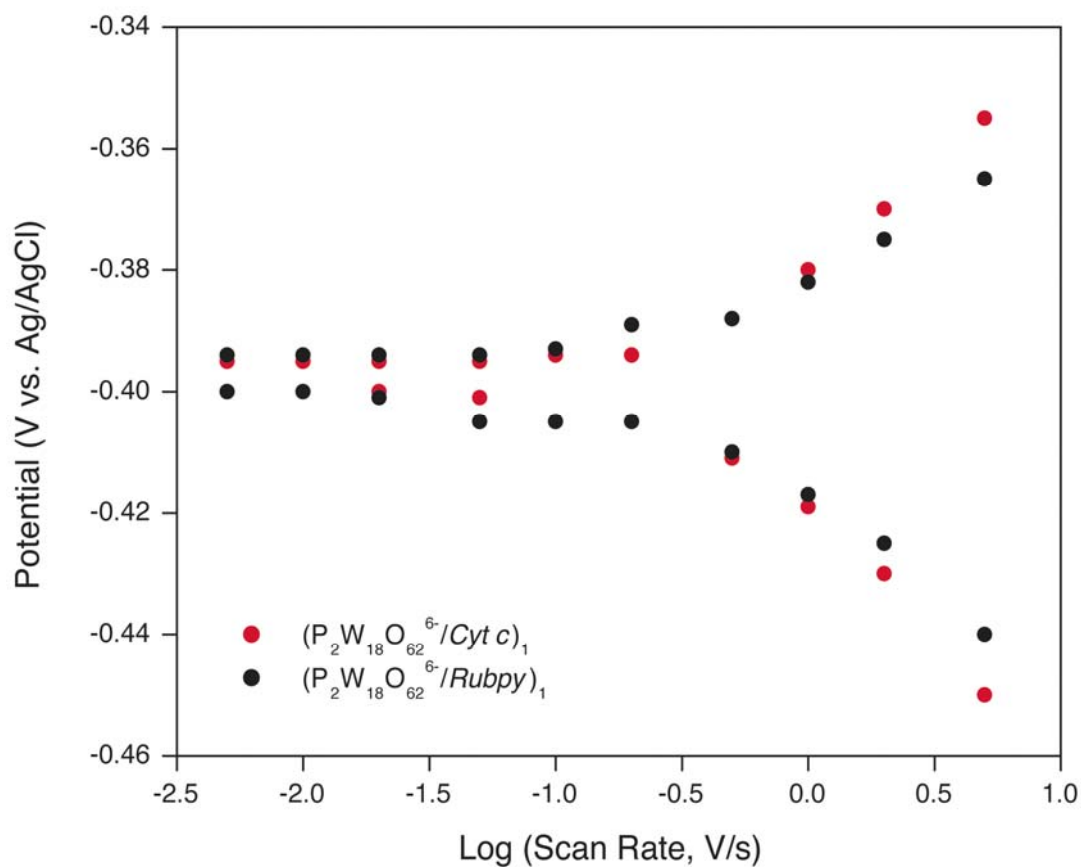
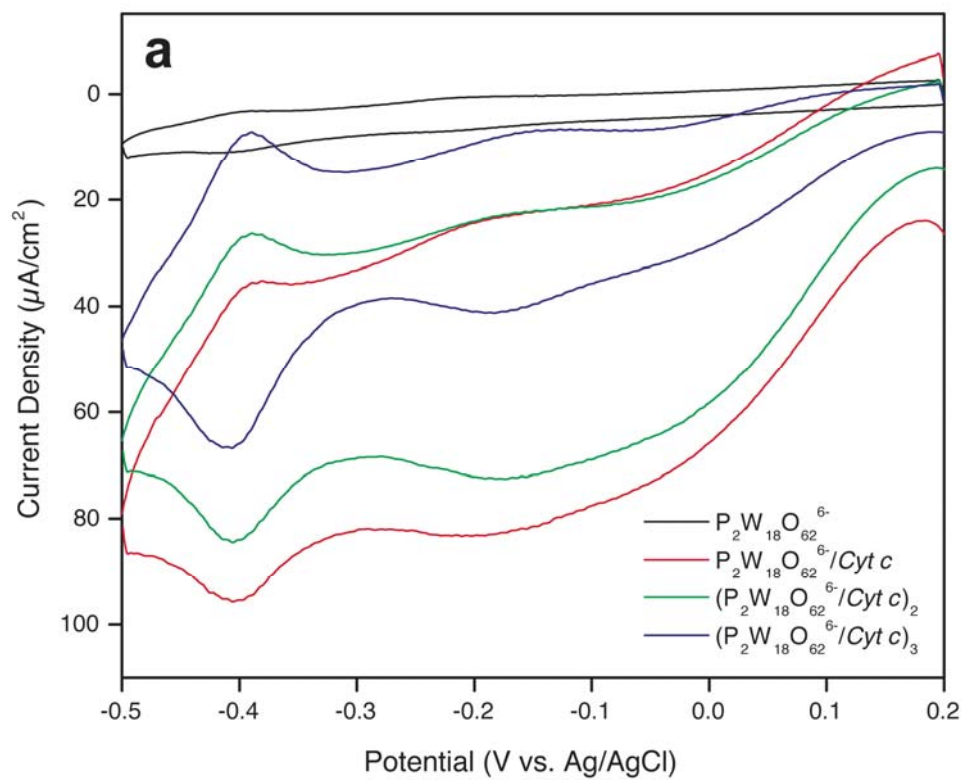


Figure 4.5. Determination of the apparent electron transfer rate constants (k_{app}) for $\{P_2W_{18}O_{62}^{6-}/cyt\ c\}_1$ and $\{P_2W_{18}O_{62}^{6-}/Rubpy\}_1$ films following Laviron method. Peak potentials were collected from the CVs at different scan rates in degassed 0.1 M H_2SO_4 aqueous solution.

Table 4.1. Change of k_{app}° as a function of number of LbL layers.

n	(POM/Rubpy) _n	(POM/cyt c) _n
1	31.7 s ⁻¹	26.4 s ⁻¹
2	20.0 s ⁻¹	19.8 s ⁻¹
5	10.6 s ⁻¹	4.0 s ⁻¹



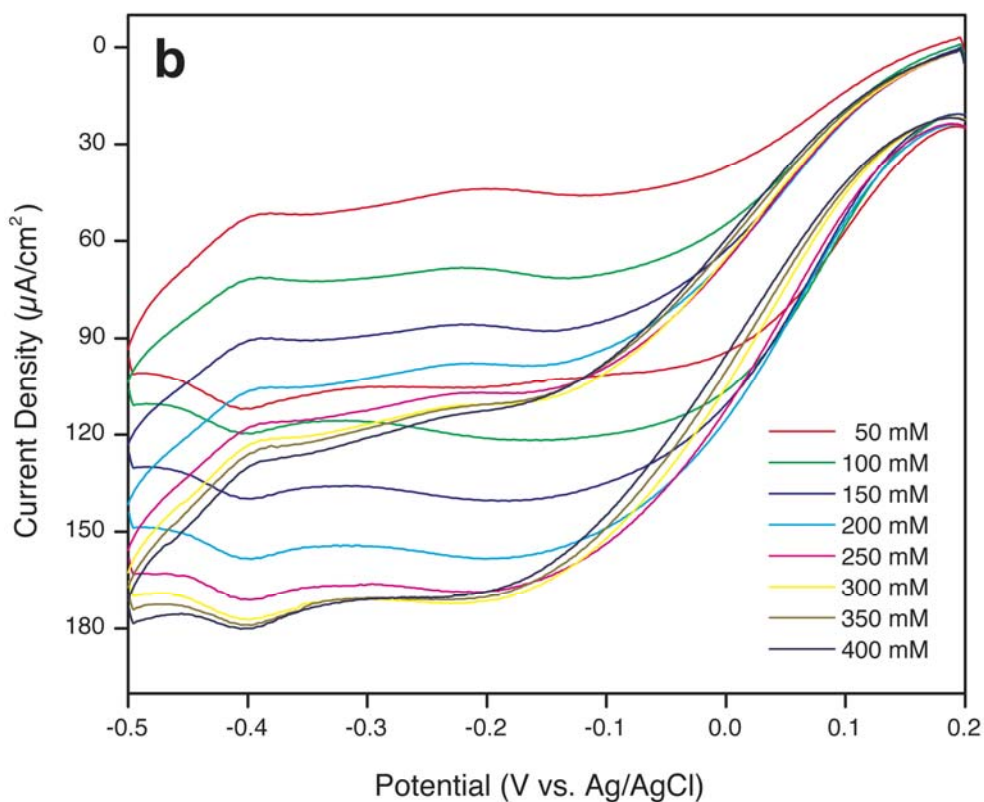


Figure 4.6. Electrocatalysis of hydrogen peroxide reduction using $\{P_2W_{18}O_{62}^{6-}/cyt\}_n$ films. (a) Dependence of catalysis efficiency on film thickness. $\{P_2W_{18}O_{62}^{6-}/cyt\}_n$ ($n = 1 - 3$) films were examined using 50 mM H_2O_2 ; supporting electrolyte: 0.1 M KCl in 0.1 M phosphate buffer (PBS), pH = 7.3; (b) Catalysis of hydrogen peroxide reduction using $\{P_2W_{18}O_{62}^{6-}/cyt\}_n$ ($n = 1$) modified GCEs at different H_2O_2 concentrations; other conditions are the same as in (a).

we found that the reduction current of H₂O₂ increases nearly linearly up to 250 mM and then levels off, which suggests that the catalysis follows the typical Michaelis–Menten behavior⁴⁶.

4.4. Conclusions

It was with two questions in mind that we set out to prepare POM/protein thin films using electrostatic LbL assembly. First, is it possible to use highly charged inorganic species such as POMs and macromolecules such as proteins to replace conventional polyelectrolytes in forming such assemblies? Many nanoscopic building blocks have been incorporated into LbL films; however, polymeric polyelectrolytes are almost always used as the counterparts in such films. In this regard, we have clearly demonstrated that polyoxometalates represent suitable materials, owing to their extremely small size, intrinsic charges and chemical stability. In fact, electrochemical and UV-vis absorption spectroscopic characterization confirm a nearly monolayer-by-monolayer growth of POMs and proteins when they are deposited by static dipping. Second, we were also curious to know if films formed using these unconventional building blocks can facilitate direct electrochemistry of redox proteins when the latter are assembled. The experiments we have done so far indicate that secondary structural considerations such as POM/protein complex formation and protein orientation may play an important role in the observed electron transfer kinetics and catalyst performance. While {P₂W₁₈O₆₂⁶⁻/cyt *c*}_n films formed by our method clearly show enhanced reduction of hydrogen peroxide, the catalytic efficiency is somewhat lower, for example, than the case where negative-charge-terminated gold nanoparticles are used to assemble *cyt c*. This result from another perspective emphasizes that many, sometimes subtle, requirements need to be met

experimentally before a strong electrochemical communication can be established between redox proteins and the electrodes. Can we design new POM structures to better accommodate redox proteins in LbL assembly? Is it possible to induce a higher level of control of the protein orientation using POMs? These are the questions we hope to find answers to in the near future. Recent studies of POM/protein interactions that show well defined binding sites and stoichiometries with no denaturation are quite promising in this regard⁴⁸.

References

1. Armstrong, F. A.; Hill, H. A. O.; Walton, N. J., *Q. Rev. Biophys.* 1985, 18, 261.
2. Zhou, Y. L.; Hu, N. F.; Zeng, Y. H.; Rusling, J. F., *Langmuir* 2002, 18, 211.
3. Shen, L.; Hu, N. F., *Biochim. Biophys. Acta-Bioenerg.* 2004, 1608, 23.
4. Shan, W. J.; He, P. L.; Hu, N. F., *Electrochim. Acta* 2005, 51, 432.
5. Sultana, N.; Schenkman, J. B.; Rusling, J. F., *J. Am. Chem. Soc.* 2005, 127, 13460.
6. Xu, J. M.; Li, W.; Yin, Q. F.; Zhu, Y. L., *Electrochim. Acta* 2007, 52, 3601.
7. Willner, I.; Katz, E., *Angew. Chem.Int. Edit.* 2000, 39, 1180.
8. Degani, Y.; Heller, A., *J. Am. Chem. Soc.* 1988, 110, 2615.
9. Willner, I.; Heleg-Shabtai, V.; Blonder, R.; Katz, E.; Tao, G. L.; Buckmann, A. F.; Heller, A., *J. Am. Chem. Soc.* 1996, 118, 10321.
10. Bernhardt, P. V., *Aust. J. Chem.* 2006, 59, 233.
11. Lvov, Y.; Ariga, K.; Ichinose, I.; Kunitake, T., *J. Am. Chem. Soc.* 1995, 117, 6117.
12. Lvov, Y. M.; Lu, Z. Q.; Schenkman, J. B.; Zu, X. L.; Rusling, J. F., *J. Am. Chem. Soc.* 1998, 120, 4073.
13. Jin, Y. D.; Shao, Y.; Dong, S. J., *Langmuir* 2003, 19, 4771.
14. Lojou, E.; Bianco, P., *J. Electroanal. Chem.* 2003, 557, 37.
15. Beissenhirtz, M. K.; Scheller, F. W.; Stocklein, W. F. M.; Kurth, D. G.; Mohwald, H.; Lisdat, F., *Angew. Chem.Int. Edit.* 2004, 43, 4357.
16. He, P. L.; Hu, N. F., *Electroanalysis* 2004, 16, 1122.
17. Lu, H. Y.; Hu, N. F., *Electroanalysis* 2006, 18, 1511.
18. Lojou, E.; Bianco, P., *Electroanalysis* 2006, 18, 2426.

19. Feng, J. J.; Xu, J. J.; Chen, H. Y., *Biosens. Bioelectron.* 2007, 22, 1618.
20. He, P. L.; Hu, N. F.; Rusling, J. F., *Langmuir* 2004, 20, 722.
21. Ingersoll, D.; Kulesza, P. J.; Faulkner, L. R., 1994, 141, 140.
22. Kuhn, A.; Anson, F. C., *Langmuir* 1996, 12, 5481.
23. Sadakane, M.; Steckhan, E., *Chem. Rev.* 1998, 98, 219.
24. Katsoulis, D. E., *Chem. Rev.* 1998, 98, 359.
25. Liu, J. Y.; Cheng, L.; Li, B. F.; Dong, S. J., *Langmuir* 2000, 16, 7471.
26. Martel, D.; Kuhn, A., *Electrochim. Acta* 2000, 45, 1829.
27. Wang, B. Q.; Cheng, L.; Dong, S. J., *J. Electroanal. Chem.* 2001, 516, 17.
28. Liu, S. Q.; Volkmer, D.; Kurth, D. G., *Anal. Chem.* 2004, 76, 4579.
29. Lin, X. Q.; Jiang, C. M., *Anal. Sci.* 2006, 22, 697.
30. Liu, T. B.; Diemann, E.; Li, H. L.; Dress, A.; Muller, A., *Nature* 2003, 426, 59.
31. Decher, G., *Science* 1997, 277, 1232.
32. Rusling, J. F.; Forster, R. J., *J. Colloid Interface Sci.* 2003, 262, 1.
33. Tang, Z. Y.; Wang, Y., *Adv. Mater.* 2006, 18, 3203.
34. Ariga, K.; Nakanishi, T.; Michinobu, T., *J. Nanosci. Nanotechnol.* 2006, 6, 2278.
35. Ginsberg, A. P., *Inorganic Syntheses*. Wiley Interscience: 1990; Vol. 27.
36. Zhan, W.; Alvarez, J.; Crooks, R. M., *Journal of the American Chemical Society* 2002, 124, 13265.
37. Xi, X. D.; Dong, S. J., *J. Mol. Catal. A-Chem.* 1996, 114, 257.
38. Pham, M. C.; Moslih, J.; Chauveau, F.; Lacaze, P. C., *J. Appl. Electrochem.* 1991, 21, 902.
39. Liu, H.; Tian, Y.; Z., D., *Langmuir* 2007, 23, 9487.

40. Kimizuka, N.; Tanaka, M.; Kunitake, T., *Chem. Lett.* 1999, 12, 1333.
41. Wood, L. L. C., S. S., *J. Am. Chem. Soc.* 1997, 119, 571.
42. Sorokulovaa, I. B.; Olsenb, E. V.; Chen, I. H.; Fiebord, B.; Barbaree, J. M.; Vodyanoyc, V. J.; Chind, B. A.; Petrenko, V. A., *Journal of Microbiological Methods* 2005, 63, 55.
43. Laviron, E., *Journal of Electroanalytical Chemistry* 1979, 101, 19.
44. Wang, J. X.; Li, M. X.; Shi, Z. J.; Li, N. Q.; Gu, Z. N., *Anal. Chem.* 2002, 74, 1993.
45. Zhao, G. C.; Yin, Z. Z.; Zhang, L.; Wei, X. W., *Electrochem. Commun.* 2005, 7, 256.
46. Kamin, R. A.; Wilson, G. S., *Analytical Chemistry* 1980, 52, 1198.
47. Zhang, H.; Hu, N., *Biosensors & Bioelectronics* 2007, 23, 393.
48. Zhang, G.; Keita, B.; Craescu, C. T.; Miron, S.; Oliveira, P.; Nadjo, L., *J. Phys. Chem. B* 2007, 111, 11253.

CHAPTER 5

SUMMARY

In the first part of this research, a polyaniline film was deposited onto a gold surface using the controlled potential method. Here, the polyaniline's state is controlled by adjusting the applied potential. The oxidized and reduced polyaniline forms were generated using potentials of +600 mV and -200 mV, respectively. MALDI-MS was used to prove that oxidized polyaniline can be nucleophilically attacked by butanethiol. The results revealed that only oxidized polyaniline can successfully be used to immobilize antibodies in order to make a good electrochemical immunosensors. As a result of this finding, a sandwich assay was developed for each of the oxidized and reduced polyaniline films and tested for a PAPP enzymatic hydrolysis. The IgG sandwich assay on oxidized polyaniline produced good cyclic voltammetry signals, with an oxidized peak current of 10^{-4} A. However, the IgG sandwich assay on reduced polyaniline film generated a peak current of only 10^{-6} - 10^{-5} A, ten times less than the immunoassay on oxidized polyaniline. When a F(ab) fragment of antibody was immobilized on the oxidized polyaniline, the biosensor layer exhibited good stability, with the peak current of the sandwich assay remaining at about 10^{-4} A. However, reacting the sensor layer with 11-mercapto-1-undecanol led to the monoclonal whole IgG molecules on oxidized polyaniline actually losing their activity. Raman spectroscopy also revealed that the F(ab) fragment of the antibody reduced the emeraldine form of polyaniline into the

leucoemeraldine form. There was no direct evidence of an interaction between the whole monoclonal antibody and polyaniline, but it was possible to confirm that only oxidized polyaniline can be used to construct effective immunosensors based on the cyclic voltammetry results. This is because the F(ab)₂ fragments of the antibodies are covalently bonded with the oxidized polyaniline through nucleophilic attachment. Therefore, arrays of the cantilever biosensors or microelectrode immunosensors could be designed that are capable of simultaneously detecting a variety of different target antigens by modifying them such that every cantilever or microelectrode is loaded with a different antibody by controlling the chemical state of the polyaniline film on the surface of the substrate.

In the second part of this research, gold nanoparticles were conjugated with bacteriophages through covalent binding. 2-iminothiolane (2-IT, or Traut's reagent) was reacted with a bacteriophage to produce thiolated bacteriophage. UV-Vis characterization of the product indicated that Traut's reagent had indeed reacted with the bacteriophage. It was also possible to confirm that a bacteriophage can attach to a gold surface after reacting with 2-IT solution based on the results of cyclic voltammetry and AFM. TEM data illustrated that bacteriophages and nanoparticles were conjugated together to form a network, and that this network formation is related to the concentration of 2-IT and gold nanoparticles added to bacteriophage solution. TEM data also revealed that most nanoparticles cannot attach to a bacteriophage if the bacteriophage had not first reacted with 2-IT. It therefore seems likely that the gold nanoparticles were conjugated with the bacteriophage via a covalent bond. Raman spectroscopy revealed a strong signal and very good surface enhancement effect in assemblies of gold nanoparticles and bacteriophage connected through 2-IT, but only a weak Raman signal from the bacteriophage in

samples prepared by mixing gold nanoparticles and the bacteriophage solution together without 2-IT. It has been reported that a covalent bond can reduce both the conformational changes and the denaturation of biomolecules that are generally caused by physical adsorption¹. These results prove that bacteriophage-gold nanoparticle networks with covalent bonds can be successfully prepared using the methods reported here. SEM data for *salmonella typhimurium* infection and SERS data for *Escherichia coli* infection of bacteriophage provided further evidence that bacteriophages retained their bioactivity in the networks fabricated for this project. This bacteriophage-gold nanoparticle network has potential applications in both cell targeting and biosensors.

In the third part of this work, results from both cyclic voltammetry and UV-Vis adsorption spectroscopic characterization confirmed that Layer-by-layer assembled ultrathin films of POMs and proteins were formed. AFM imaging indicated that the thickness of ten layers of POM/*Cyt c* is about 40 nm, which is reasonable given the dimensions of the POM (~1 nm) and the protein (~3x3x4 nm). Electrochemical data showed that formation of the POM/protein slowed the electron transfer process as the film became thicker and enhanced the reduction of hydrogen peroxide. The catalytic activity of this LbL film for hydrogen peroxide was dominated by the protein's contribution (*cyt c*).

Reference

1. Hermanson, G. T.; Smith, P. K., *Immobilized Affinity Ligand Techniques*, Academic: London, 1992.